Progress in Energy and Combustion Science 000 (2020) 100876

Contents lists available at ScienceDirect

Progress in Energy and Combustion Science

journal homepage: www.elsevier.com/locate/pecs

What fuel properties enable higher thermal efficiency in spark-ignited engines? ☆

James P. Szybist[a,*], Stephen Busch[b], Robert L. McCormick[c], Josh A. Pihl[a], Derek A. Splitter[a], Matthew A. Ratcliff[c], Christopher P. Kolodziej[d], John M.E. Storey[a], Melanie Moses-DeBusk[a], David Vuilleumier[b], Magnus Sjöberg[b], C. Scott Sluder[a], Toby Rockstroh[d], Paul Miles[b]

[a] Oak Ridge National Laboratory, 2360 Cherahala Blvd, Knoxville, TN 37932, United States
[b] Sandia National Laboratories, United States
[c] National Renewable Energy Laboratory, United States
[d] Argonne National Laboratory, United States

ARTICLE INFO

Article history:
Received 10 July 2019
Accepted 30 July 2020
Available online xxx

Keywords:
Octane
Knock
Spark ignition
Flame speed
Heat of vaporization
Particulate matter
Efficiency
Alternative fuels

ABSTRACT

The Co-Optimization of Fuels and Engines (Co-Optima) initiative from the US Department of Energy aims to co-develop fuels and engines in an effort to maximize energy efficiency and the utilization of renewable fuels. Many of these renewable fuel options have fuel chemistries that are different from those of petroleum-derived fuels. Because practical market fuels need to meet specific fuel-property requirements, a chemistry-agnostic approach to assessing the potential benefits of candidate fuels was developed using the Central Fuel Property Hypothesis (CFPH). The CFPH states that fuel properties are predictive of the performance of the fuel, regardless of the fuel's chemical composition. In order to use this hypothesis to assess the potential of fuel candidates to increase efficiency in spark-ignition (SI) engines, the individual contributions towards efficiency potential in an optimized engine must be quantified in a way that allows the individual fuel properties to be traded off for one another. This review article begins by providing an overview of the historical linkages between fuel properties and engine efficiency, including the two dominant pathways currently being used by vehicle manufacturers to reduce fuel consumption. Then, a thermodynamic-based assessment to quantify how six individual fuel properties can affect efficiency in SI engines is performed: research octane number, octane sensitivity, latent heat of vaporization, laminar flame speed, particulate matter index, and catalyst light-off temperature. The relative effects of each of these fuel properties is combined into a unified merit function that is capable of assessing the fuel property-based efficiency potential of fuels with conventional and unconventional compositions.

Contents

☆ This manuscript has been authored by four National Laboratories under contract with the US Department of Energy (DOE): Oak Ridge National Laboratory managed by UT-Battelle, LLC, under contract DE-AC05-00OR22725; National Renewable Energy Laboratory managed by Alliance for Sustainable Energy, LLC, under contract No. DE-AC36-08GO28308; Argonne National Laboratory managed by UChicago Argonne, LLC, under contract DE-AC02-06CH11357; and Sandia National Laboratories managed and operated by National Technology and Engineering Solutions of Sandia, LLC., a wholly owned subsidiary of Honeywell International, Inc, for DOE's National Nuclear Security Administration under contract DE-NA0003525. The US government retains and the publisher, by accepting the article for publication, acknowledges that the US government retains a nonexclusive, paid-up, irrevocable, worldwide license to publish or reproduce the published form of this manuscript, or allow others to do so, for US government purposes. DOE will provide public access to these results of federally sponsored research in accordance with the DOE Public Access Plan (http://energy.gov/downloads/doe-public-access-plan).

* Corresponding author.
E-mail address: szybistjp@ornl.gov (J.P. Szybist).

https://doi.org/10.1016/j.pecs.2020.100876

α	Average catalyst heating rate
AFM	Air-fuel mixture
AFR	Mass air-to-fuel ratio
AKI	Antiknock index
ATDC	After top dead center
BMEP	Brake mean effective pressure
BOB	Blendstock for oxygenate blending
CAD	Crank-angle degree
CAFE	Corporate Average Fuel Economy
CARB	California air resources board
CFPH	Central fuel property hypothesis
CFR	Cooperative fuels research
CO	Carbon monoxide
CO_2	Carbon dioxide
COV	Coefficient of variation
c_v	Heat capacity at a constant volume
DBE	Double bond equivalent
DF	Downsize factor
ΔF_{LO}	Fuel penalty during cold start
Δf_{LO}	Instantaneous difference between the cold and hot fuel consumption rates
DI	Direct injection
E85	Fuel mixture containing nominally 85 vol % ethanol
EGR	Exhaust gas recirculation
EISA	Energy Independence and Security Act
EIVC	Early intake valve closing
EPA	Environmental Protection Agency
f_C	Fuel consumption rate during cold start
F_{FTP}	Total fuel consumed during the FTP cycle
f_H	Fuel consumption rate during hot start
FSN	Filter smoke number
FTP	EPA Federal Test Procedure for the city driving cycle
γ	Ratio of specific heats of a working fluid
GPF	Gasoline particulate filter
g/mi	Gram per mile
η_b	Brake efficiency
HC	Hydrocarbon
HCCI	Homogeneous charge compression ignition
HPD	High power density
η_{comb}	Combustion efficiency
η_{GE}	Gas exchange efficiency
η_{ideal}	Ideal efficiency
η_{mech}	Mechanical efficiency
η_{OE}	Overexpanded cycle efficiency
η_{Otto}	Otto cycle efficiency
H	Heaviside function
HoV	Heat of vaporization
IAT	Intake air temperature
$IMEP_g$	Gross indicated mean effective pressure
$IMEP_n$	Net indicated mean effective pressure
ITE	Indicated thermal efficiency
K	Engine operating variable in OI
KLSA	Knock limited spark advance
KP	Knock point
LHV	Lower heating value
LIVC	Late intake valve closing
LPD	Low power density
LSPI	Low speed preignition
LTHR	Low temperature heat release
MAT	Mixture air temperature
MON	Motor octane number
MSS	Microsoot sensor
NA	Naturally aspirated
NMOG	Non methane organic gases
NOx	Oxides of nitrogen
NTC	Negative temperature coefficient
NVH	Noise, vibration and harshness
OI	Octane index
PFI	Port fuel injection
p_i	Example fuel property
$p_{i,ref}$	Reference example fuel property
PM	Particulate matter
PMEP	Pumping mean effective pressure
PMI	Particulate matter index
PM_{soot}	Soot or solid carbon portion of the particulate matter
PN	Particle number
PPR	Peak pressure rise
PR	Preignition rating
PRF	Primary reference fuel
PRR	pressure rise rate
P_{ST}	Cylinder pressure at spark timing
θ	Crank angle
$Q_{fuel\ total}$	Total fuel energy
Q_{HR}	Total energy release through combustion of the fuel
Q_{HT}	Total energy lost via wall heat transfer
r_c	Compression ratio
RON	Research octane number
RPM	Revolutions per minute
S_{octane}	Octane sensitivity
σ_{HT}	Proportion of energy remaining after wall heat transfer
SI	Spark ignition
σ_{ideal}	The degree to which the actual heat release profile resembles the ideal profile
S_L	Laminar flame speed
SOC	Start of combustion
T	Temperature
T50	Temperature at which 50% of the fuel is evaporated
T70	Temperature at which 70% of the fuel is evaporated
T_{amb}	Ambient temperature
$T_{c,90}$	TWC light-off temperature
TEL	Tetraethyl lead
t_{LO}	Time required for TWC light-off for 90% conversion
TSF	Toluene standardization fuels
TWC	Three-way catalyst
UDDS	Urban dynamometer driving schedule
V	Volume
Vc	Clearance volume
VCR	Variable compression ratio
Vd	Displacement volume
VOC	Volatile organic compound
VP	Vapor pressure
W	Work per cycle
WOT	Wide open throttle
YSI	Yield sooting index

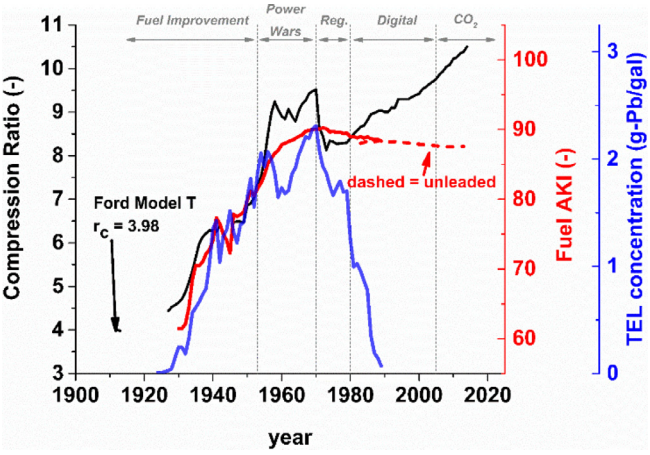

Fig. 1. Historically representative averaged trends in compression ratio (black), fuel AKI (red), and fuel TEL concentration (blue) for the United States as a function of year, Figure from Splitter *et al.* [1]. (For interpretation of the references to color in the text, the reader is referred to the web version of this article.)

1. Efficiency trends in spark ignition engines

1.1. Historical trends in spark ignition engines (1900–2000)

The composition and properties of fuel for spark ignition (SI) engines have historically been affected by many factors dating to the invention of the SI engine. Engine performance has only been one of the factors, while others are related to fuel production resources and technology, engine technology, regulations, and societal acceptance. Most of this review article focuses on the ways in which fuel affects engine performance and efficiency, but this section includes discussion of the larger societal and regulatory impacts for context.

Recently, Splitter *et al.* [1] provided an in-depth review of the coevolution of SI engines and fuels that relied on the antiknock index (AKI) as the primary performance metric of the fuel. In a review of knocking combustion, Wang *et al.* [2] describe knock as the noise associated with autoignition of a portion of the fuel-air mixture ahead of the propagating flame front, and add that knock is an inherent problem that plagues SI engines. The AKI is intended to be a metric of knock resistance, and is the average of the research octane number (RON, ASTM D2699 [3]) and motor octane number (MON, ASTM D2700 [4]), which are standardized tests under two different engine operating conditions. In general, the more resistant a fuel is to autoignition or knock, the more efficient an SI engine can be. Section 3 provides a more detailed analysis of the relationship between knock resistance and engine efficiency, including the shortcomings of the RON, MON, and AKI metrics, as well as other fuel properties that affect knock. However, from a historical perspective on the evolution of fuel quality, we will rely on the analysis from Splitter *et al.* [1], which used AKI.

In an effort to better understand the historical trends, Splitter *et al.* [1] identified developments and segmented the history of fuels into finite time frames or "ages," which are bounded by the onset of, or changes to, technical, societal, and regulatory factors. These ages are indicated in Fig. 1, which also illustrates the average engine compression ratio (r_c) of all vehicles sold on an annual basis, the average AKI of regular-grade gasoline, and the concentration of tetraethyl lead (TEL), a fuel additive that was used to increase the AKI of gasoline in the United States from the 1920s until the late 1980s.

The initial age pointed out in Splitter *et al.* [1] consisted of engine and fuel coevolution that stemmed from fuel improvements. Specifically, improvements to refining and fuel additives (e.g., TEL) greatly influenced the history and coevolution of fuels and engines, not only in the "fuel improvement age" but also throughout the twentieth century. Beginning in the late 1910s through the 1930s, researchers identified engine and fuel relationships between knock, compression ratio, performance, and efficiency [5].

Despite concerns about toxicity [6–9], TEL became an economically viable pathway to increase AKI, and allow corresponding increases in r_c, as shown in Fig. 1. However, the toxicity concerns did limit its concentration, to initially 3.17 g-Pb/gal in 1925 [6], followed by an increase in 1959 to 4.23 g-Pb/gal [10]. Refining advancements provided an additional path to increased AKI, including continuous process vacuum distillation, improved thermal reforming in the late 1920s and 1930s, catalytic cracking during World War II, and platinum reforming in the 1950s [11]. These factors allowed the AKI of both regular and premium grade gasoline to increase by more than 9 points from 1953 to 1970.

Simultaneous with AKI increases in the 1950s and 1960s, the real price of gasoline decreased (i.e., adjusted for inflation) [1], resulting in the "Power Wars" age (Fig. 1) where the fleet average horsepower doubled between 1953 and 1969 with virtually no increase in vehicle weight (127 vs. 284 HP and 3850 vs. 3879 lb, respectively). While improvements in AKI enabled power increases through higher r_c, there were also other contributing factors. Specifically, because there were no criteria emission standards at that time, increasing power through fuel enrichment was widespread. Fuel enrichment is when there is more fuel than can be burned to completion with the amount of air present in the combustion chamber, and while this increases power, it also reduces fuel economy and increases emissions of unburned hydrocarbons (HCs) and carbon monoxide (CO). Until oxygenated compounds were added to fuel at appreciable levels starting in the late 1990s and early 2000s, the stoichiometric mass air-fuel ratio (AFR) for gasoline was approximately 14.5. The fleet-average AFR decreased from approximately 15:1 in 1955 to approximately13:1 by 1961 and persisted at approximately 13:1 through 1965 [12]. The combined trajectories of these effects are presented in Fig. 2.

The rapid advances in performance during the late 1950s through the 1960s ("power wars age" in Fig. 1), were quickly halted by emissions regulations resulting from urban air quality concerns and fuel economy regulations resulting from geopolitically-caused fuel shortages in the 1970s. In 1970, the US Congress passed the Clean Air Act, which included the first national tailpipe emissions standard that regulated tailpipe emissions of CO, volatile organic compounds (VOCs), and oxides of nitrogen (NO_x), and went into full effect by 1975.

In order to implement the emission standards of the Clean Air Act, the composition of the fuel had to be changed so that the exhaust was compatible with the emerging catalytic aftertreatment technologies. Specifically, beyond the widespread contamination of the environment with lead, which had known negative health effects [13–19], TEL tended to cause deposit formation inside the combustion chamber. In order to prevent deposits, halogenate antideposit fuel additives such as dichloroethane and dibromoethane were developed in the 1920s and added to gasoline to prevent metal deposits from rapidly forming on combustion chamber surfaces [16,20,21]. Initially these anti-deposit additives were not a technical concern, but it was found that they poisoned catalysts and prevented compliance with the Clean Air Act. Thus, to enable catalyst use in 1975, the U.S. Environmental Protection Agency (EPA) defined the associated fuel lead phasedown process in 1973 [22], ruling that unleaded gasoline must be offered by all point-of-sale vendors by July 1974 [22]. Despite improved refining technologies, removing the TEL from gasoline caused the AKI to decrease by approximately 2 points from 90 AKI in 1970 to 88 AKI in 1974, as seen in Fig. 1.

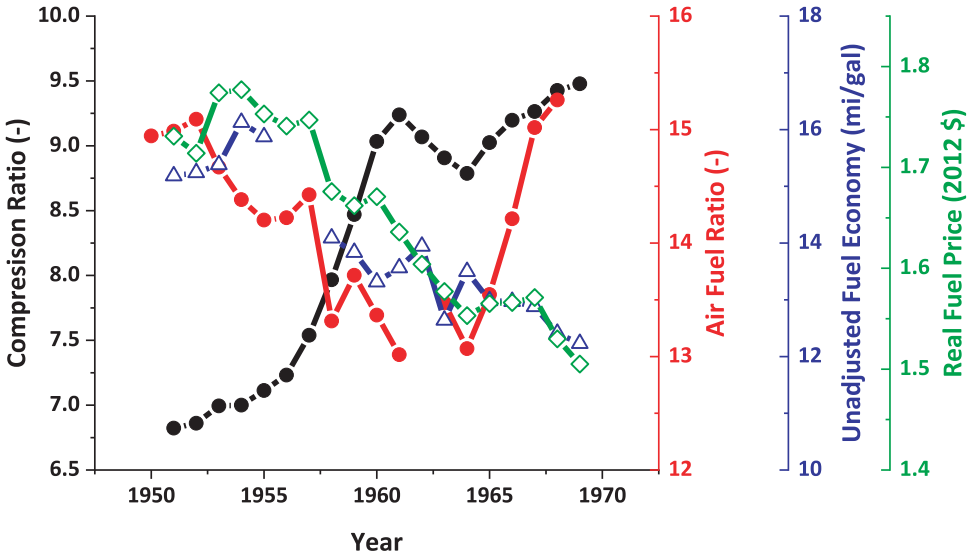

Fig. 2. Historically representative average trends in compression ratio (black), air-fuel ratio at wide open throttle (red), fuel economy (blue), and fuel price (green), figure from Splitter *et al.* [1]. (For interpretation of the references to color in the text, the reader is referred to the web version of this article.)

Initially, emission standards were met with the use of an oxidation catalyst to treat CO and VOC emissions, and by reducing NO_x emissions through in-cylinder methods [23]. The widespread methods to reduce NO_x emissions in-cylinder were to reduce r_c and to introduce exhaust gas recirculation (EGR) [23,24]. The reduced r_c to comply with NO_x emission standards also had the effect of masking the reduced performance of the lower AKI unleaded fuel [11,21,22,25–27]. To meet the more stringent NOx emission standards in 1981, three-way catalysts (TWCs) were developed and deployed, simultaneously reducing NO_x while oxidizing CO and VOC emissions [27]. These efforts proved successful at reducing emissions and improving air quality, including reducing NOx emissions by a factor of 4 by 1981 relative to a pre-regulations vehicle, from 4 g/mi NO_x to 1.0 g/mi [23,27]. However, reducing r_c to comply with NO_x emission standards decreased the maximum theoretical and achievable efficiency of the engine [28]. Fig. 2 shows that the fuel economy of vehicles in the mid-1960s was higher than that of vehicles in the early 1970s.

Motivated by fuel supply volatility in the 1970s, the United States passed the Energy Policy Conservation Act of 1975 [29], which among other things, imposed fuel economy standards to reduce fuel consumption. The average fuel economy standards were 15, 19, and 20 mpg for the model years 1978, 1979, and 1980, respectively, and an eventual requirement of 27.5 mpg for 1985 [29] that automakers met primarily through sharp reductions in vehicle weight—nearly 20%—from 1976 to 1980. Further fuel economy improvements, as well as engine performance improvements were necessary, but unlike in the fuel improvement and power war ages, AKI of the gasoline was not increasing, as shown in Fig. 1, and therefore could not be used as a basis for engine improvements.

Further engine improvements were enabled during the digital age, which, as shown in Fig. 1, effectively enabled r_c to be decoupled from AKI. The digital age accelerated advances in engine design through computer-aided simulations, and through electronic controls combined with low-cost sensors and computing. On-board controls included knock sensors [30] coupled with active spark control [31] to mitigate knock, and improved air-fuel-ratio control [32–34] to enable higher catalyst conversion efficiency at stoichiometric operation [23,35,36]. Both computational design tools and on-vehicle controls became critical to building vehicles that complied with increasingly stringent exhaust tailpipe emissions limits and fuel economy standards [23]. As a result, in the 1980s and 1990s it was possible to increase r_c and performance without changes to fuel AKI, thereby increasing both performance and efficiency. This allowed vehicle power and acceleration to be increased an average of 4% every year from 1980 to 2004 without improvements in AKI [37].

1.2. Recent trends in SI engines (2000–Present)

The *2018 EPA Automotive Trends Report* provides recent fuel economy data [38] and, as shown in Fig. 3, vehicle fuel economy has been increasing sharply since 2005. This recent fuel economy increase comes after a period of fuel economy decrease between 1986 to 2005, likely due to several circumstances. The oil glut of the mid 1980's resulted in a return to very inexpensive gasoline after the price shocks of the 1970's. During the Reagan Administration in 1986, the corporate average fuel economy (CAFE) standards enacted in 1975 were frozen at 26.0 mpg for cars and 19.5 for trucks, instead of the 27.5 mpg and 20.0 mpg, respectively as designated in the Clean Air Act [39]. Under the George H. W. Bush Administration in 1989, the standards returned to 27.5 mpg and 20.0 mpg, but attempts to raise them further were thwarted through the Bush Administration and the Clinton Administration [39]. At the same time, consumer preference was shifting markedly from small cars to heavier light trucks and SUVs, thus resulting in an overall decrease in real-world fuel economy [39]. Safety concerns also led to increases in vehicle weight as body reinforcements and other safety systems added to the weight of the vehicles. In 2000, late in the Clinton Administration, Congress lifted the freeze on fuel economy that had been in place since 1989, setting the stage for future CAFE increases. This occurred during the George W. Bush Administration when Congress passed the Energy Independence and Security Act (EISA) which increased CAFE as a fleet-wide average for all vehicles to 35 mpg by 2020, and then was increased further during the Obama Administration. Interestingly, while vehicle weight has been largely level since 2005, horsepower has continued to increase as fuel economy has improved.

The increase in vehicle fuel economy is partly attributable to engine technologies and partly attributable to non-engine technologies. Non-engine technologies include advancements in transmissions [40] that allow the engine to be operated at higher-efficiency operating conditions throughout a drive cycle [41], advancements in the light weighting of vehicles [42], and the energy

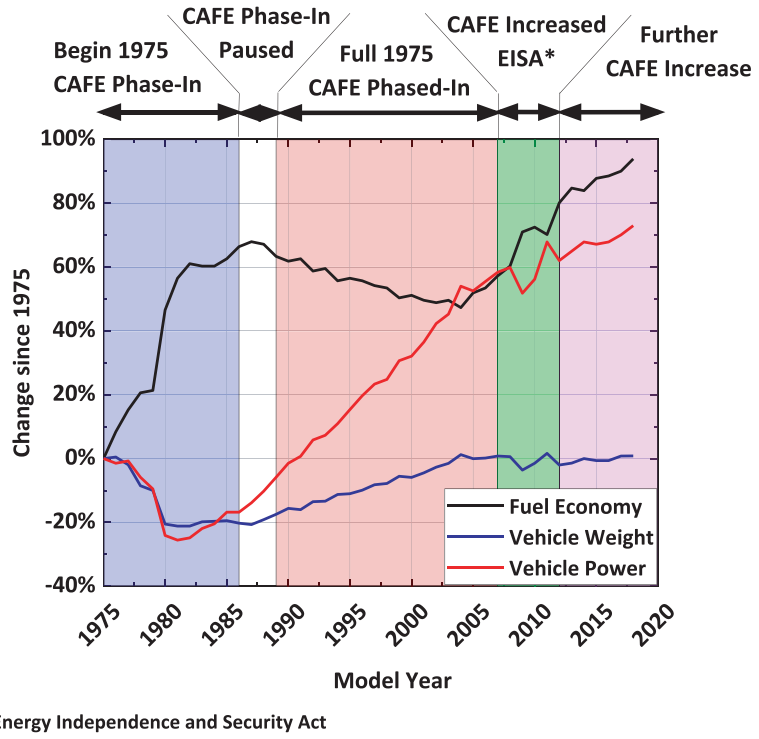

Fig. 3. Trends of fuel economy, horsepower, and vehicle weight from 1975 to 2018. Data from EPA Automotive Trends Report [38].

recovered through regenerative braking in hybrid electric powertrains [43]. Those technologies are very important to vehicle fuel consumption and efficiency, but they are beyond the scope of this article, which focuses specifically on engine efficiency and the role that fuel properties can play to maximize engine efficiency.

Many of the engine technologies employed to enable a simultaneous increase in vehicle power and fuel efficiency have been combined in complementary ways. Broadly speaking, there are two dominant pathways to increase vehicle efficiency: one pathway with high power density (HPD) that aims to decrease the engine displacement through engine downsizing, which allows engines to be used in more efficient operating regions; and another pathway with lower power density (LPD) that aims to use an overexpanded Atkinson or Miller cycle to increase the peak engine efficiency. An overview of these two pathways is given in Sections 1.2.1 and 1.2.2, respectively; the pathways are compared in Section 1.2.3. The thermodynamic basis for each of the contributing technologies is discussed in Section 2.2; the way that fuel properties can interact with these technologies to provide further efficiency improvements is discussed in Section 3.

1.2.1. High vehicle efficiency pathway 1. engine downsizing through high power density

Engine downsizing is the process of using a smaller-displacement engine than was used in the previous generation of vehicle to deliver equivalent or improved performance. The extent of downsizing is shown in Fig. 4 as the production share of engines having 3, 4, 6, or 8 cylinders as a function of time [38]. During the increase in fuel economy from 2005 to the present, shown in Fig. 3, the production share of four-cylinder engines has increased from just over 25% to more than 60%. Further, during this same time period, vehicle power continued to increase, which is also shown in Fig. 3 [38]. Thus, there has been a dramatic increase in the power per unit displacement, also known as specific power, of light-duty vehicles since 2005.

Increasing the power density of an engine can be accomplished by increasing the maximum engine load, increasing the maximum engine speed, or through a combination of these. Conventional naturally-aspirated (NA) engines achieve maximum brake mean effective pressures (BMEPs) of less than 15 bar. High-power concepts are defined as anything that exceeds that threshold. Similarly, engine speeds above 7000 rpm are generally considered to be high-speed concepts [44–46], as shown graphically in Fig. 5. For high efficiency, modern downsized engines operate at high loads using charge boosting rather than higher speeds, where the friction penalties increase, and typically combine direct injection (DI) fueling and boosting through the use of turbochargers. Typical forms of charge boosting increase the BMEP to about 20 bar, but further increases in high-load engine concepts employing more aggressive downsizing strategies are possible, with some production engines achieving 30 bar BMEP, and several researchers reporting engine operation up to 35 bar BMEP [47–52].

Turner *et al.* defined a downsizing factor; as follows:

$$DF = \frac{V_{d_{NA}} - V_{d_{Downsized}}}{V_{d_{NA}}} \quad (1)$$

where DF is the downsizing factor and $V_{d_{NA}}$ is the displacement volume for comparably-powered NA and downsized engine alternatives [52]. They reported that most downsized gasoline engines in current production vehicles have a DF of about 35% to 40%. Some prototypes with a DF of 60% have been shown [47,52]. For production engines, downsizing is most often combined with down speeding as an effective measure to improve fuel efficiency, and benefits of up to 10% have been shown in vehicle applications [44].

The penetration of downsized boosted engines in the market has increased dramatically since 2005 during the recent increase in fuel economy. The percentage of boosted engines sold increased from 1.7% in 2005 to 30.8% in 2018 [38]. Table 1 provides three examples comparing the conventional and downsized engine configurations with approximately constant vehicle configuration and engine power. The examples shown include a small car (Honda Civic

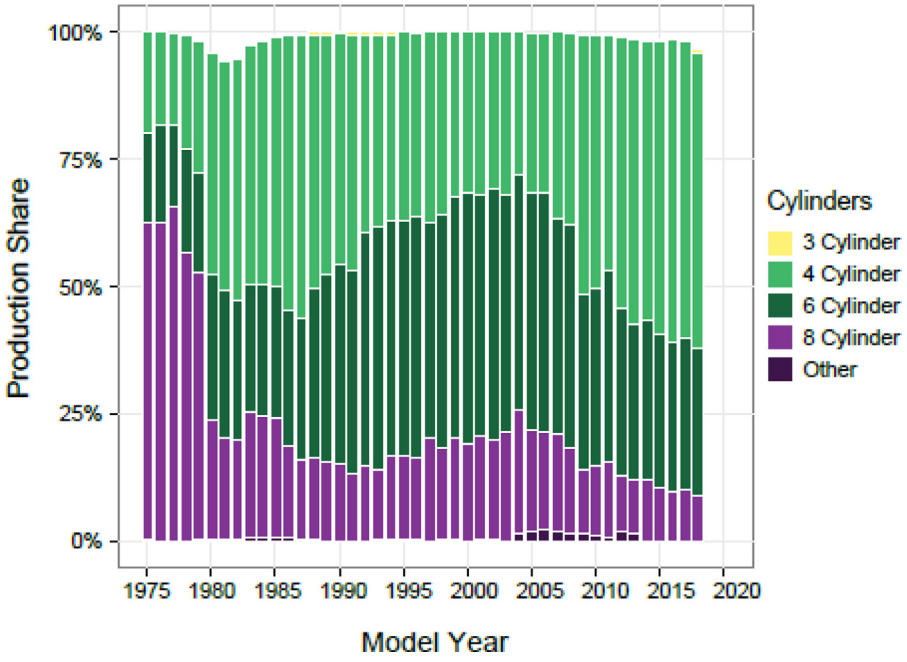

Fig. 4. Production share of spark-ignition light-duty engines in the United States by cylinder count from 1975 through 2018 from the EPA Automotive Trends Report [38]. Note that the bars do not add to 100% because light-duty sales of diesel engines are not included in this figure.

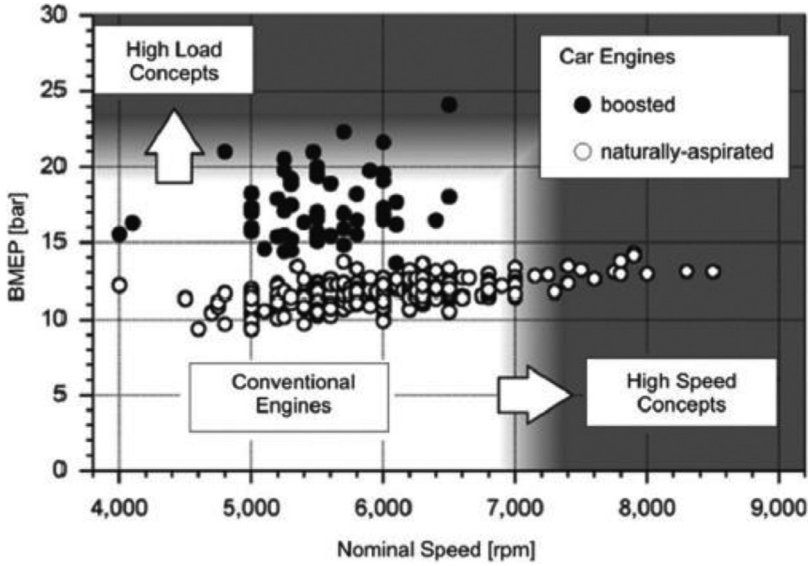

Fig. 5. BMEP and nominal engine speed for boosted and naturally aspirated engine concepts. Reprinted from Schumann *et al.* [46] with permission of Sage Publishing.

Table 1
Examples of downsized engine applications.

Vehicle	Downsize Factor	Model Year	Displacement	Maximum Power	Power Density	U.S. EPA Combined Fuel Economy
Honda	37.6%	2015	2.4 L	153 kW @ 7000 rpm	64 kW/L	26.5 MPG
Civic		2017	1.5 L	153 kW @ 5700 rpm	102 kW/L	33.0 MPG
Ford	36.0%	2013	2.5 L	125 kW @ 6000 rpm	50 kW/L	26.0 MPG
Escape		2013	1.6 L	129 kW @ 5700 rpm	81 kW/L	28.0 MPG
Chevrolet	37.2%	2019	4.3 L	212 kW @ 5300 rpm	50 kW/L	18.5 MPG
Silverado		2019	2.7 L	231 kW @ 5600 rpm	86 kW/L	21.5 MPG

SI) through a full-sized pickup truck (Chevrolet Silverado), and in each case the downsized engine application provides an increase in fuel economy of between 7 and 25%.

1.2.2. High vehicle efficiency pathway 2. Low power density

The technologies for the high-efficiency pathway that utilizes LPD vary to some degree but generally include direct fuel injection and overexpanded engine cycles combined with high r_c. Some of the engines in this category also utilize cooled EGR. As will be discussed in more detail in Section 2, the overexpanded Atkinson

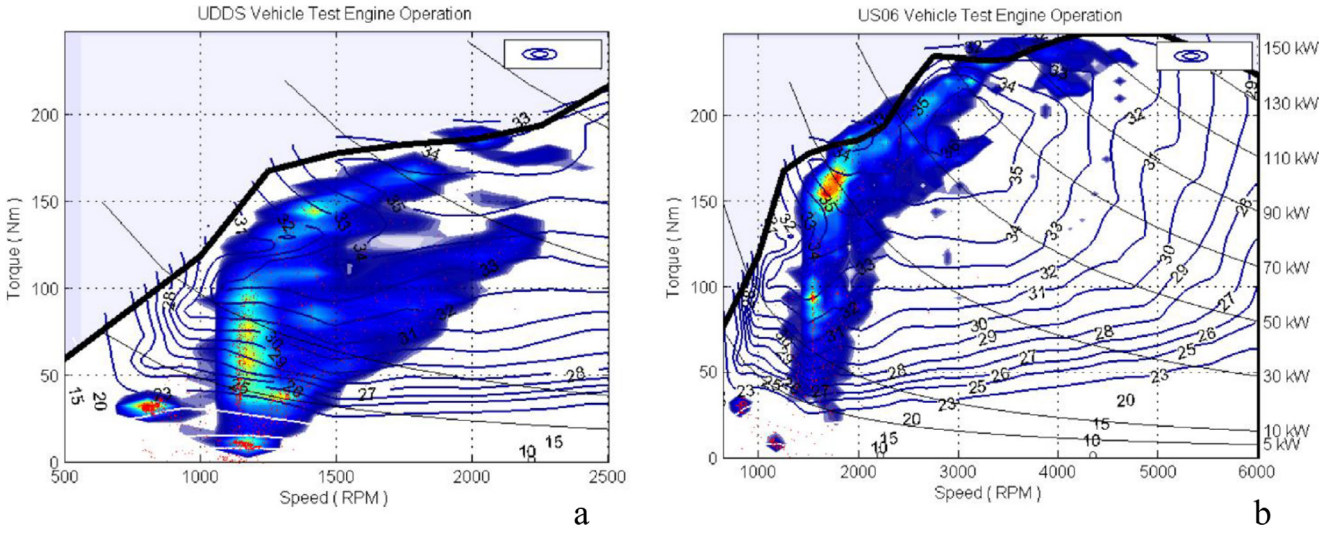

Fig. 6. Energy-weighted fuel consumption as a function of torque and speed for a mid-sized sedan with a continuously variable transmission during drive cycles for (a) the UDDS cycle, and (b) the US06 drive cycle. Contour lines indicate brake thermal efficiency, and shading represents energy consumption. Reprinted from Newman *et al.* [58] with permission of SAE International.

or Miller cycle, combined with the high r_c, delivers higher peak efficiencies than the downsized engines can achieve, but because the displacement volume is not fully utilized with overexpanded cycles, the power densities of the engines are lower.

The US EPA benchmarked one of these engines, the 2014 Mazda 2.0 L SKYACTIV-G engine [53]. As opposed to the downsized boosted engines discussed in the previous section, this engine had a very high r_c (13:1), allowing it to produce a high peak η_b (37.9%) [53]. However, it also had a significantly lower power density (57.5 kW/L) than the boosted HPD engines.

LPD engines that include EGR can increase η_b even more. Two examples of research involving hybrid-specific engines are reported by Hwang *et al.* [54], who provided an overview of a 2016 1.6 L engine from Hyundai-Kia Corporation, and by Matsuo *et al.* [55], who reported on a 1.8 L engine from Toyota Motor Corporation. The two studies produced similar results. Both engines achieved 40% η_b by combining DI fueling, Atkinson cycle operation, high geometric r_c (13.0:1), and high levels of cooled EGR dilution (20% [54] and 25% [55], respectively). Because they utilized high levels of EGR dilution, the engines had low specific power outputs of 48.3 kW/L[54] and 39.4 kW/L [55].

A similar design approach was taken by Hakariya *et al.* [56], who presented a 2.5 L engine from Toyota, which was then later benchmarked by the US EPA [57]. This engine achieved an η_b of 40% using DI fueling, Atkinson cycle operation with late intake valve closing (LIVC), a high mechanical compression ratio (13:1), and up to 25% cooled EGR dilution. The difference with the 1.8 L Toyota engine is that the 2.5 L engine was intended for a conventional power train rather than a hybrid application, and it achieved a higher power density (60 kW/L) than the Mazda SKYACTIV-G [53].

1.2.3. Comparison of the high vehicle efficiency pathways

Relative to the boosted HPD, the LPD pathway can produce a higher peak engine efficiency, up to 40% η_b [54–56]. The higher η_b is largely due to these engines having a higher r_c, but can also include the use of overexpanded engine cycles and EGR, which are discussed in more detail in Section 2.2. However, peak engine efficiency alone is not a good predictor of vehicle fuel economy because the engine power demands can vary dramatically based on vehicle drive cycle, and the majority of engine operation during drive cycles is not at the peak-efficiency. Fig. 6 shows the energy-weighted speed and torque and corresponding energy efficiency over the course of the urban dynamometer driving schedule (UDDS) and the US06 driving cycle for a mid-sized sedan with a continuously variable transmission [58]. The UDDS is a light-load driving cycle. Most of the fuel is consumed at less than 50% of the peak load and at speeds between 1000 and 1500 rpm. In contrast, the US06 driving cycle is much more aggressive, and a much larger fraction of the fuel is consumed at higher loads and at speeds over 2000 rpm.

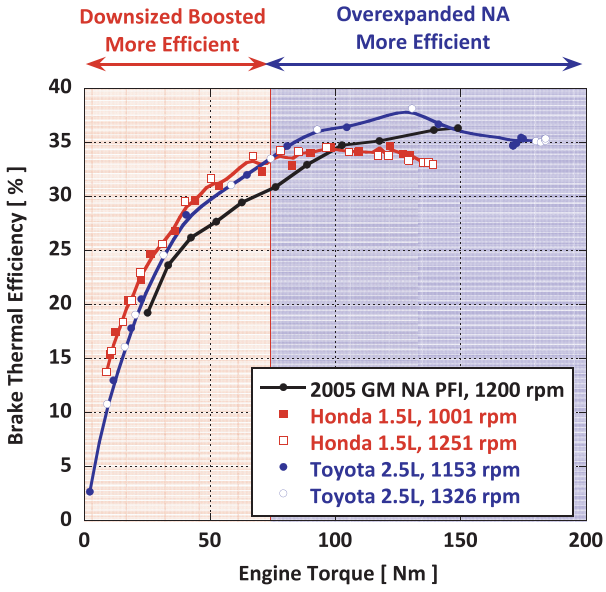

Fig. 7. η_b as a function of torque for a baseline 2.4 L NA PFI engine at 1200 rpm [59], a boosted downsized 1.5 L engine from Honda at two different engine speeds [60], and a Toyota 2.5 L engine using an Atkinson cycle engine and EGR dilution [57].

The HPD and LPD pathways differ in that they provide an efficiency benefit from different portions of the load range. To illustrate the difference, Fig. 7 shows efficiency as a function of engine torque for an NA port fuel injection (PFI) engine from 2005 to serve as the baseline, a boosted HPD engine to represent high-efficiency pathway 1 (Section 1.2.1), and a LPD engine to repre-

sent high-efficiency engine pathway 2 (Section 1.2.2). The baseline engine data are from a GM 2.4 L 2005 NA PFI engine with a maximum power of 132 kW presented by Dugdale *et al.* [59], from which a plot of brake specific fuel consumption at 1200 rpm was digitized and then converted to η_b assuming a fuel lower heating value (LHV) of 43.5 kJ/g. The downsized boosted data are from a Honda 1.5 L engine with a maximum power output of 130 kW that was benchmarked by Stuhldreher [60]. The η_b data for this engine were not available at 1200 rpm. Thus, the η_bs at both 1001 rpm and 1251 rpm are plotted to illustrate that η_b changes very little as a function of speed within that speed range. The overexpanded LPD Atkinson cycle engine of a Toyota 2.5 L engine with a maximum power output of 150 kW was presented by Hakariya *et al.* [56] and was later benchmarked by Kargul *et al.* [57]. The η_b data from Kargul *et al.* [57] were available at 1153 and 1326 rpm.

Fig. 7 shows that, relative to the 2005 GM NA PFI engine, there are efficiency advantages for both the high-power-density pathway using a downsized boosted engine and the low-power-density pathway using an overexpanded Atkinson cycle and EGR dilution. At the lightest engine loads, the HPD pathway provides more of an efficiency benefit than the overexpanded cycle, but at higher engine loads, the LPD pathway provides more of a benefit. Thus, the way that the engines are used in a vehicle, in terms of transmission pairing and vehicle duty cycle, determines which of the engines can provide the most efficient vehicle. As a result, both are viable pathways moving forward.

2. Factors that increase efficiency in SI engines

Prior to understanding how fuels can improve efficiency in SI engines, it is important to understand the thermodynamic basis for efficiency, as well as the engine technologies that are being deployed by engine manufacturers to improve efficiency. Thus, Section 2.1 provides a thermodynamic framework by which to evaluate the ways that higher efficiency can be attained in an engine and Section 2.2 provides a discussion of the effect that individual technologies can have on efficiency from a thermodynamic standpoint. Section 2.3 then introduces the role of fuel properties on increasing engine efficiency in the context of the engine thermodynamics and other engine technologies being deployed for high efficiency.

2.1. Thermodynamic expressions for efficiency in an SI engine

Brake thermal efficiency may be expressed as the following product of component efficiencies:

$$\eta_b = \eta_{mech}\eta_{comb}\eta_{GE}\sigma_{HT}\sigma_{ideal}\eta_{ideal} \tag{2}$$

These component efficiencies are defined below.

η_{mech} is the mechanical efficiency, the ratio of brake work to net indicated work:

$$\eta_{mech} = \frac{BMEP}{IMEP_n} \tag{3}$$

where *BMEP* is the brake mean effective pressure (the shaft work performed in one cycle divided by the engine's displacement volume) and $IMEP_n$ is the net indicated mean effective pressure (the indicated work performed in one cycle divided by the engine's displacement volume). The main difference between indicated and brake work can be attributed to engine friction.

η_{comb} is the combustion efficiency (the ratio of total heat released by combustion to the amount of available fuel energy):

$$\eta_{comb} = \frac{Q_{HR}}{Q_{fuel,\ total}} \tag{4}$$

where Q_{HR} is the total amount of energy released through combustion of the fuel and $Q_{fuel,\,total}$ is the amount of useful fuel energy supplied or the theoretical maximum amount of fuel energy available to perform work (typically assumed to be equal to the fuel's LHV).

$\eta_{GE}$is the gas exchange efficiency (representing the work penalty required to move air into the engine):

$$\eta_{GE} = 1 + \frac{PMEP}{IMEP_g} \tag{5}$$

where *PMEP* is the pumping mean effective pressure (the net amount of work performed during the gas exchange process divided by the engine's displacement volume; for boosted operation, *PMEP* can be positive, so it is possible for η_{GE} to be larger than unity). For reference, Section 2.2.3 includes a discussion of minimizing *PMEP*, including a visualization of the pumping work on a pressure-volume diagram in Fig. 10.

$IMEP_g$ is the gross mean effective pressure (the amount of work performed during the compression and expansion strokes divided by the engine's displacement volume).

σ_{HT} is the proportion of total heat release available after wall heat losses have removed energy from the system:

$$\sigma_{HT} = 1 - \frac{Q_{HT}}{Q_{HR}} \tag{6}$$

where Q_{HT} is the total energy lost via wall heat transfer during one engine cycle.

η_{ideal} is the efficiency of the ideal working cycle, which is frequently represented as the ideal Otto cycle (η_{Otto}), Eq. 7. As is discussed in Section 2.2.3, however, η_{ideal} can be represented by other cycles as well.

$$\eta_{Otto} = 1 - {r_c}^{1-\gamma} \tag{7}$$

where r_c is the geometric compression ratio of the engine, γ is the ratio of specific heats for the working fluid.

σ_{ideal} is degree to which the actual heat release profile resembles the ideal profile.

In this case, σ_{ideal} is the degree of constant volume combustion:

$$\sigma_{ideal} = \frac{1}{\eta_{Otto}Q_{HR}} \int_{SOC}^{EOC} \left(1 - \left(\frac{V_d + V_c}{V(\theta)}\right)^{1-\gamma}\right) \frac{dQ_{HR}}{d\theta} d\theta \tag{8}$$

where

SOC is the start of combustion,
EOC is the end of combustion,
V_d is the displacement volume of one cylinder,
V_c is the clearance volume of one cylinder,
$V(\theta)$ is the crank angle dependent volume of one cylinder,
θ is the crank angle.

The impact of changes in friction, combustion efficiency, pumping losses, heat transfer, and combustion speed/phasing may be expressed in terms of their contributions to relative changes in brake thermal efficiency. To this end, the total differential of η_b is divided by η_b:

$$\frac{d\eta_b}{\eta_b} = \frac{d\eta_{mech}}{\eta_{mech}} + \frac{d\eta_{comb}}{\eta_{comb}} + \frac{d\eta_{GE}}{\eta_{GE}} + \frac{d\sigma_{HT}}{\sigma_{HT}} + \frac{d\eta_{ideal}}{\eta_{ideal}} + \frac{d\sigma_{ideal}}{\sigma_{ideal}} \tag{9}$$

2.2. High-Efficiency Engine Technologies

For engine technologies to increase η_b and ultimately to decrease vehicle fuel consumption, they must affect one or more of the terms on the right-hand side of equation 9. The individual technologies that enable these efficiency increases are discussed in Sections 2.2.1 through 2.2.7. Many of the technologies are ultimately used to increase r_c within the acceptable knock limitations, which maximizes η_{ideal}, as described by Eq. 7, or they are used to minimize pumping, maximizing η_{GE}. Thus, these two goals are discussed before the individual technologies.

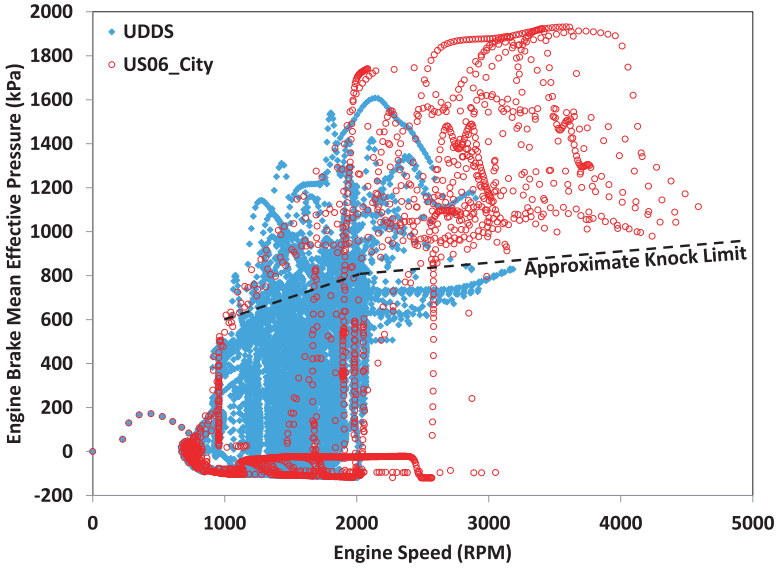

Fig. 8. Engine operating conditions predicted by vehicle system modeling for a mid-size sedan on the UDDS and city portion of the US06 driving cycles. Reprinted from Sluder *et al.* [61] with permission of CRC.

All engines aim to minimize friction to maximize η_{mech}. However, while recognizing the importance of friction, this review article is focused on in-cylinder and emissions processes where fuel properties can provide an impact. Thus, direct friction-reducing technologies are out of scope for this study, such as surface treatments and low-friction lubricants. However, fuels can have an indirect impact on engine friction through downsizing. The downsizing effect is accounted for empirically through the downsizing efficiency multiplier in Section 3.1.5.

In order to achieve an acceptable compromise between efficiency and power density, all modern SI engines are knock-limited over the high-load portion of their operating range. This is illustrated by Sluder *et al.* [61] in Fig. 8, which shows speed-load operating points over two different engine driving cycles, and which of those are knock-limited [61]. These results are specific to the engine and vehicle combination studied, which was typical of mid-size sedans in the U.S. market. While other combinations of engines and vehicles yield somewhat different percentages, the majority of driving conditions on both schedules for a wide variety of engine and vehicle combinations are not knock-limited. Interestingly, Sluder *et al.* report that 92% of the engine operating conditions over the UDDS driving cycle are not knock-limited. The city portion of the US06 cycle is a much more aggressive driving schedule, but even that schedule results in over 67% of the engine operating conditions occurring in the knock-free region [61]. Engines are designed such that r_c is as high as possible while still being able to achieve the maximum load of the engine at a predetermined level of knock mitigation. Thus, the selection of r_c is a compromise between maximizing efficiency over the lower load portions of the engine operating map while maintaining a high power density.

At loads higher than the knock limit, spark ignition is retarded to later in the engine cycle, which is effective at mitigating knock because it reduces the pressure and temperature of the unburned gas prior to the consumption of the end-gas, slowing the autoignition reactions that cause knock. Retarding the ignition also decreases σ_{ideal} by moving the heat release away from the point of minimum cylinder volume. The lost opportunity to extract work that is caused by late combustion phasing for knock avoidance was illustrated by Szybist and West [62] and is shown in Fig. 9.

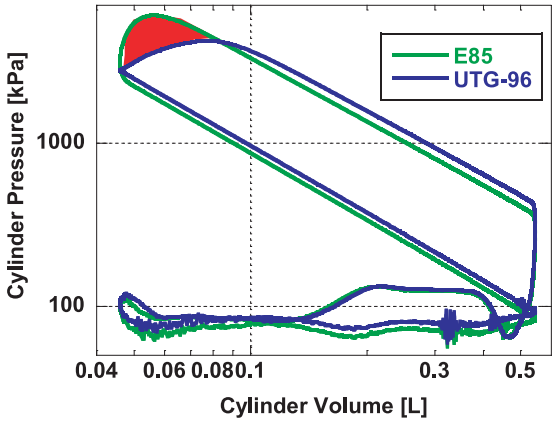

Fig. 9. Pressure-volume diagram illustrating the effect of late combustion phasing on engine efficiency at an engine load of 10 bar $IMEP_n$ at 2000 rpm. One fuel (E85, green) is not knock-limited and advanced combustion timing is possible. The other fuel (UTG-96, blue) is phased later due to knock avoidance. The shaded area in red represents a lost opportunity to extract work from the engine cycle due to retarded combustion phasing for knock mitigation. Reprinted from Szybist and West [62] with permission of SAE International.

Boosted HPD engines, as discussed in Section 1.2.1, typically utilize a lower r_c than is used by LPD Atkinson-cycle engines, discussed in Section 1.2.2. This difference is partly due to engines becoming more knock-prone at higher engine loads and partly due to the LPD Atkinson-cycle engines having a lower effective r_c because of the valve timing strategy being used, as will be discussed in Section 2.2.3. Another emerging engine technology that aims to maximize r_c throughout the engine operating map is the use of variable compression ratio, which is discussed in more detail in Section 2.2.6.

Minimizing pumping work, or maximizing η_{GE}, is another strategy that is commonly applied to various engine technologies, and there are numerous methods to achieve it. Pumping work at light engine operating load conditions occurs because the mass of fuel in-cylinder needs to be limited, and due to the requirement of a stoichiometric mixture for the effective function of the TWC, the mass of air also needs to be limited. Historically, this was achieved by throttling the intake airflow to lower the manifold pressure, re-

sulting in the primary source of pumping losses. Using boosted HPD engines is itself a strategy to minimize pumping work because, relative to a naturally aspirated engine, the intake manifold pressure only needs to be maintained below ambient pressure for the lightest loads and is above ambient pressure for much of the operable load range. Such a situation reduces the use of intake throttling. This de-throttling effect is what makes HPD boosted engines more efficient than LPD engines at the lightest operating loads, as shown in Fig. 7.

LPD engines, and to a lesser extent HPD engines, utilize a host of additional technologies to maximize η_{GE} by reducing pumping work. The technologies include overexpanded engine cycles (Section 2.2.3) and cylinder deactivation (Section 2.2.7), both of which reduce the effective displacement of the engine under part-load conditions. They also include utilization of cooled EGR dilution (Section 2.2.4), which maximizes the in-cylinder mass for a given load condition without increasing the air or fuel mass. Some technologies provide additive or even synergistic benefits in fuel consumption; others may compete with one another because they represent different approaches to addressing the same efficiency losses. For example, combining overexpanded engine cycles and cylinder deactivation technologies has diminishing returns because both attempt to reduce pumping work by decreasing the effective engine displacement.

2.2.1. Boosted engine operation

As Heywood [63] explains, the maximum load that a given engine can deliver is limited by the amount of fuel that can be burned inside the engine cylinder, and the amount of fuel that can be burned is limited by the amount of air that can be inducted. Compressing the air to a higher density increases the air mass that can be inducted, which enables the engine to operate at higher load operation relative to a naturally aspirated engine. Thus, boosting the air system is a key enabling technology for HPD downsized engines.

Boosting the intake manifold pressure can be done through either turbocharging, which uses exhaust gases to drive a compressor, or through supercharging. While superchargers are effective at increasing engine power, they typically use mechanical power from the engine to drive a compressor, leading to efficiency loss. It is worth pointing out that electric superchargers can be paired with electricity recovered from regenerative braking in a mild hybrid configuration, resulting in some high efficiency synergies [64]. However, such use of electric superchargers is still under development and further consideration of this configuration is outside the scope of this review. Turbochargers, on the other hand, are energy recovery devices that use waste heat in the exhaust to perform compression work on the intake air, making them a more efficient technology than superchargers. With the trend of engine downsizing, the use of turbochargers in gasoline engines has become common, and the sale of boosted engines has risen from 1.7% in 2005 to 30.8% in 2018 [38].

2.2.2. Direct injection fueling

DI fueling uses either central-mount or side-mount fuel injectors to deliver fuel directly into the combustion chamber and is differentiated from PFI or carbureted fueling, which introduce the fuel upstream of the combustion chamber. DI fueling is advantageous for knock mitigation relative to PFI fueling because more of the heat of vaporization (HoV) of the fuel comes from the charge air itself rather than the metal surfaces of the engine [65]. Additionally, a combination of DI fueling with variable valve phasing, over-scavenging, or some fresh air blowing directly through the cylinder during gas exchange can be used to remove all burnt gases without introducing un-burnt air-fuel mixture into the exhaust gas stream because of the flexibility in timing the injection [66–68]. Together, these technologies act to reduce the in-cylinder temperature with DI fueling, thereby mitigating knock and allowing r_c to be increased. DI fueling also increases the in-cylinder turbulence, which serves to shorten the combustion duration [69], which benefits σ_{ideal}. Using modern injection hardware and advanced engine calibration, DI fueling can also reduce fuel-wall interactions by tailoring spray patterns and injection durations to the combustion chamber and the intake-generated flow [70]. This makes more of the fuel available to the combustion event and increases combustion efficiency (η_{comb} in Eq. 9).

When the first generation of modern gasoline DI engines was launched, in the late 1990s, the emphasis of improved efficiency was squarely placed on the ability to run fuel-lean in stratified charge mode [44,67,68]. Due to the need for complicated NOx emission controls systems and the restricted fuel efficiency gains made as a result of the limited operating range in that mode, automotive manufacturers soon switched to a homogeneous stoichiometric charge mode while utilizing the benefits of DI, thus achieving an increase in power density [45,66,71,72], thereby enabling engine downsizing.

Thus, DI fueling combined with turbocharging are the essential technologies for the HPD engine pathway with downsized engines discussed in Section 1.2.1. Additionally, DI fueling is a key technology enabler to LPD engines. Because LPD engines are also knock-limited, they can take advantage of the HoV of the fuel for charge-cooling, which helps to mitigate knock. Further, the additional turbulence from the DI fuel injection is useful for extending the EGR dilution tolerance, which is discussed in Section 2.2.4.

2.2.3. Overexpanded engine cycles

The Otto cycle gives up potential for additional work extraction from exhaust gasses which are at higher than ambient pressure at the end of the expansion event. Over-expanded cycles, namely the Atkinson and Miller cycles, utilize expansion ratios which are larger than the r_c to allow further expansion of the exhaust gases for additional work extraction [73]. Thus, the ideal efficiency for an overexpanded cycle, η_{OE}, is higher than η_{Otto} for a given compression ratio.

Over-expanded engine cycles can also have a second major effect of increasing the gas exchange efficiency (η_{GE}) by decreasing pumping work when the over-expansion ratio is continuously varied to act as a form of variable displacement. Most overexpanded cycles function by utilizing only a portion of the displacement volume of the intake stroke. This is typically accomplished by using either early intake valve closing (EIVC) or LIVC. With EIVC, the intake valve closes during the intake stroke, causing cylinder pressure to temporarily decrease below the intake manifold pressure, before returning to manifold pressure and above during the compression stroke, with the effect of reducing the trapped air and fuel mass without requiring throttling. Similarly, LIVC reduces the trapped air and fuel mass by drawing in a full cylinder charge, but then expelling a portion of the charge mass back into the intake manifold before the intake valve is closed. The effect of these two valve timing strategies on pressure-volume diagrams is illustrated in Fig. 10 [74].

Numerous mechanical strategies can be used to implement EIVC and LIVC, including some strategies that use multiple cam profiles through a lost-motion system [75,76] and some that use a cam-in-cam arrangement [77]. Using EIVC or LIVC to produce a high-efficiency engine allows the use of high mechanical r_c, as is evident in the numerous production engines with r_c = 13:1 (see Section 1.2.2). This is possible because the effective r_c is lower than the mechanical r_c when the compression stroke is only partially utilized.

Overexpanded engine cycles are becoming common with LPD NA engines. However, numerous studies have shown that it is pos-

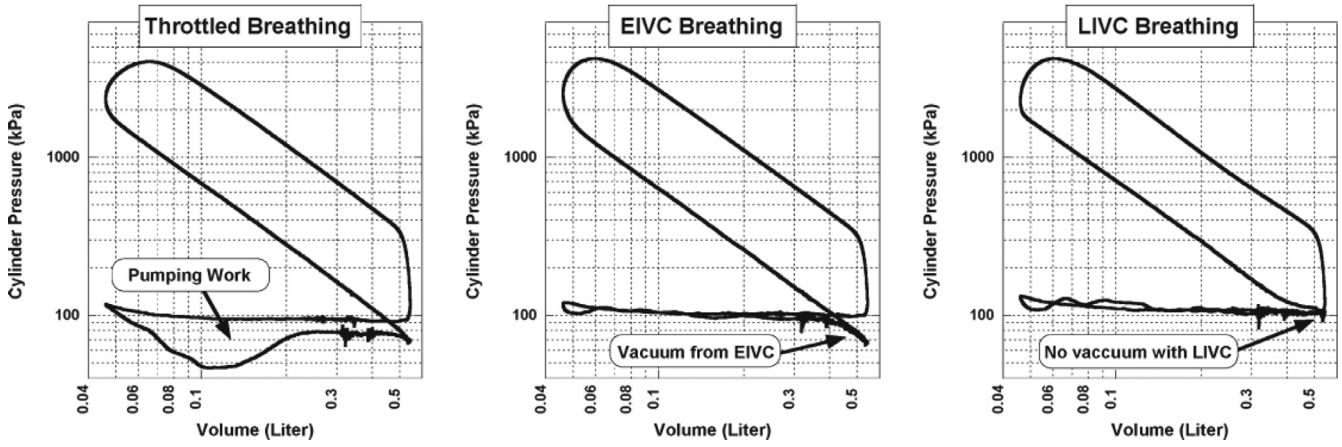

Fig. 10. Pressure-volume diagrams of engine operation at 1500 rpm, 8 bar BMEP with conventional throttled operation, an EIVC valve strategy, and an LIVC valve strategy. Reprinted from Szybist *et al.* [74] with permission of American Chemical Society.

sible to combine the downsized boosted pathway with overexpanded technologies for further efficiency gains (for example, see Osborne *et al.* [78]).

2.2.4. Exhaust gas recirculation

Cooled EGR is an engine technology that is being deployed as a method to increase engine efficiency. When cooled external EGR is used, a fraction of the exhaust is cooled and mixed with the incoming fresh air. This technology benefits the η_{GE}, σ_{HT}, and η_{ideal} terms, but it can adversely impact the η_{comb} and σ_{ideal} terms.

The overall efficiency advantages for high-EGR conditions are summarized in a thermodynamic modeling study by Caton [79]. The additional mass added by the EGR causes the manifold pressure to increase without increasing the intake oxygen flow, thereby maintaining a stoichiometric charge while decreasing engine pumping and increasing engine efficiency at part-load conditions, benefiting the η_{GE} term in Eq. 9. Additionally, the adiabatic flame temperature decreases with EGR dilution, typically causing the heat transfer to decrease, benefiting the σ_{HT} term in Eq. 9. Also, due to a combined thermal and composition effect, the ratio of specific heats (γ) of the working fluid increases with EGR, benefiting the η_{ideal} term in Eq. 9, as described by Eq. 7.

In addition to the γ benefit for η_{ideal}, Alger *et al.* [80] showed that EGR also reduces the knock propensity, through the reduced in-cylinder temperature, which could allow r_c to be increased. Alger *et al.* [80] also concluded that every one percent increase of EGR was equivalent to a 0.5 octane number increase. Splitter *et al.* [81,82] confirmed the reduced knock propensity effect using 15% EGR, which allowed the maximum load limit to be increased by more than 10% in a single-cylinder engine experiment.

EGR can also alter the combustion process in ways that have adverse impacts on the terms in Eq. 9. Specifically, EGR decreases the laminar flame speed (S_L) of the fuel, resulting in a longer combustion duration [83,84], adversely impacting the σ_{ideal} term in Eq. 9. In addition to a decrease in σ_{ideal}, the use of EGR dilution is limited because of increased cycle to cycle combustion variability, as measured by the coefficient of variation (COV) of $IMEP_g$ [73,85,86]. Ozdor *et al.* showed that the increase in COV of $IMEP_g$ was directly attributable to the decrease in S_L and, in particular, the increased duration of the initial flame kernel development [86]. Additionally, Szybist and Splitter [84] showed that EGR decreases the combustion efficiency, adversely affecting the η_{comb} in Eq. 9.

2.2.5. Advanced Ignition Systems

Conventional electrical ignition systems are comprised of either inductive coils or capacitor discharge units, and the underlying physics of these spark ignition processes are well-understood [63,87]. The total spark energy delivered to the gas in the spark plug is generally around 30 mJ [88], which is one to two orders of magnitude greater than the minimum ignition energy required for stoichiometric combustion with low dilution. Using an advanced ignition system can impact the terms in Eq. 9 to provide improved efficiency: decreased combustion duration for a higher σ_{ideal} as well as higher η_{comb}. Further, advanced ignition systems can enable higher levels of EGR dilution, which is thermodynamically advantageous as discussed in Section 2.2.4. Several types of advanced ignition systems are listed below:

- Multiple spark plugs [88,89]
- Discharging multiple ignition events in a single cycle [90,91]
- An extended spark discharge ignition event [92]
- Breakdown or blast wave ignition units [93–96]
- Laser ignition systems [97]
- Corona discharge ignition systems [96–99]
- Plasma jet and rail plug ignition systems [100–106]
- Low temperature plasma ignition systems [107–110]
- Pre-chamber ignition systems [111–118]

2.2.6. Variable compression ratio

Variable compression ratio (VCR) technologies enable the use of increased mechanical r_c in the region of the engine operating map that is not knock-limited. This is done by varying the clearance volume at top dead center through four categories of mechanisms that do not involve varying the stroke of the engine:

- vary the position of the crankshaft relative to the engine head (e.g., install the crankshaft in an eccentric cradle) [119];
- vary the effective linkage distance between the crankshaft and piston, which can include using a variable-length connecting rod [120–122] or an intermediate linkage between the crank throw and connecting rod [123–125];
- move the head relative to the crankshaft [126,127]; or
- use movable elements in the head as well as within the piston to contract or enlarge the clearance volume [128–133].

VCR strategies can be implemented in a continuously variable manner within a range of authority or can instead be designed in a two-step manner, where the system can vary between two discrete values of r_c. The benefits of both types of systems have been quantified. Shelby *et al.* estimated the benefits of both continuous and two-step VCR for an r_c range of 10:1 to 13:1 and found that a two-step implementation reduced fuel consumption 2.5% to 3.6% and that a continuously variable strategy was similar, offering a

2.7% to 3.7% improvement [134]. Wolfgang *et al.* [122] estimated a larger fuel consumption decrease of 8.5% by combining VCR with an overexpanded engine cycle.

2.2.7. Cylinder deactivation

One early application of cylinder deactivation occurred in 1916, but it was not until the 1980s that several more attempts were made. In recent years, cylinder deactivation has become a mainstream technology that is being used to reduce vehicle fuel consumption, and in 2018, 12% of vehicle sales incorporated this technology [38].

Cylinder deactivation is a technology that can be employed to change the effective displacement of the engine. In addition to stopping the fuel injection, both the intake and exhaust valves stop actuating so that there is no excess air present in the exhaust, allowing the TWC to maintain high NO_x conversion efficiency. Cylinder deactivation increases engine efficiency primarily by decreasing pumping work, or increasing η_{GE}. For example, if half the cylinders are deactivated, the remaining cylinders are required to double their net power to maintain demanded power, allowing those cylinders to operate more efficiently at conditions that reduce throttling losses [135].

Cylinder deactivation has historically been limited by transient control and noise, vibration, and harshness (NVH) constraints [135]. In recent years, however, many of those constraints have been overcome. NVH constraints have been overcome with cylinder deactivation largely due to improved control technologies, and the next generation of advanced control for cylinder deactivation, Dynamic Skip Fire technology [136,137], has recently been commercialized and promises to extend the market penetration of cylinder deactivation even further. Struhldreher [138] baselined a 4.3 L six-cylinder engine with and without cylinder deactivation and found that, at conditions between 1 and 4 bar BMEP at 1250 rpm, deactivation can increase η_b by more than three percentage points, which is more than a 20% relative improvement at the lightest loads.

2.3. Fuel Property Impacts on SI Engine Efficiency

Like the engine technologies discussed in Section 2.2, fuel properties that enable increases in η_b do so through changes to one or more of the terms on the right-hand side of Eq. 9. Changes to the terms may be the direct result of the fuel property, or they may be indirect effects resulting from changes in engine design and operation enabled by the fuel or required to mitigate undesirable effects of a fuel property. These effects may be analyzed through knowledge of the impact of each fuel property on each term on the right-hand side of Eq. 9.

To evaluate the merits of new fuel formulations in terms of their expected impact on engine efficiency, the combined impact of the fuel's properties on brake thermal efficiency must be quantified. It is useful to compare the merits of a new fuel with a reference fuel, such that the relative improvement in thermal efficiency resulting from the use of the new fuel may be estimated. To this end, the merit function is defined as the relative change in brake thermal efficiency computed as a linear combination of the new fuel's properties:

$$Merit = \frac{\Delta\eta_b}{\eta_b} = \sum_i \frac{1}{\eta_b}\frac{\partial\eta_b}{\partial p_i}\left(p_i - p_{i,ref}\right) \tag{10}$$

where p_i stands for the fuel properties that influence brake thermal efficiency and $p_{i,ref}$ stands for the corresponding properties of the reference fuel.

This Eq. is the basis for the Co-Optima SI efficiency merit function [139], the definition of which depends on

- the identification of the fuel properties p_i,
- an established set of reference properties $p_{i,ref}$, and
- knowledge of the sensitivity of brake thermal efficiency to each property ($\frac{\partial\eta_b}{\partial p_i}$).

Identifying the fuel properties that can enable increases in efficiency, and subsequently quantifying the potential efficiency contribution of each individual fuel property in an optimized engine configuration, is not straight-forward. Performing these tasks was the major focus of the Co-Optima initiative's efforts on SI engines as well as the focus of the remainder of this article. Section 3 describes the fuel properties that have an efficiency impact through in-cylinder processes affected by knock-resistance metrics, HoV, S_L, and PMI. Section 4 describes how fuel properties can impact vehicle efficiency due to the emissions controls required. In particular, Section 4 focuses on the catalyst light-off temperature and the sooting tendency of the fuel.

3. How fuels affect in-cylinder efficiency

A guiding principle of the Co-Optima initiative is the central fuel properties hypothesis (CFPH), which states that fuel properties provide an indication of the performance and emissions of the fuel, regardless of the fuel's chemical composition. Historically, some gasoline standards have been performance-based, which implicitly align with the CFPH. For instance, the composition of the fuel is not considered for the distillation and volatility specifications in the ASTM standard for gasoline [140] or in the octane number measurements. Rather, they are performance-based indicators of fuel quality. However, other fuel standards are composition-based, such as the sulfur content of gasoline [140] and the California requirement to limit the aromatic content of the gasoline to 35 vol % and the olefin content to 10 vol % [141].

Within the Co-Optima initiative, fuel components derived from biomass are being considered for blending with gasoline feedstocks, and the evaluation criteria extend beyond fuel performance in an engine. The Co-Optima initiative is also evaluating the life-cycle environmental and economic impacts of bio-derived fuels and the technology readiness and scalability of the fuel production technology [142]. The combined analysis of engine performance aspects with environmental, economic, and scalability considerations can be found in a report by Farrell *et al.* [143]. The present study aims to provide an in-depth review of the engine performance aspects of the Co-Optima initiative.

A number of the fuel components and blending streams identified within the Co-Optima initiative have oxygen-containing functional groups that are not conventionally associated with fuels for SI engines. Historically, fuel for SI engines has been limited to petroleum-derived hydrocarbon streams from refineries (alkanes, olefins, aromatics, and naphthenes), along with a small number of oxygenated compounds, namely ethanol, methanol, and methyl tertiary butyl ether. The potential for significant changes in gasoline composition calls into question whether performance-based metrics that align with the CFPH are accurate indicators of performance across the full engine operating map with changing fuel chemistry.

To develop a better understanding of the contributions of individual fuel properties and their adherence to the CFPH, Section 3 focuses on the role that fuel properties have on in-cylinder processes that can impact efficiency. Subsection 3.1 considers the various ways to measure and quantify antiknock properties as well as their ability to accurately predict knock propensity under different operating conditions. Subsection 3.2 focuses on the impact of the various ways that HoV affects engine efficiency, after which the role of S_L is considered in Subsection 3.3.

Table 2
Properties of the Co-Optima fuels, as given by Fouts *et al.* [144].

	RON	MON	S_{octane}	Saturates	Aromatics	Olefins	Ethanol
Unit	-	-	-	vol %	vol %	vol %	vol %
ASTM Method	D2699	D2700	-	D1319	D1319	D1319	D5599
$alkylate_{Co\text{-}Optima}$	98.0	96.6	1.4	100.0	0.0	0.0	0.0
$E30_{Co\text{-}Optima}$	97.4	86.6	10.8	57.1	5.0	8.1	30.6
$aromatic_{Co\text{-}Optima}$	98.1	87.8	10.3	65.0	30.8	4.2	0.0
$olefinic_{Co\text{-}Optima}$	98.2	88.0	10.2	58.1	10.6	31.3	0.0
$cyclo\text{-}alkane_{Co\text{-}Optima}$	98.0	87.1	10.9	70.3	28.2	1.5	0.0

Subsection 3.4 examines the current state of knowledge on the impact of fuel properties on low-speed preignition (LSPI).

References are made to the Co-Optima fuels throughout Sections 3 and 4. The five Co-Optima fuels were designed within the Co-Optima initiative as a means to test the CFPH (detailed descriptions of these fuels are given in Fouts *et al.* [144]). The five Co-Optima core gasolines all have matched nominal RON of 98. One of these fuels, referred to as $alkylate_{Co\text{-}Optima}$, has low octane sensitivity (S_{octane}), which is the difference between RON and MON and is discussed further in Section 3.1.2, while the other four fuels have nominally matched S_{octane} between 10.2 and 10.9. Despite nominally matched fuel properties, the four fuels with high S_{octane} have significantly different chemical compositions, as shown in Table 2.

3.1. Knock resistance

3.1.1. Historical antiknock metrics

The knock phenomenon was observed as early as 1876 [145], but it was not until around 1900, when the advent of the carburetor solved the major challenge of providing a combustible gas mixture, that knock became problematic and garnered more serious attention [146]. Knock was initially diagnosed to occur as a result of preignition, but by 1905, Ricardo concluded that it was the shock of a gaseous wave striking the walls of the cylinder, which he called "detonation" [146]. This inspired research into the knock phenomenon and the effect of fuels, including development of VCR research engines [147,148].

In conjunction with VCR engines to study knock, there was also a need to develop detailed cylinder pressure analysis to measure knock events. Midgley and Boyd, working with the National Bureau of Standards, improved upon the original cylinder-pressure indicator designs invented by Watt for steam engines [149]. They also compared techniques used to measure "detonation" in engines, such as using the listening method, cylinder pressure indicator method, temperature, and the bouncing pin, and concluded that the bouncing pin method was superior [149]. This method consisted of a free pin placed loosely in a guide with the lower end placed on the cylinder head. During non-knocking operation the pin merely floated with the small flexing of the cylinder head, however, under knocking combustion "the cylinder head would flex so violently that the pin was thrown free of its contact." [5]. The bouncing-pin mechanism was able to provide a robust measurement device for quantifying knock by comparison of results obtained with reference fuels by measuring the bouncing pin fluctuation in a given time period using an electrolytic cell containing sulfuric acid and distilled water [149], as shown in Fig. 11. This device was ultimately implemented in the standard knock-testing equipment, the Cooperative Fuels Research (CFR) engine [150–153].

Several groups recognized the need to have standard reference fuels to characterize the knock tendency of a test fuel, measured at the same time and under the same conditions [149,154,155]. Midgley and Boyd investigated using aromatics (benzene and toluene) as the non-knocking fuel and diethyl ether as the knock-enhancing fuel, but these were rejected because their knock tendency was extremely sensitive to AFR [149]. Other potential reference fuels proposed by Midgely and Boyd included cyclohexane, hexane, diethyl selenide, and a hexane-isopropyl nitrite [149].

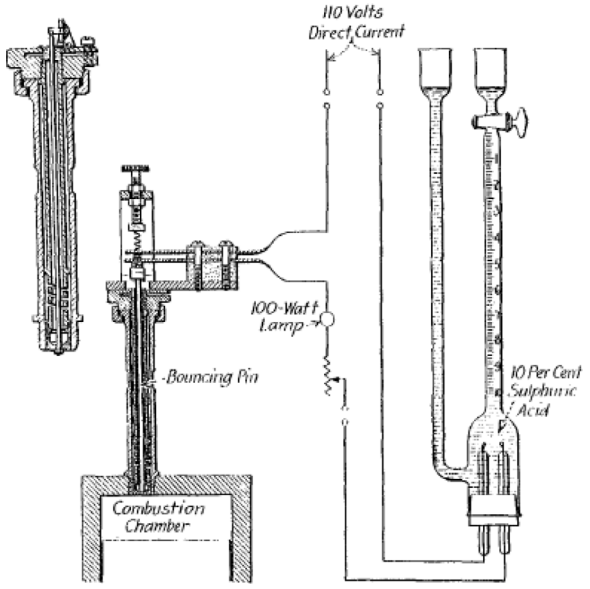

Fig. 11. Midgley–Dickenson bouncing pin. Reprinted from Midgley [149] with permission of SAE International.

The Ethyl Corporation subsequently proposed using n-heptane and 2,2,4 trimethyl pentane (iso-octane) as the reference fuels for octane rating [155], and those fuels are still used today in the RON [3] and MON [4] tests and are known as the primary reference fuels (PRFs). They argued that using iso-octane was deemed to be more suitable than toluene due to having a very similar hydrogen-carbon ratio and similar specific gravity as well as viscosity to that of n-heptane [155]. By 1931 the CFR Committee implemented the PRF octane number scale as part of the knock-testing equipment and designated it the Research Method, which later became the RON.

It was soon discovered that the combustion chamber surface temperatures of the CFR engine during the RON test were not representative of automobile engines at the time. Although they met the RON specification, some samples of gasoline were found to behave differently in the field. To rectify that, the MON test method was developed based on modifications to the RON test. Specifically, the engine speed and intake mixture temperature were increased to obtain combustion chamber surface temperatures representative of engines at the time [156-159].

While the RON [3] and MON [4] standardized tests are still used as the basis to quantify the knock tendency of a fuel, there has been a significant amount of recent research to develop a better understanding of what is measured in the RON and MON tests. Specifically, the instrumentation of the CFR octane rating engine does not respond to the pressure oscillations after autoignition, but

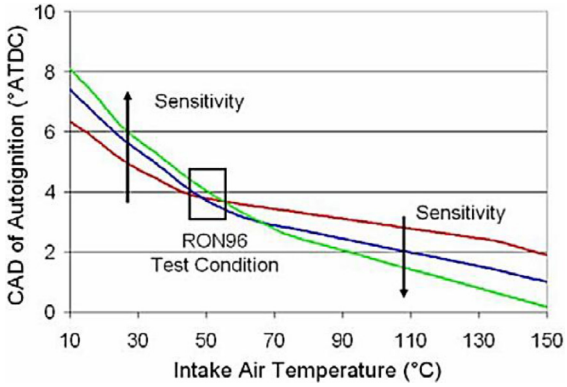

Fig. 12. Autoignition timing as a function of intake temperature for three fuels with a RON rating of 96: Red $S_{octane} = 0$, Blue $S_{octane} = 11$, Green $S_{octane} = 17$. Reprinted from Mittal *et al.* [170] with permission of SAE International.

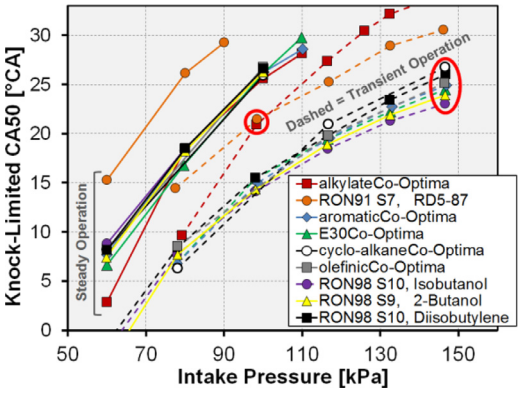

Fig. 13. Knock-limited phasings of nine fuels under steady-state (solid lines) and transient conditions (dashed lines), with fixed engine speed (1400 RPM) and stoichiometric operation. Reprinted from Vuilleumier *et al.* [171] with permission of SAE International.

rather the sharp pressure inflection prior to the oscillation [160–164]. However, in a more recent study, Rockstroh et. al. [165] concluded that these phenomena were closely correlated.

3.1.2. Octane index and the importance of octane sensitivity

The MON test was developed after the RON test because the in-vehicle performance of the fuel was not adequately being characterized by the RON test [156–159]. The need for this was not simply in absolute terms, but also in relative terms. In other words, the highest RON fuel would underperform lower RON fuels in application. Thus, the MON test conditions were an effort to address the reality that the relative ranking of knock resistance among a set of fuels changes as the engine conditions change. As a measure of this, the concept of S_{octane} was introduced, defined as the difference between RON and MON.

Leppard [166] investigated the chemical origin of S_{octane}, focusing on different chemical classes. For alkanes, there is a two-stage ignition process: low-temperature heat release (LTHR) followed by a negative temperature coefficient (NTC) region wherein the reaction rate becomes inversely proportional to the temperature. Those processes are followed by a high-temperature heat-release event. The chemical origins and dependencies of the two-stage ignition process were later elucidated in the development of chemical kinetic mechanisms for the PRFs, n-heptane [167] and iso-octane [168], the paraffinic fuels that define the RON and MON scales. The PRFs undergo knock at about the same r_c in the RON and MON tests even though the intake manifold temperature increases significantly. Thus, the NTC behavior makes the fuels insensitive to changes in intake temperature. The insensitivity of autoignition to intake temperature with NTC was recently confirmed by Splitter *et al.* in a more modern gasoline DI engine where the knock limited combustion phasing did not change significantly when intake temperature was increased from 90°C to 160°C [169]. Because other paraffinic fuels also exhibit two-stage ignition behavior, low S_{octane} is ubiquitous among paraffinic fuels. In contrast, Leppard [166] showed that neither aromatics nor olefins exhibited the two-stage ignition behavior, and as a consequence, the r_c for those fuels at the knocking condition in the RON test is significantly different than at the knocking condition in the MON test, meaning that they have higher S_{octane}.

The effect of S_{octane} was further investigated by Mittal *et al.* [170] in a chemical kinetic modeling study of an engine using three fuels with a RON of 96 and with S_{octane} varying from 0 to 17. Fig. 12 shows the crank angle of autoignition as a function of temperature for these fuels. At an intake temperature of 50°C, which is similar to the RON test, all of the fuels autoignited at a similar crank angle. At cooler temperatures, the fuel with lowest S_{octane} was the most prone to autoignition, but the trend is reversed at high intake temperature, where the fuel with the highest S_{octane} is the most prone to autoignition. With the intake air temperature range of 50°C to 150°C, the fuel with the lowest S_{octane} is the least sensitive to the impact of changes in intake temperature, which is in agreement with Leppard [166], who found that the NTC behavior of paraffinic low-S_{octane} fuels made them insensitive to changes in intake temperature.

In validation of the crossover in modeled autoignition propensity by Mittal *et al.* in Fig. 12 [170], a crossover in the knock resistance between different fuels as engine conditions change has also been observed experimentally in modern engines by Vuilleumier *et al.* [171] and by Szybist and Splitter [172]. Vuilleumier *et al.* [171] observed the change in the rank ordering of fuel knock limits as a function of intake manifold pressure using nine fuels of varying compositions, shown in Fig. 13, using a fuel matrix that included the Co-Optima core fuels discussed in Section 3 and described by Fouts *et al.* [144]. Knock limits were measured for both conventional steady-state continuously fired operation with a 100% duty cycle and skip-fired operation with a lower 20% duty cycle. The skip-fired operation has lower surface and gas temperatures and represents the knock response during a transient from low to high load, which engines experience during vehicle acceleration. Under the transient conditions, the knock-limited combustion phasing of the low- S_{octane} $\text{alkylate}_{\text{Co-Optima}}$ fuel crosses over that of the research gasoline representative of commercial regular-grade gasoline (RD5–87). Relative to the $\text{alkylate}_{\text{Co-Optima}}$, the RD5–87 has a lower RON (91 vs 98 RON) and a higher S_{octane} (7 vs. 1.4 S_{octane}). Thus, despite its significantly higher RON, the $\text{alkylate}_{\text{Co-Optima}}$ fuel is only more knock-resistant at low intake manifold pressures; it becomes more knock-prone under boosted conditions.

Recently, the chemical origins of S_{octane} have been further investigated by Westbrook *et al.* [173]. They conclude that electron delocalization caused by features of molecular structure, such as a carbon-carbon double bond incorporated in, or a hydroxyl group attached to, a carbon chain, leads to preferential hydrogen abstraction on sites that have a low probability of leading to isomerization after characteristic low-temperature oxygen addition reactions. The low rates of isomerization reduce the overall rate of low-temperature chain branching, which is responsible for LTHR. This leads to reduced low-temperature reactivity and reduced NTC behavior, causing a difference in behavior between these types of fuels (e.g., olefins, alcohols) relative to paraffins, which is expressed as S_{octane}.

Independent kinetic modeling studies performed by Yates *et al.* [174] and Mehl *et al.* [175] demonstrated that the RON and

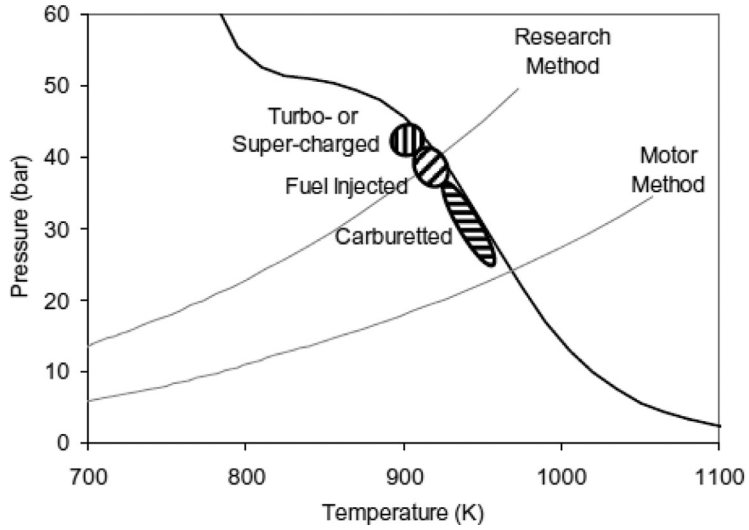

Fig. 14. Pressure-temperature trajectories of the of the Research Method (RON) and Motor Method (MON) plotted over a line of constant ignition delay (4 ms). Additionally, the typical knock-limited pressure-temperature conditions for different engine technologies are highlighted. Reprinted from Yates *et al.* [174] with permission of SAE International.

MON tests represent two different pressure-temperature trajectories, as shown in Fig. 14. The MON trajectory has a higher temperature at a given pressure and consequently avoids the pressure-temperature conditions that result in LTHR before encountering the pressure-temperature conditions of the NTC region. In contrast, the RON trajectory has a lower temperature at a given pressure, leading to conditions that yield a much stronger LTHR event prior to entering the pressure-temperature conditions of the NTC region. The stronger LTHR raises the temperature of the unburned fuel-air mixture, leading to increased knock propensity under these conditions. Thus, the relative knock-resistance order of fuels can change depending on the pressure-temperature trajectory, and the relative change in order is largely dependent on S_{octane}. Further, Yates *et al.* [174] showed that carbureted engines operate at pressure-temperature trajectories between RON and MON, PFI engines operate closer to the RON trajectory, and boosted DI engines can operate at pressure-temperature trajectories outside the bounds of RON and MON. While Yates *et al.* [174] describe these engine technologies in terms of their fueling technologies, the movement toward the RON trajectory can be attributed to a variety of technologies that reduce the temperature of the charge at intake valve closing, with engine-breathing technologies being particularly important. There is also a significant timescale difference between these tests such that the MON test (900 rpm) operates at an engine speed that is 50% faster than the RON test (600 rpm). However, considering that both of these tests operate at engine speeds that are significantly slower than the speeds of modern engines, both tests represent long-timescale conditions.

To relate the specific performance of an engine and fuel to the RON and MON tests, Kalghatgi [176, 177] pioneered a practical method to correlate the RON and MON values to knock-limited spark advance (KLSA). This method requires a parameter, K, which is dependent on the engine operating conditions, to act as a weighting factor between RON and MON. The resultant octane index (OI) rating (Eq. 11) correlates to the actual knock propensity of the fuel much more strongly than either RON or MON in modern engines [177–179]. This allows the relative knock resistance of fuels to be determined at conditions in real engines, which differ from the RON and MON tests, as shown by Kalghatgi in Fig. 15 [176].

$$OI = RON - K{*}S_{Octane} \tag{11}$$

The variable K in Eq. 11 is a heuristic that allows the changing knock propensity for different engine conditions to be understood. By definition, $K_{RON} = 0$ and $K_{MON} = 1$, but for all other operating conditions K is derived empirically and does not have a fundamental underpinning. In his early work, Kalghatgi [176,177] explained that K is determined through a multivariable linear regression analysis of KLSA. Since then, a variety of methods have been introduced to estimate K, including an empirical correlation that was dependent on the temperature at a compressive pressure of 15 bar [180], nonlinear regression analyses [181,182], and direct comparisons with PRFs [179]. Zhou et al. [183] compared four methods of calculating K and determined that each method had strengths and weaknesses. For the linear and nonlinear regression methods, the determination of K was very sensitive to the design of the fuel matrix. In particular, if RON and S_{octane} were highly correlated, the determination of K was unreliable. When attempting to determine K from direct comparisons with PRFs, only OI values below 100 may be compared with PRFs, because the maximum OI for a PRF blend ($S_{octane} = 0$) is 100. Extension of the PRF scale to values $>$ 100 requires the addition of TEL [3, 4], which introduces a different chemical pathway to knock mitigation, a conceptual deviation from the $<$100 RON and MON scale, and more uncertainty. This is of particular consequence when K is negative because negative K values coupled with high-S_{octane} fuels can yield OI values in the 110 to 150 range, making direct comparison between a high-S_{octane} fuel and a lead-free PRF impossible at those conditions. Considering the various ways in which K can be estimated for a given engine and operating condition, combined with a lack of first-principles physicality associated with K, a regression from experimental data is the most accepted method to determine K, judged by representation in the literature [171,176,178,180,184,185].

Kalghatgi [176,177] also explained that, although an empirical correlation is the most reliable method of determination, K is also a descriptor of the trajectory of the compression process in the engine through the pressure-temperature domain. Pressure-temperature trajectories that have a negative K value are “beyond RON” because they have a higher pressure at a given temperature than the RON test. Pressure-temperature trajectories that have a K value that is greater than unity are “beyond MON” because they have a temperature that is greater than the MON test at a given pressure. Boosted SI engines typically correspond to a negative K value under knocking conditions [184,185], whereas homogeneous

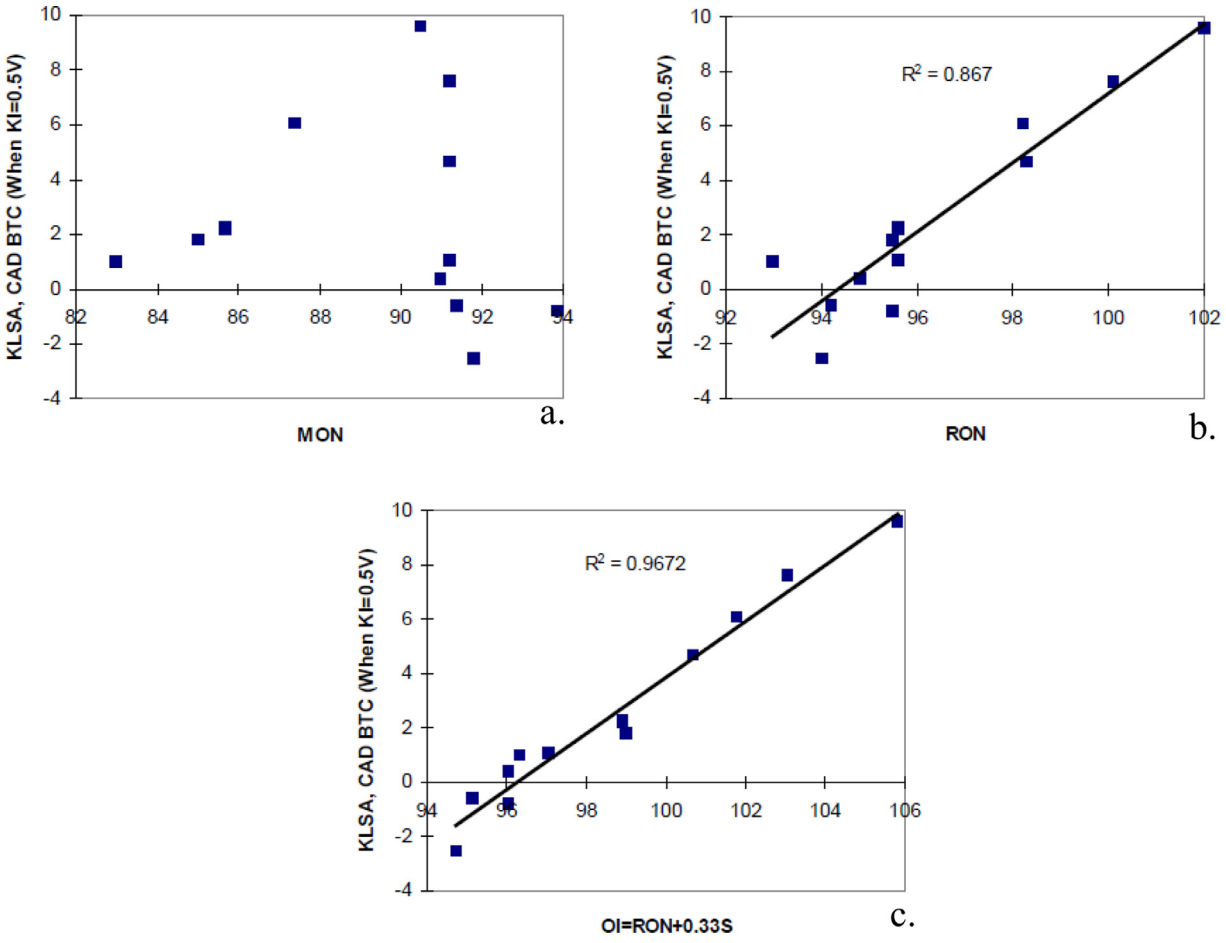

Fig. 15. Knock-limited spark advance as a function of (a) MON, (b) RON, and (c) OI. Reprinted wfrom Kalghatgi [176] with permission of SAE International.

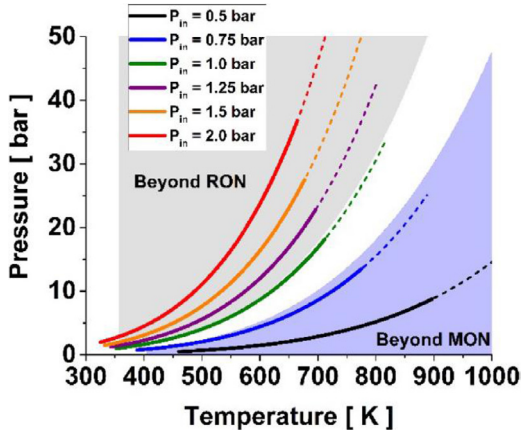

Fig. 16. Pressure-temperature trajectories of the RON and MON tests as well as a graphic illustration of the "Beyond RON" and "Beyond MON" regions. Reprinted from Szybist *et al.* [189] with permission of SAE International.

charge compression ignition (HCCI) engines correspond to K values greater than unity [179–184,186–188].

This pressure-temperature framework was illustrated graphically by Szybist *et al.* [189] and paired with a notional model of pressure-temperature trajectory across a range of intake pressures, as is shown in Fig. 16. The results of the notional model illustrate that the trajectory through the pressure-temperature domain changes significantly with intake manifold pressure. At the two lowest intake manifold pressures, 0.5 and 0.75 bar, the pressure-temperature trajectory is in the "beyond MON" region. At an intake manifold pressure of 1 bar, the pressure-temperature trajectory is close to that of the RON test. All the boosted operating conditions are "beyond RON." This trend also agrees closely with the variation of unburned gas temperature with different conditions shown by Amer *et al.* [184].

Szybist and Splitter [190] explored the relationship between the physicality of the pressure-temperature trajectory and the K factor as determined by a linear regression analysis for boosted operating conditions. The analysis involved varied intake temperatures and EGR rates at stoichiometric operation for seven different fuels, including three of the Co-Optima core fuels discussed previously in Section 3 [144]. Their findings, shown in Fig. 17, illustrate that the physical description of K representing a trajectory in the pressure-temperature domain is incomplete or that it is not completely descriptive of the physical phenomenon. As expected, the most negative K value has the pressure-temperature trajectory that is the pressure-temperature trajectory furthest beyond the RON. However, their results show that there is a maximum K value where K approaches zero and that it then starts to decrease again as the RON condition is approached. Thus, while the physical explanation of the K factor explains much of the trend, it does not fully explain the phenomenon.

K is not strictly a representation of the compression trajectory in the pressure-temperature domain; however, thinking of it as such can provide useful insights. Specifically, several studies have shown that the fuel can shift the trajectory in the pressure-temperature domain and hence can change K. Szybist and Splitter [190] and Ratcliff *et al.* [191] show that fuels with higher HoV

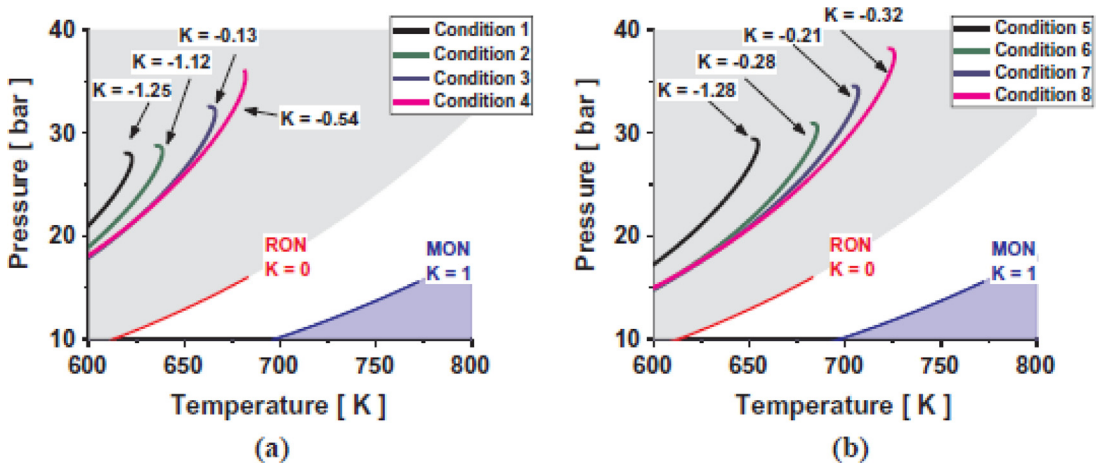

Fig. 17. Pressure-temperature trajectories and corresponding K values as determined by linear regression for an intake temperature of (a) 35 °C and (b) 90°, where conditions 1–8 represent different EGR and backpressure combinations at a constant fueling rate nominally producing 18 bar $IMEP_g$ at 2000 rpm. The different pressure-temperature trajectories represent different EGR and back-pressure conditions. Reprinted from Szybist and Splitter [190] with permission of Elsevier.

such as ethanol blends can cause lower temperature at intake valve closing, hence producing a lower temperature trajectory. Additionally, the exhaust temperature is affected by the knock-limited combustion phasing [192], which has an effect on the trapped residual fraction and intake valve closing temperature and ultimately on the pressure-temperature trajectory. Thus, K may best be viewed as a factor that is not strictly an indication of the engine operating condition, but as a variable that can be affected by engine design, engine operating condition, and fuel-engine interaction.

In a separate study, Szybist and Splitter [172] present results to show that the regions of LTHR that lead to knock do not vary linearly with S_{octane}. Their results, shown in Fig. 18, illustrate that the regions of LTHR that lead to low-S_{octane} fuels being more knock-prone in the beyond-RON region can be identified through kinetic modeling. The regions of LTHR are fuel-specific but are generally larger for the low- S_{octane} fuels, thereby providing a directionally correct kinetic basis for OI.

3.1.3. Accuracy and limitations of octane index

While the OI approach to ranking fuel knock resistance has proven to be a more effective predictor of knock than RON, MON, or AKI [176,178,180,184], the OI metric is not fully predictive for knock-limited SI operation. Szybist and Splitter [190] investigated seven fuels at eight different boosted knock-limited operating conditions and reported R^2 correlation coefficients ranging from 0.60 to 0.88. Similarly, Vuilleumier and Sjöberg [171] reported an R^2 value of 0.84 using nine different fuels, including the Co-Optima core fuels, under boosted knock-limited conditions [144]. However, Fig. 19 shows that even with an R^2 correlation coefficient of 0.84, the departures from the predicted combustion phasing can be significant, with knock-limited combustion phasing differences of up to 4 crank angle degrees (CAD) for fuels of similar OI [171]. The study encompassed an uncertainty assessment which suggested that these deviations are caused by real fuel effects that the OI approach cannot fully capture, but the chemical and/or physical causes for the deviations were not determined.

In addition to individual fuels behaving as a outliers when determining K at a given operating condition in a specific engine, the determination of K does not appear to be transferrable between different engines. Vuilleumier and Sjöberg [171] reported a K value of -3.2 under a load-transient condition when the intake pressure was 146 kPa. In contrast, under steady-state conditions with a similar intake manifold pressure of 143 kPa, Szybist and Splitter [190] reported a K value of -1.25. While these experiments had many differences, including engine speeds (1400 rpm vs 2000 rpm) and r_c (12:1 vs. 9.2:1), this is a very large difference in K value given the similar intake manifold pressures. Similarly, in a vehicle study, Prakash *et al.* [185] found a wide range of K values for similar operating conditions, including values as low as -4, which they considered to be nonphysical. They concluded that the roles of other fuel properties, specifically the effect of vapor pressure on the fuel-air mixing process, can have a large impact on the K value determination, and that those effects can be vehicle-specific. In supporting this conclusion, Rockstroh *et al.* [193] determined that K was highly dependent on the fuel subset that was used to determine K. For a single operating condition, they found that K could vary from -0.68 to +0.69 simply by the choice of the fuel subset used. This is consistent with Zhou et al. [183] who reported that the determination of K via regression analyses was highly sensitive to the fuel matrix that was used. The lack of transferability demonstrates the challenges of attempting to capture the differences in engine design, engine operating conditions, and fuel-engine interactions into a single term.

The results of Szybist and Splitter [190] and Vuilleumier and Sjöberg [171] are somewhat in contrast to other works in the literature, which demonstrate good agreement between the OI and observations of knock resistance in stoichiometric SI engines, often yielding R^2 values of 0.90–0.99 [178,180] . These discrepancies naturally lead to questions regarding the underlying causes. However, it has previously been shown that extending the OI framework beyond conventional stoichiometric operation, and specifically to HCCI operation, has had mixed results, indicating that universal application to autoignition problems is not appropriate. Kalghatgi [186] reported that the OI framework could be extended to HCCI operating conditions in which the charge conditions differ from those found in stoichiometric SI engines. However, conditions have been identified in which the OI approach to ranking fuel behavior does not hold. Risberg et. al. [194] found that internal EGR rates above 50% by mass leading to high in-cylinder temperatures in beyond-MON-type HCCI conditions caused all tested fuels to behave similarly despite varying RON and MON ratings. Shibata et. al. [195] demonstrated the lack of physicality of the K factor arising from NTC behavior and suggested that this makes the OI inappropriate for use with HCCI engines. These studies raise the question of what are the ranges of conditions under which the OI is applicable; it is clear that, as autoignition conditions deviate too far from the RON and MON conditions, eventually an extrapolation of these data points will not be sufficient.

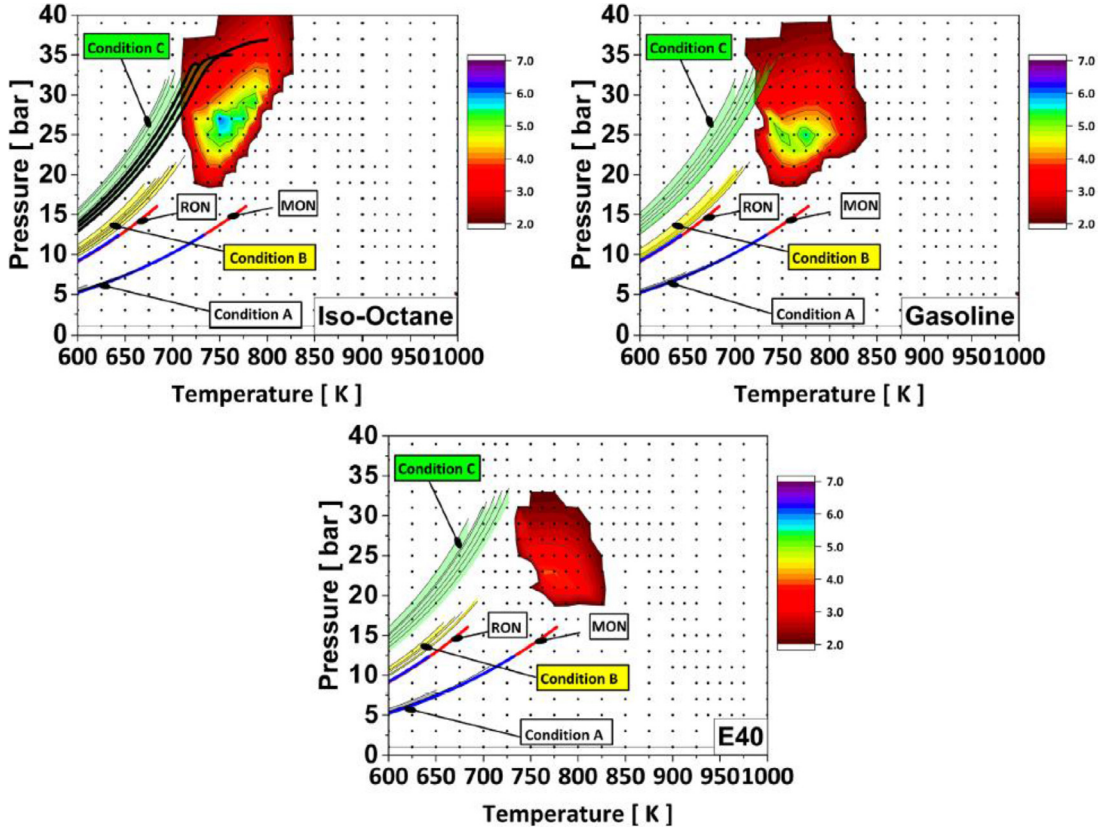

Fig. 18. Contour plots of regions of LTHR, where the contours indicate the difference in ignition delay (shown in ms) between LTHR ignition as indicated by a 50 K temperature rise and high temperature ignition for iso-octane (RON = 100, $S_{octane} = 0$), gasoline (RON = 100, $S_{octane} = 6$), and E40 (RON = 100, $S_{octane} = 12$) with pressure-temperature trajectories from three different operating loads (nominally 10, 15, and 20 bar $IMEP_g$ for Conditions A, B, and C, respectively). Fuels with the lower S_{octane} have larger regions of LTHR. Reprinted from Szybist and Splitter [172] with permission of Elsevier.

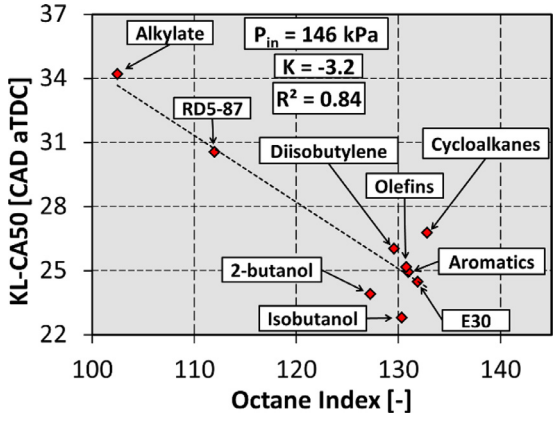

Fig. 19. Best-fit relationship between OI and knock-limited phasing for nine fuels at a transient, boosted operating condition, with a most-probable K value of -3.2. Reprinted from Vuilleumier *et al.* [171] with permission of SAE International.

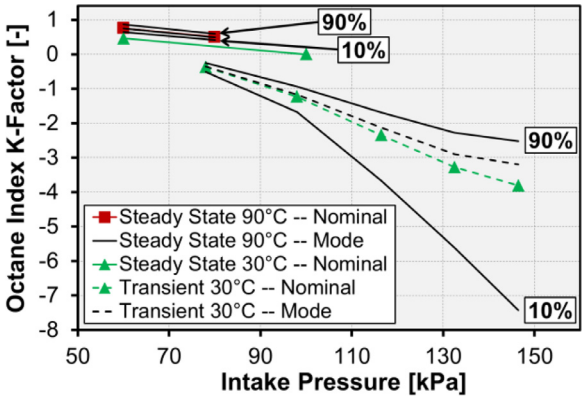

Fig. 20. Nominal and mode of distribution Octane Index K values over a range of operating conditions. Also shown is the 80% probability range (10th to 90th percentile range). Reprinted from Vuilleumier *et al.* [171] with permission of SAE International.

To better understand the uncertainty associated with OI, and specifically the K factor determination, Vuilleumier et. al. [196, 197] performed a detailed uncertainty analysis using the data shown in Fig. 19 [171] of matched RON and MON fuels to assess the relative contributors of different sources of uncertainty and how the relative uncertainty varies with operating conditions (as represented by K). The uncertainty analysis was carried out through Monte Carlo simulations, which perturbed the inputs to the linear regression used to determine K—namely the RON, MON, and knock-limited phasing of each fuel at each condition based on the individual uncertainties associated with each measurement. They determined that there were probabilistic distributions of the K value and that a high degree of uncertainty exists in the linear regression of K for highly negative K values. Fig. 20 summarizes the results of the Monte Carlo simulations across a range of conditions, plotting the nominal K value (regressed with nominal data), the mode K value of the distribution (peak of the probability distribution in [171]), and 10th and 90th percentile values of the distribution. This figure highlights the characteristic increase in uncertainty in the OI as the operating conditions are extrapolated to $K << 0$, which is a condition that may be encountered for boosted SI operation.

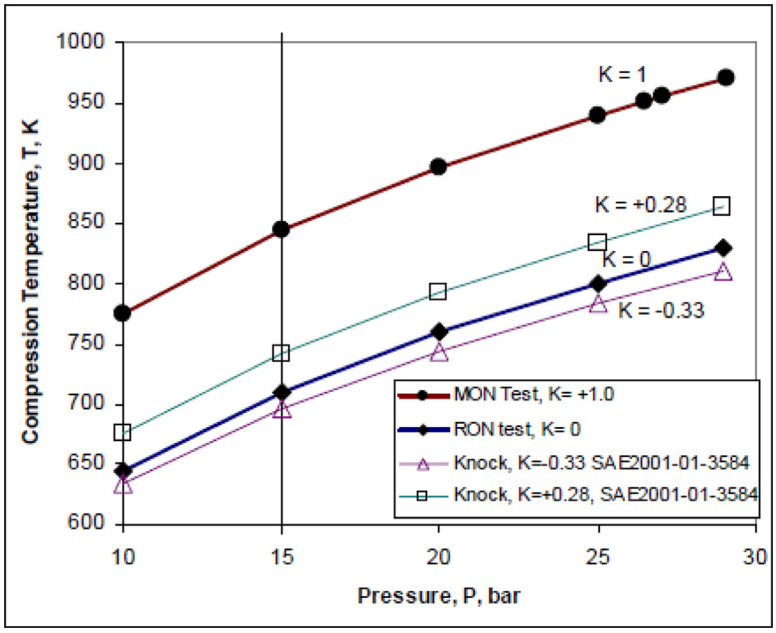

Fig. 21. Pressure-temperature trajectories associated with K values ranging from −0.33 to 1. Reprinted from Kalghatgi [180] with permissions of SAE International.

Returning to the question of the extent of the applicability of OI, both HCCI and SI engine studies have demonstrated that such limits can be exceeded. Considering the K values in Fig. 20, it is shown that a relatively moderate level of intake pressure increase leads to highly negative K values at a low-temperature, transient operating condition. Kalghatgi [180] shows the pressure-temperature trajectories associated with various K values ranging from -0.33 to 1, shown in Fig. 21. The nonlinearity of K as a function of temperature at a constant pressure, and particularly the steep decrease in K for K values < 0, hints that if the charge temperature is decreased significantly below the RON test temperature, the K value will become highly negative, leading to greater errors in extrapolating the RON and MON test results, as was found to be the case in the global sensitivity analysis performed by Vuilleumier et. al. for a negative K condition [171]. Further insights into the uncertainty of the OI in the negative K value regime are provided by Prakash et. al. [185], where the octane appetites of modern vehicles were assessed using both steady-state and transient testing methodologies. Prakash *et al.* demonstrated both the low K values that can be encountered in the operation of modern vehicles and the uncertainty associated with assessing the K value. Steady-state testing at 1500 RPM with two of the vehicles used in the study yielded K values of -4.2 and -6.1; the authors reveal that these two vehicles are in fact of the same make and model and that they deliver a significantly different assessment of K, highlighting the variations in K value determination caused by presumably small differences in the vehicles or testing.

3.1.4. The impact of knock resistance on efficiency

In Subsection 3.1.3 it was shown that much about the OI rating and K value determination remains uncertain. However, there is an overwhelming dataset that shows that the performance of OI is superior to other standard antiknock metrics that have been developed, as discussed in Section 3.1.2. Thus, OI will be used as the basis to determine the thermodynamic impact of a fuel's knock resistance on efficiency. If the increased knock resistance provided by a fuel is exploited to increase the engine's r_c and decrease its displacement volume, knock resistance can affect η_b in several ways:

- Increasing a fuel's knock resistance enables increases in r_c and therefore in the ideal thermal efficiency, η_{ideal}
- The higher η_{ideal} that is enabled by a higher knock resistant fuel and higher r_c increases the engine power if the engine displacement is held constant. Thus, for a given power requirement, the engine can be downsized (a decrease in V_d), which affects pumping losses and changes η_{GE} for a given torque level.
- For a given torque, increasing r_c and downsizing may both affect the mechanical efficiency η_{mech}.
- For a given torque, increasing r_c and downsizing may both affect the heat transfer factor σ_{HT}.

Even when the r_c is not increased and the engine is not downsized in response to improved knock resistance of the fuel, increasing knock resistance typically allows spark timing to be advanced for operating points that would otherwise be knock-limited, as illustrated in Fig. 9. Advanced combustion phasing increases the degree of constant volume combustion, σ_{ideal}, and thereby increases η_b. This effect is expected at high loads that are infrequently experienced in light-duty drive cycles (see, for example, Chow *et al.* [65]). However, it is neglected for this analysis because the impact of such operating points on the total fuel consumed during a typical drive cycle is expected to be small (see Fig. 8).

A merit function term will now be defined to quantify the combined effects of knock resistance on η_b as described above, using the OI as the characteristic property. The chain rule is used to describe how efficiency changes as a function of r_c, V_d, and OI as follows:

$$\frac{1}{\eta_b}\frac{\partial \eta_b}{\partial OI} = \frac{1}{\eta_b}\left[\frac{\partial \eta_b}{\partial \eta_{mech}}\left(\frac{\partial \eta_{mech}}{\partial V_d}\frac{\partial V_d}{\partial r_c}+\frac{\partial \eta_{mech}}{\partial r_c}\right)\frac{\partial r_c}{\partial OI}+\frac{\partial \eta_b}{\partial \eta_{GE}}\left(\frac{\partial \eta_{GE}}{\partial V_d}\frac{\partial V_d}{\partial r_c}+\frac{\partial \eta_{GE}}{\partial r_c}\right)\frac{\partial r_c}{\partial OI}+\frac{\partial \eta_b}{\partial \sigma_{HT}}\left(\frac{\partial \sigma_{HT}}{\partial V_d}\frac{\partial V_d}{\partial r_c}+\frac{\partial \sigma_{HT}}{\partial r_c}\right)\frac{\partial r_c}{\partial OI}+\frac{\partial \eta_b}{\partial \eta_{ideal}}\frac{\partial \eta_{ideal}}{\partial r_c}\frac{\partial r_c}{\partial OI}\right] \tag{12}$$

Simplifications lead to

$$\frac{1}{\eta_b}\frac{\partial \eta_b}{\partial OI} = \frac{\partial r_c}{\partial OI}\left(\frac{1}{\eta_{mech}}\left(\frac{\partial \eta_{mech}}{\partial V_d}\frac{\partial V_d}{\partial r_c}+\frac{\partial \eta_{mech}}{\partial r_c}\right)+\frac{1}{\eta_{GE}}\left(\frac{\partial \eta_{GE}}{\partial V_d}\frac{\partial V_d}{\partial r_c}+\frac{\partial \eta_{GE}}{\partial r_c}\right)+\frac{1}{\sigma_{HT}}\left(\frac{\partial \sigma_{HT}}{\partial V_d}\frac{\partial V_d}{\partial r_c}+\frac{\partial \sigma_{HT}}{\partial r_c}\right)+\frac{1}{\eta_{ideal}}\frac{\partial \eta_{ideal}}{\partial r_c}\right) \tag{13}$$

3.1.5. Estimating the Impact of Knock Resistance on Efficiency from Literature

Defining the terms of Eq. 13 is not a simple exercise, as they are influenced by engine design parameters as well as details of the engine operating conditions within the speed/load map. Chow *et al.* [65] and Leone *et al.* [198] approach this with a three-step method.

The first step is an assumption about the degree to which an increase in OI enables an increase in r_c, expressed as $\frac{\partial r_c}{\partial OI}$. Leone *et al.* provide a range of values for the increase in r_c enabled by increases in knock resistance based on experimental studies (RON + improved knock resistance from HoV, to be addressed in Section 3.2). They show that the value of this term can vary widely but estimate its value to be 1/3 for a well-developed combustion system that has been optimized for the higher compression ratio [198]. This is similar to Yokoo *et al.*, who found the value to be 0.3 for a naturally aspirated engine [199]. Chow *et al.* assume this value to be ¼ but do not provide further support for their assumption [65]. For this derivation, it is assumed that the increase in RON is equal to the increase in octane index; S_{octane} is assumed to remain constant. A value of 1/3 is used for $\frac{\partial r_c}{\partial OI}$, meaning that an increase in octane index of three points is assumed to enable an increase in compression ratio of one point. This is a critical assumption and the range of fuel properties, engine designs, and engine operation over which it is valid remains to be demonstrated.

The second step is to estimate the change in efficiency that results from this increase in compression ratio. In the context of Eq. 13, this is equivalent to the following sum:

$$\frac{1}{\eta_b}\frac{\partial \eta_b}{\partial r_c} = \frac{1}{\eta_{ideal}}\frac{\partial \eta_{ideal}}{\partial r_c} + \frac{1}{\eta_{GE}}\frac{\partial \eta_{GE}}{\partial r_c} + \frac{1}{\sigma_{HT}}\frac{\partial \sigma_{HT}}{\partial r_c} + \frac{1}{\eta_{mech}}\frac{\partial \eta_{mech}}{\partial r_c} \tag{14}$$

Leone *et al.* provide data for experimental and theoretical studies that indicate $\frac{1}{\eta_b}\frac{\partial \eta_b}{\partial r_c}$ decreases as the engine's initial r_c increases and that it is in the approximate range of 1% to 3% per unit compression-ratio increase for compression ratios between 9:1 and 12:1 [198]. Engine system modeling using GT-Power software was performed by Chow *et al.* and supports this finding for r_c between 10:1 and 11:1 [65]. Based on the data provided in the two studies, a conservative estimate for the value of $\frac{1}{\eta_b}\frac{\partial \eta_b}{\partial r_c}$ is 1.6% per unit compression-ratio increase.

The third step in estimating $\frac{1}{\eta_b}\frac{\partial \eta_b}{\partial OI}$ is to determine the additional efficiency benefits that result from downsizing an engine to maintain its performance level after the r_c increase. These benefits depend on the engine operating point, the degree to which the engine's operation is knock-limited, and whether the engine is turbocharged. While Smith *et al.* [200] report a downsizing efficiency-multiplier factor of 1.6, this is an aggressive estimate that is specific to boosted engines. Leone *et al.* suggest downsizing efficiency-multiplier factors of 1.3 and 1.1 for NA and turbocharged engines, respectively [198]. To make the analysis broadly applicable to both boosted and NA engines, an average value of 1.2 is assumed in this discussion and the following analysis.

To summarize the process described above to estimate $\frac{1}{\eta_b}\frac{\partial \eta_b}{\partial OI}$, the conclusion based on several studies reported in the literature indicate that an increase in OI of three points allows the compression ratio to be increased by a single point, thus increasing the efficiency by 1.6%. With the efficiency multiplier of 1.2 due to downsizing, the three-point OI increase results in a 1.9% efficiency increase. Therefore, $\frac{1}{\eta_b}\frac{\partial \eta_b}{\partial OI}$ may be estimated as $\frac{1.2(1.6\%)}{3\ OI\ units} = \frac{1\%}{1.6\ OI\ units}$. This is a more conservative estimate than the value of $\frac{3.52\%}{4\ OI\ units} = \frac{1\%}{1.1\ OI\ units}$ used by Chow *et al.* [65].

While the OI provides a useful structure, it is not expressed using measurable fuel properties. Eq. 15 puts $\frac{1}{\eta_b}\frac{\partial \eta_b}{\partial OI}$ in a merit function term that is related to a reference fuel and incorporates the fuel properties RON and S_{octane} directly, along with an explicit K value input. The results are the most significant terms of Eq. 10:

$$\frac{1}{\eta_b}\frac{\partial \eta_b}{\partial OI}\left(OI - OI_{ref}\right) = \frac{\left(RON - RON_{Ref}\right)}{1.6} - K\frac{\left(S_{octane} - S_{octane,Ref}\right)}{1.6} \tag{15}$$

Table 3
Parameters for GT-Power simulations for compression ratio and displacement volume variations.

Bore [mm] × Stroke [mm]	Baseline: 86 × 86.07 Downsized engine: 83.05 × 83.05
Displacement volume [L]	Baseline: 2.0 Downsized engine: 1.8
r_c [-]	9.5:1, 10.5:1
BMEP [bar]	0.5, 1.0, 1.5, 2.0, 2.5, 3.0, 4.0, 5.0, 6.0, 7.0
Engine speed [rpm]	1500, 2000, 2500, 3000
CA50 [CAD ATDC[1]]	8 CAD ATDC
EGR Rate [%]	10%

[1] ATDC: After top dead center

3.1.6. Estimating the impact of knock resistance through simulation and analysis

Because knock resistance is the fuel property with the most potential to enable improvements in efficiency, further validation of the value of $\frac{1}{\eta_b}\frac{\partial \eta_b}{\partial OI}$ beyond estimations based on the literature is warranted, particularly because there is a significant discrepancy between the conservative value of $\frac{1\%}{1.6\ OI\ units}$ developed in the previous section and the more optimistic value of $\frac{1\%}{1.1\ OI\ units}$ suggested by Chow *et al.* [65]. The right-hand side of Eq. 13 is evaluated with a combination of theoretical analysis and one-dimensional numerical simulations. The latter are achieved using a model of a turbocharged, four-cylinder engine based on the example provided in the GT-Power software, with the addition of a high pressure EGR loop. Simulations are run for a range of engine speeds and loads at two different r_c values and for two different V_d values. Heat release profiles are simulated using a Wiebe function. Combustion duration is assumed to be a function of engine speed, and combustion phasing is retarded at lower speeds and higher loads to simulate knock-limited operation. The parameters for these functional relationships are taken from engine experiments and/or from the four-cylinder turbocharged engine example in GT-Power. These combustion phasing and duration relationships are maintained regardless of r_c and V_d. Less than 8% of the UDDS driving cycle and less than 33% of the US06 cycle may be expected to involve knock-limited operation, so the impact of these simplifying assumptions on cumulative fuel consumption is expected to be limited [61], as shown in Fig. 8. The simulation parameters are summarized in Table 3.

Two terms on the right-hand side of Eq. 13 are evaluated through theoretical analysis: $\frac{\partial \eta_{ideal}}{\partial r_c}$ can be trivially derived from the definition of the Otto cycle efficiency:

$$\frac{\partial \eta_{ideal}}{\partial r_c} = (\gamma - 1)r_c^{-\gamma} \tag{16}$$

where γ is the ratio of specific heats and, for this simplified analysis, is assumed to be equal to 1.34.

The degree of downsizing with respect to r_c, $\frac{\partial V_d}{\partial r_c}$, is the result of design decisions influenced by factors such as the desired peak torque and power and is subject to knock considerations. Yet more factors play a role if the engine is turbocharged, as turbocharger constraints and/or peak cylinder pressure limits determine the possible output power (a more detailed discussion is given by Leone *et al.* [198]). A rigorous estimation of $\frac{\partial V_d}{\partial r_c}$ is beyond the scope of

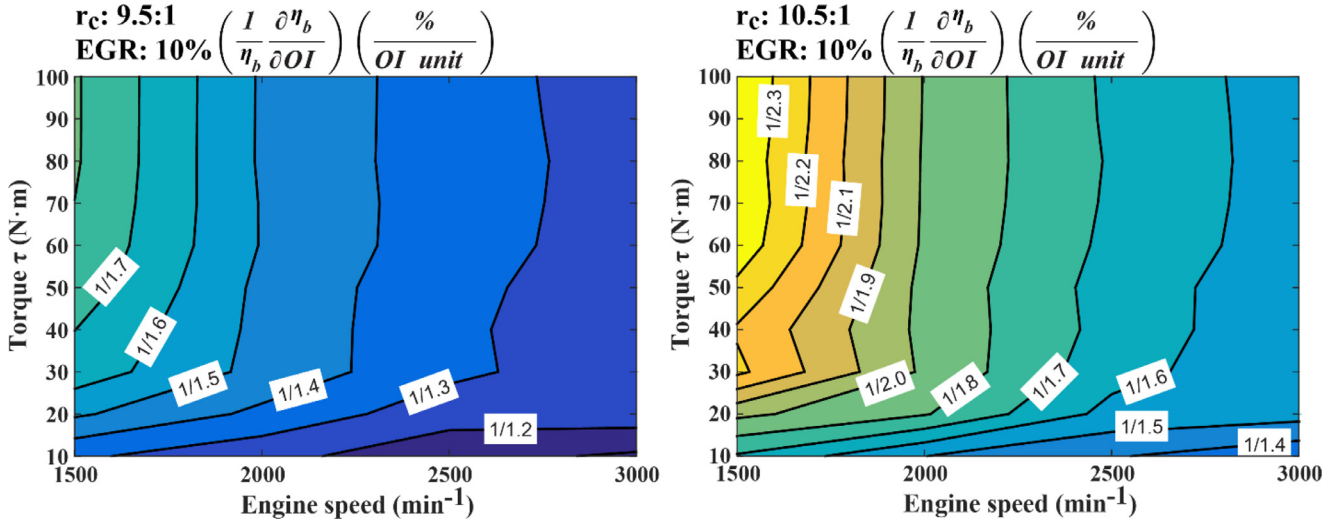

Fig. 22. Estimated relative efficiency gain due to changes in octane index for an initial r_c of 9.5:1 (left) and 10.5:1 (right) and an initial displacement volume of 2.0 L. OI most effectively enables efficiency improvements at high engine speeds and low loads.

this work, but a simple Otto-cycle analysis can be performed for stoichiometric, naturally aspirated, wide-open-throttle operation to provide a rough estimate of $\frac{\partial V_d}{\partial r_c}$. This analysis is based on Heywood [73], which may be expressed for a four-stroke engine as

$$V_d = \frac{2W(1+AFR_{stoichiometric})c_v T_1}{P_{atm}(LHV_{mix}+HoV_{mix})}(\gamma-1)\left(\frac{r_c-1}{r_c}\right)\left(\frac{1}{1-r_c^{1-\gamma}}\right) \quad (17)$$

where

W is the work per cycle and is calculated using Eq. 17 for a known displacement volume;

c_v is the constant-volume specific heat of the working fluid, estimated as 0.8 $\frac{kJ}{kg\ K}$;

T_1 is the temperature of the working fluid before compression, assumed to be 90°C;

P_{atm} is the assumed cylinder pressure at the beginning of the compression stroke: 100 kPa;

LHV_{mix} is the lower heating value of the fuel mixture (43.4 $\frac{MJ}{kgfuel}$), and HoV_{mix} is the heat of vaporization of the fuel mixture (304.9 $\frac{kJ}{kgfuel}$).

From Eq. 17, $\frac{\partial V_d}{\partial r_c}$ can be directly calculated as

$$\frac{\partial V_d}{\partial r_c} = \frac{2W(1+AFR_{stoichiometric})c_v T_1}{P_{atm}(LHV_{mix}+HoV_{mix})}(\gamma-1) \times\left(\frac{1}{r_c^2}\left(\frac{1}{1-r_c^{1-\gamma}}\right)+\frac{r_c-1}{r_c}\frac{(1-\gamma)r_c^{-\gamma}}{\left(1-r_c^{1-\gamma}\right)^2}\right) \quad (18)$$

The remaining unknown partial derivatives in Eq. 13 are $\frac{\partial \eta_{GE}}{\partial V_d}$, $\frac{\partial \eta_{GE}}{\partial r_c}$, $\frac{\partial \sigma_{HT}}{\partial V_d}$, $\frac{\partial \sigma_{HT}}{\partial r_c}$, $\frac{\partial \eta_{mech}}{\partial V_d}$, and $\frac{\partial \eta_{mech}}{\partial r_c}$; their values are estimated using the GT-Power simulations. The gas exchange efficiency η_{GE}, wall heat loss term σ_{HT}, and mechanical efficiency η_{mech} are computed via interpolation of simulation results for a range of torque values at each engine speed and for each displacement volume. The partial derivatives are estimated using a simple difference method. In this way, Eq. 13 is evaluated as a function of engine speed and brake torque for various initial compression ratios.

Fig. 22 shows estimated values of $\frac{1}{\eta_b}\frac{\partial \eta_b}{\partial OI}$ as a function of engine speed and load for r_c of 9.5:1 (left) and 10.5:1 (right) and an EGR rate of 10%. The change in OI that is needed to improve efficiency by 1% is smallest at lower loads and higher speeds. The largest contributor to this efficiency improvement is the increase in ideal cycle efficiency due to the increased r_c. However, heat transfer losses also increase as r_c is increased; the benefits of increased OI are reduced at lower engine speeds, as more time is available for heat transfer to occur. Increasing r_c also increases throttling losses for a given torque output, but downsizing the engine and maintaining this torque output results in a net increase in gas exchange efficiency, especially at lower loads where throttling losses are more significant. Finally, downsizing the engine decreases friction more at low loads than at high loads, so the mechanical efficiency is improved most at low loads. Thus, the amount OI must be increased to achieve a 1% efficiency improvement is lowest for high engine speeds and low loads.

While the efficiency benefits of increasing OI depend strongly on engine design and operation, the intention of the merit function is to provide a basis for evaluation and comparison of alternative fuel candidates. The strong nonlinearity in engine efficiency at lower loads leads to strong dependence of relative efficiency improvements on OI. Powertrain design decisions that determine engine operating speeds will also influence the potential relative efficiency benefit for a given increase in OI. The extent to which an increase in OI can enable an increase in r_c has been assumed to be constant for this analysis, but it may be expected to decrease at higher r_c due to changes in chemical kinetic behaviors for different fuels. Changes in knock-limited operation have been neglected for this analysis, specifically the engine load at which the engine initially encounters knock-limited operation and the extent of combustion phasing retard at peak load. While any changes made to these design inputs will affect the realizable efficiency benefits as OI increases, there is insufficient information available to provide insight on the magnitude of these changes. Furthermore, wall heat transfer has a significant impact on the efficiency benefits that may be realized as fuel knock resistance is increased, and changes in engine design may alter these efficiency benefits.

Nonetheless, these one-dimensional numerical simulations provide validation for the value of $\frac{1}{\eta_b}\frac{\partial \eta_b}{\partial OI}$ of $\frac{1\%}{1.6\ OI\ units}$ identified in Section 3.1.5. The simulations revealed that the possible efficiency gains are complex and are not constant over the engine map, but for the purpose of a merit function, a value of $\frac{1}{\eta_b}\frac{\partial \eta_b}{\partial OI} = \frac{1\%}{1.6\ OI\ units}$ is reasonable. The analyses presented in this work suggest that the value of $\frac{1}{\eta_b}\frac{\partial \eta_b}{\partial OI}$ given by Chow *et al.*, $\frac{1\%}{1.1\ OI\ units}$, may be somewhat optimistic. Thus, the value of $\frac{1\%}{1.6\ OI\ units}$, which is expanded to the

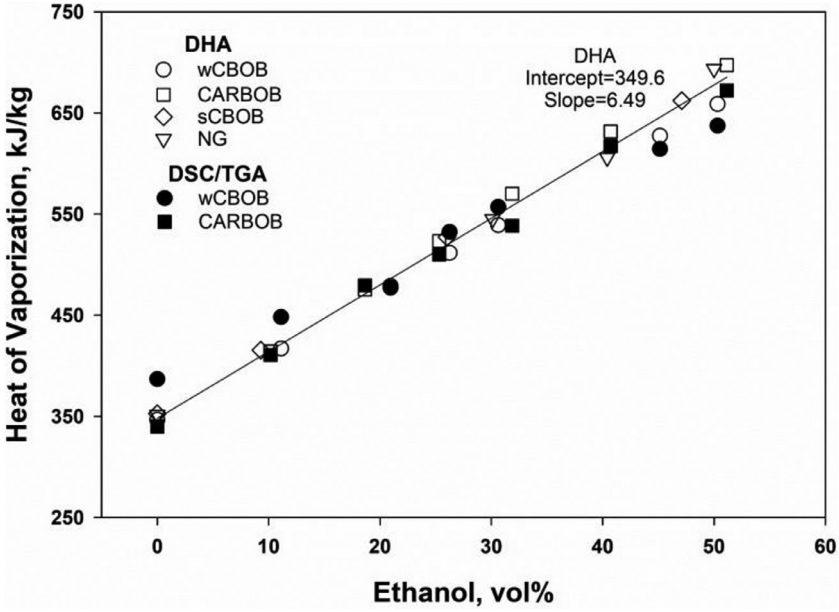

Fig. 23. HoV as a function of ethanol content measured by differential scanning calorimetry/thermogravimetric analysis (DSC/TGA) at 23 °C and calculated from detailed hydrocarbon analysis (all blends) at 25 °C. Winter conventional BOB (wCBOB), California reformulated (CARBOB), summer conventional BOB (sCBOB), and natural gasoline (NG) represent different hydrocarbon blending streams. Reprinted from Chupka *et al.* [207] with permission of SAE International.

full merit function format in Eq. 15, appears to be more representative of operating points that may be encountered during a typical drive cycle for compression ratios near 10.0:1 [65].

3.2. Heat of vaporization

3.2.1. Thermodynamic impacts of HoV on engine efficiency

The fuel's HoV can impact efficiency in multiple ways. The first is through its influence on the fuel's knock resistance. For DI engines, the in-cylinder fuel vaporization process reduces the charge temperature. This increases charge density, resulting in either increased power output or increased throttling requirements through improved volumetric efficiency, and the reduced charge temperature can provide improved efficiency through knock mitigation [201–205]. Cooling for hydrocarbon fuels provides the same effect as an increase of roughly 5 OI units in a boosted DI engine relative to a PFI-fueled engine [198]—consistent with an earlier estimate that 7 K of cooling is equivalent to a 1 octane number increase [206].

Low-molecular-weight alcohols such as methanol and ethanol exhibit much higher HoV than gasoline boiling range hydrocarbons. Blending of ethanol into gasoline has been shown to significantly increase HoV, as shown in Fig. 23 [207]. The thermodynamic maximum charge cooling can be estimated by assuming that the fuel is evaporating into the air at the same temperature, evaporation is completed during the intake stroke, and there is no heat transfer. The temperature change for this ideal adiabatic cooling is shown in Fig. 24 for stoichiometric mixtures of ethanol blended into several gasoline blendstocks at different fuel/air starting temperatures [207]. The amount of cooling decreases with increasing temperature because HoV decreases with increasing temperature, ultimately becoming zero at the critical temperature (for a pure component). Kasseris and Heywood showed that, for their test engine, between 70% and 80% of the theoretical maximum cooling was typically achieved [202]. Based on simulations, they suggested that a higher percentage of the theoretical maximum cooling could be obtained at higher intake air temperatures.

While the benefits of DI are well established, and many of those benefits are derived from charge cooling and increased charge motion, there is a lack of consensus in the literature regarding the magnitude of the effect of additional charge cooling from methanol or ethanol blending. For example, Wyszynski and coworkers measured a 9% improvement in volumetric efficiency for DI versus PFI using a hydrocarbon gasoline at wide open throttle (WOT), and a further 3% improvement for a 10 vol % methanol or ethanol blends [205]. Kasseris and Heywood report that increased HoV increases the effective octane rating at a rate of about 0.15 octane number/vol % ethanol, and that the rate of increase is approximately linear in ethanol fraction, as summarized in Fig. 25 [203]. Stein and coworkers found that the chemical octane and evaporative cooling effects of ethanol blends on knock were of comparable importance [208]. In contrast, a comprehensive multicylinder engine study has indicated that, for ethanol fractions of less than 30%, there is a negligible impact of HoV on knock-limited spark advance at low to moderate loads, and only a small effect at high loads, when RON and MON are held constant (Fig. 26) [209]. The authors suggest that the charge cooling effect of added ethanol is at least partially captured in the RON test because intake air temperature is set upstream of the carburetor [3].

Foong and coworkers studied evaporative cooling from ethanol blends on the RON test [210]. They showed that increased evaporative cooling reduced the intake mixture temperature to below that observed with the hydrocarbon fuels for ethanol blends up to about 40 vol % ethanol (Fig. 27a). No further cooling was observed above that ethanol level, likely because the fuel-air mixture was saturated and liquid fuel droplets were being inducted into the engine. A modified RON test was developed where the intake air was heated to maintain intake mixture temperature at the same level as observed for hydrocarbon-only fuels. A comparison of RON and the modified RON for ethanol blends from zero to 100% (Fig. 27b) shows little impact of increased HoV on RON up to approximately 30 to 40 vol % ethanol, but at higher ethanol levels RON was significantly higher on the standard RON test. Note that heating the intake air temperature caused the ethanol blends to have higher knock intensity, and therefore lower modified RON ratings than their initial standard RON ratings. From those results, Leone *et al.* concluded that the effect of HoV may be fully accounted for in the RON test for blends up to approximately E30 [209].

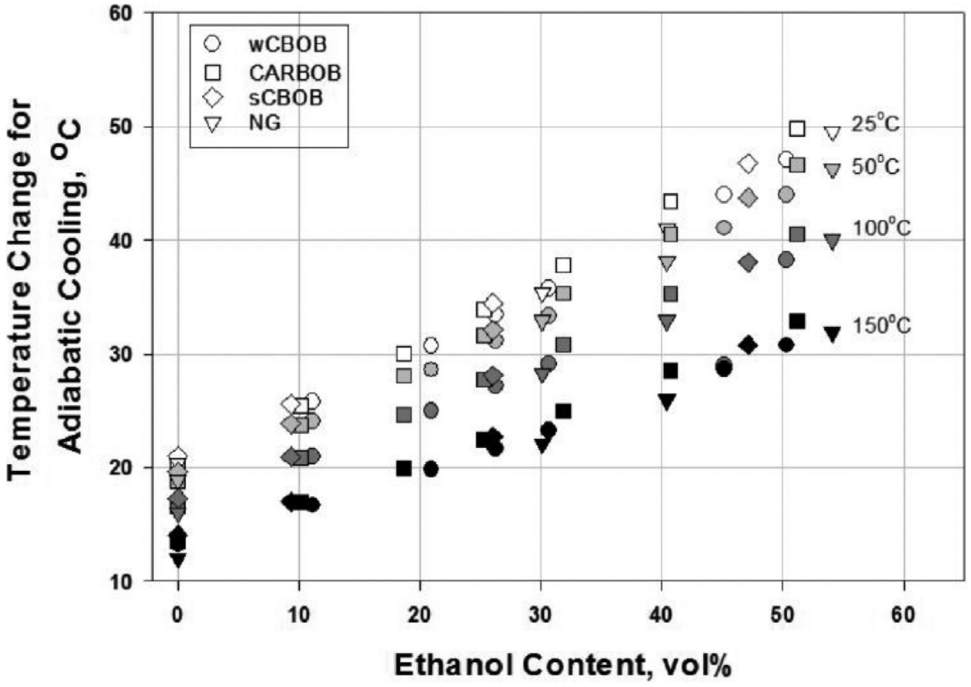

Fig. 24. Temperature change for adiabatic cooling of stoichiometric air-fuel mixtures at different initial temperatures (listed at right). Reprinted from Chupka *et al.* [207] with permission of SAE International.

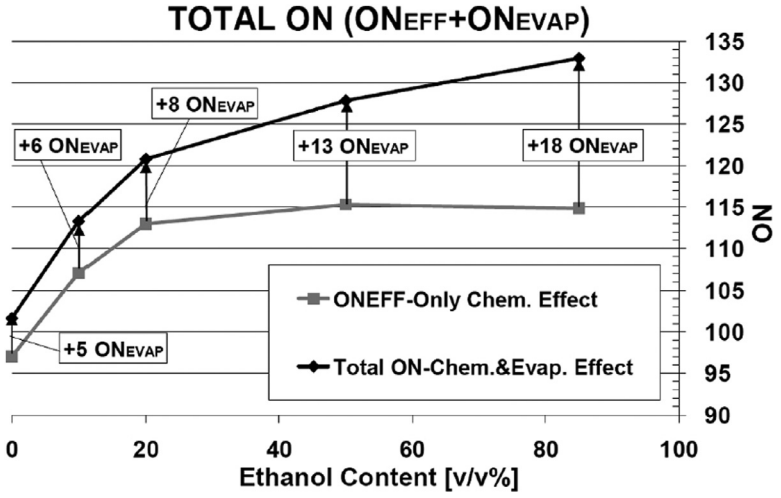

Fig. 25. Total octane number (ON_{EFF}+ON_{EVAP}) vs. fuel ethanol content. While ON_{EFF} only shows the chemical effect, which is realized in both DI and PFI engines, the total octane number includes chemical as well as evaporative antiknock effects, which are mostly realized in a DI engine. Reprinted from Kasseris and Heywood [203] with permission of SAE International.

Kolodziej *et al.* [211] used an instrumented CFR engine to further study Foong's modified RON method, which heats the upstream intake air temperature (IAT), before the carburetor, for fuels with higher HoV to match the downstream mixture air temperature (MAT), after the carburetor, to that of PRFs. This was done using PRFs (mixtures of n-heptane and iso-octane) blended with 0 to 50 vol % ethanol while holding RON = 98 constant. Consistent with the findings by Foong *et al.*, increasing the IAT temperature of the ethanol blends to match the MAT caused them to have higher knock intensities relative to the blend containing no ethanol (PRF98), resulting in a reduced RON rating. However, it was also found that increasing the IAT upstream of the carburetor introduced three test artifacts to the modified test method: reductions to the cylinder pressure at spark timing (P_{ST}), the engine load ($IMEP_g$), and fueling rate, shown in Fig. 28. To compensate for the reduced P_{ST}, intake pressure to the engine was increased in small increments through a compressed-air system until P_{ST} matched those of the initial standard RON conditions. This allowed for a comparison of the original standard RON rating (RON_{STD}) of the ethanol blends with their compensated RON rating (RON_{Comp}). By removing the HoV effect, RON_{Comp} were lower than RON_{STD} in proportion to the HoV of the fuel. When both the cooling effect of the increased HoV of the fuel and the reduced P_{ST} were compensated for, the estimated effect of HoV on the RON of a given PRF-ethanol blend approximately doubled. However, the effect of HoV on RON was still ≤1 ON for 10 and 20 vol % ethanol blends. For 30–50 vol % ethanol, the effect of HoV on RON was estimated to be approximately 1.3–2.8 ON, respectively.

Fig. 29 shows four methods for estimating the HoV effect on RON. The first is the methodology from Foong *et al.* [210] of in-

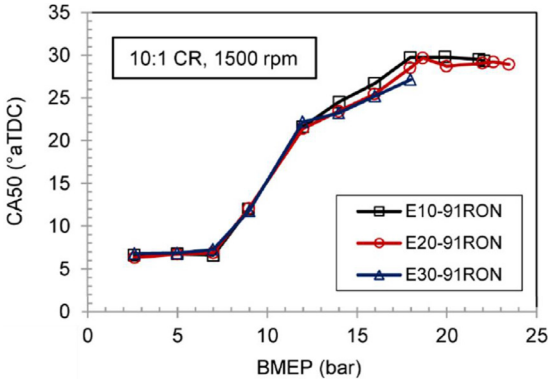

Fig. 26. Combustion phasing for load sweeps at 1500 rpm at 10:1 r_c for matched blends having the same RON and S, but varying ethanol content and HoV. Reprinted from Leone *et al.* [209] with permission of SAE International.

creasing IAT until the MAT matched that of PRF98. The second case also matched MAT with the PRF98, but additionally compensated P_{ST} until it was the same as PRF98. The third case (demonstrated on the right side of Fig. 28) matched MAT with PRF98, but matched P_{ST} of each ethanol blend to the P_{ST} of that fuel at standard RON conditions. Most knock-limited spark advance studies of fuels on modern engines are carried out at constant $IMEP_g$. Therefore, the fourth case matched MAT with PRF98 for each ethanol blend but also increased the intake pressure until the same $IMEP_g$ was achieved for all ethanol blends as PRF98. The HoV effect was estimated to have approximately a factor of 2 higher effect on RON with both cylinder pressure and MAT compensation than with only matching MAT [210]. When the intake pressure was increased to achieve constant $IMEP_g$ conditions for all ethanol blends as PRF98, the HoV effect on RON was estimated to be even higher, approximately 3.5 times higher than the Foong *et al.* IAT heating method [210]. In all methods, the effects of HoV on RON were $\leq$1 RON for 10 and 20 vol % ethanol blends. However, possibly important contributions from HoV start to occur for 30 vol % ethanol levels and higher.

Sluder and coworkers [212] observed that, in studies showing an HoV benefit, HoV and S_{octane} are covariant because blending of

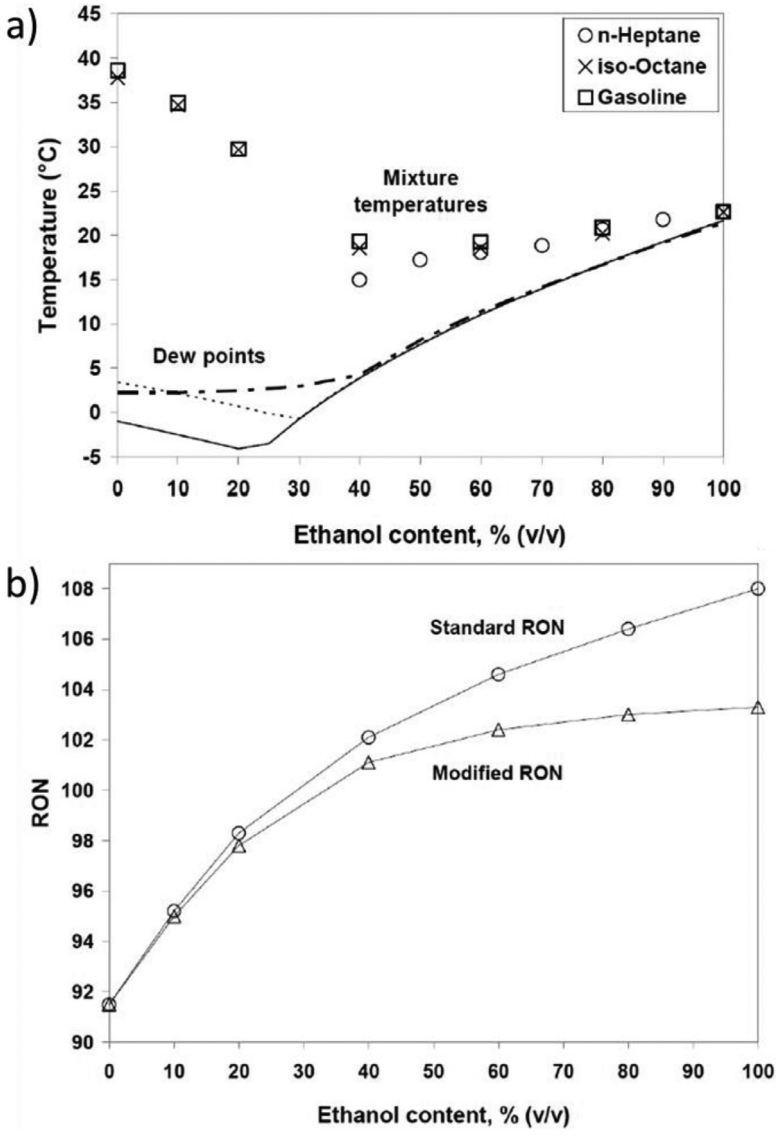

Fig. 27. (a) Measured intake mixture temperatures and dew points calculated from the Peng-Robinson Eq. of state for the standard RON test. (b) Comparison of standard RON values and values from a modified test where the intake air was heated to maintain intake mixture temperature at a constant 36 °C. Reprinted from Foong *et al.* [210] with permission of SAE International.

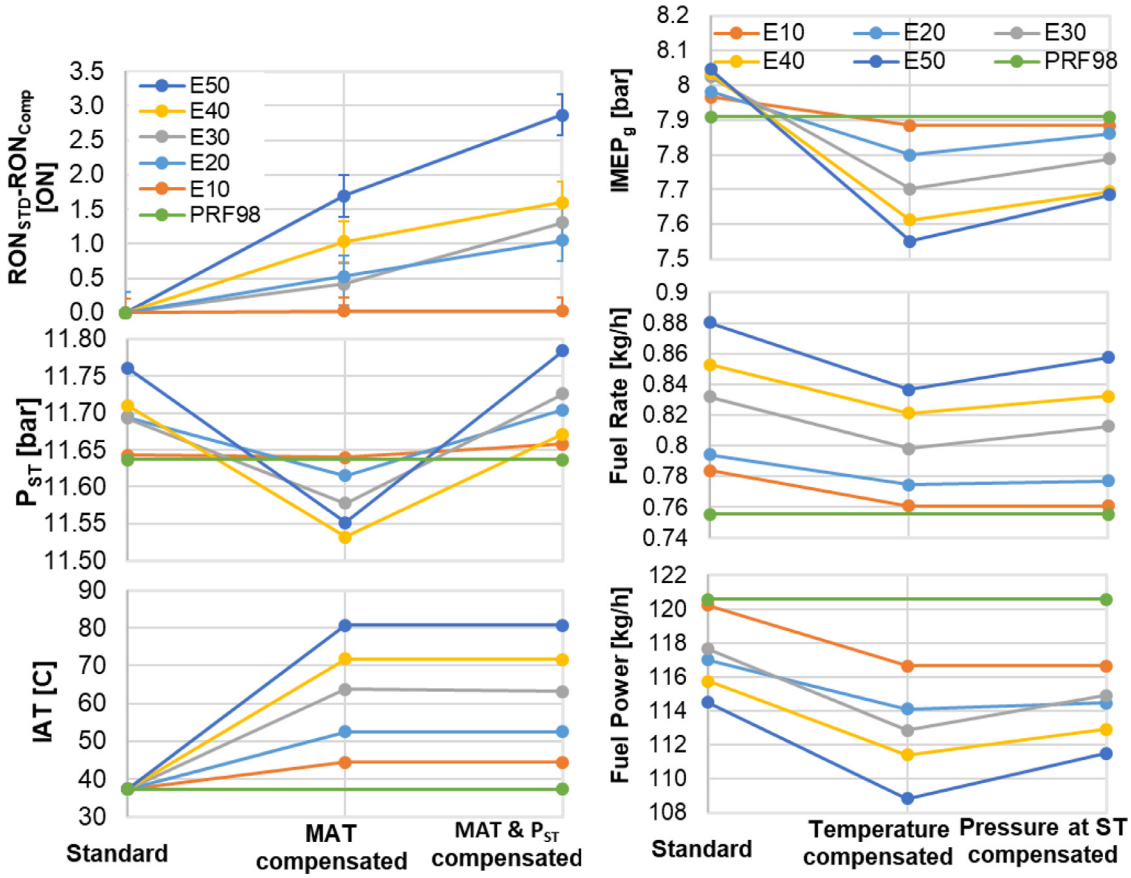

Fig. 28. Effects of Foong modified RON method (MAT compensation only) and both MAT and P_{ST} compensated method on the change in RON, P_{ST}, $IMEP_g$, fuel rate, and fuel power delivery. Adapted from Kolodziej *et al.* [211].

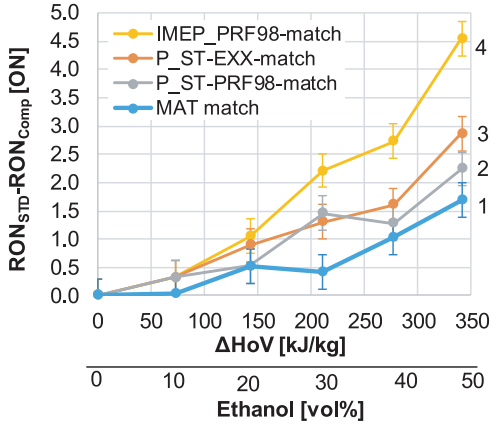

Fig. 29. Various methods proposed to estimate the HoV effect on the RON method: (1) increase IAT until MAT matches that of PRF98, (2) match MAT and compensating P_{ST} to match PRF98, (3) match MAT and compensating P_{ST} until that of the ethanol blend under standard RON conditions, and (4) match MAT and compensating the engine $IMEP_g$ to that of PRF98. Adapted from Kolodziej *et al.* [211].

ethanol increases both HoV and S_{octane} [202,203,208,213]. They also observed that studies that employed match blending to hold S_{octane} constant while varying HoV do not show additional knock benefit for higher-HoV fuels [209,214]. They proposed that HoV be considered as a thermal component to S_{octane}. While this theory holds at many conventional operating conditions, subsequent research has determined that even with matched S_{octane}, HoV might have additional knock mitigation potential under some operating conditions [191,215]. Ratcliff and coworkers showed that, for fuels with matched RON and S_{octane} but different HoV, there was no difference in knock tendency at low intake-manifold temperature [191]. However, a substantial advantage was observed at higher intake-manifold temperatures. This group noted that as IAT was increased, the fraction of theoretical (adiabatic) cooling observed for the intake mixture based on the temperature at the time the intake valve is closed also increased, likely because of more rapid evaporation and reduced heat transfer [202]. These results can be understood by again considering the OI, where, as discussed in the previous section, K is not strictly a representation of the compression trajectory in the pressure-temperature domain, but thinking of it as such can provide useful insights. With this view, the reduced temperature produced from the high-HoV fuels moves the compression curve in the pressure temperature domain to lower temperatures. This physical representation implies lower values of K for high HoV fuels (in agreement with Stein and coworkers [208]), enhancing the effect of S_{octane} on knock resistance. A similar trend of shifting the pressure-temperature trace to lower temperatures for high-HoV fuels was observed in another study conducted within the Co-Optima initiative using the Co-Optima core fuels [190]. At high engine speeds when engine breathing becomes less efficient, the higher trapped residuals act to increase the intake valve closing temperature, indicating conditions where the HoV may play a more significant role in knock reduction.

Until further clarification is obtained, we conservatively assume that a fuel's effective OI is affected only modestly by HoV and increases at a rate of about 0.01 OI units per kJ/kg of HoV. In other words, $\frac{\partial OI}{\partial HoV} = 0.01 \frac{OI\ units}{kJ/kg}$. This value is supported by the increase in the RON value for the IMEP-matched condition in Fig. 29 and

is equivalent to 0.06 ON/ethanol vol %, which is significantly lower than the level reported for splash-blended fuels by Kasseris and Heywood of 0.15 ON/ethanol vol % and the value suggested for ethanol blends above E40 of 0.16 ON/ethanol vol % by Leone *et al.* [198,203].

Since blending of alcohols is the primary way to increase fuel HoV, increasing the HoV is accompanied by a reduction in the amount of air required to form a stoichiometric air-fuel mixture. For this reason, the HoV is expressed in units of $\frac{kJ}{kg_{AFM}}$, where the subscript AFM stands for air-fuel mixture. For stoichiometric mixtures,

$$HoV_{AFM} = HoV\frac{m_{fuel}}{m_{AFM}} = \frac{HoV}{1+AFR_s} \tag{19}$$

where m_{fuel} is the mass of fuel, m_{AFM} is the combined mass of the fuel mixture and the air required to form a stoichiometric mixture of fuel and air, and AFR_s is the stoichiometric air-fuel mass ratio for the given fuel mixture. As the heat of vaporization of a fuel mixture changes, so does the heat of vaporization of the corresponding stoichiometric air-fuel mixture. The relationship between these rates of change is expressed as $\frac{\partial HoV}{\partial HoV_{AFM}}$, which is estimated to have a value of 8.5 using data from Foong *et al.* [210] (see Fig. 30).

The HoV of a fuel mixture affects brake thermal efficiency by several other mechanisms. Jung *et al.* performed experiments and analysis to determine the mechanisms by which efficiency is improved with a blend of 15% gasoline and 85% ethanol (E85) compared to operation with gasoline for throttled conditions [214]. With the E85 fuel, HC and carbon dioxide (CO_2) emissions are reduced, and η_{comb} increases. However, the increased evaporative cooling of the E85 reduces the cylinder pressure during the intake stroke and therefore increases the pumping work, thus decreasing η_{GE}, although that effect was very small for E85 and would be even less significant for mid-level ethanol blends. Lower temperatures before and after combustion with E85 reduce wall heat losses, thereby increasing σ_{HT}. These lower temperatures act to increase the specific heat ratio, so both η_{ideal} and σ_{ideal} are increased with higher HoV of a fuel mixture. Lower temperatures may have an additional effect of decreasing heat release rates, thereby further decreasing σ_{ideal}. The fuel mixture's HoV acts to reduce the measured value of the heat of combustion in a way that is not representative of the fuel injection and vaporization process in the engine, because the fuel begins in the liquid phase in the HoV measurement [216]. Thus, the actual amount of chemical energy that can be released as heat in the combustion chamber is higher than the measured LHV for any fuel with a positive HoV [217]. Because E85 has a higher HoV than gasoline, the amount of chemical energy that can be released as heat during the combustion process is larger than is indicated by the LHV. This effect accounted for roughly half of the part-load efficiency improvement observed for E85 and is considered in the definition of combustion efficiency:

$$\eta_{comb} = \frac{Q_{HR}}{m_{fuel}(LHV + HoV)} \tag{20}$$

where *LHV* is the lower heating value of the fuel.

The aggregate of the HoV effects described above is given by:

$$\frac{1}{\eta_b}\frac{\partial\eta_b}{\partial HoV_{AFM}} = \left[\frac{1}{\eta_b}\frac{\partial\eta_b}{\partial OI}\frac{\partial OI}{\partial HoV}\frac{\partial HoV}{\partial HoV_{AFM}}\right] + \left[\frac{1}{\eta_b}\frac{\partial HoV}{\partial HoV_{AFM}}\left(\frac{\partial\eta_b}{\partial\eta_{comb}}\frac{\partial\eta_{comb}}{\partial HoV} + \frac{\partial\eta_b}{\partial\eta_{GE}}\frac{\partial\eta_{GE}}{\partial HoV} + \frac{\partial\eta_b}{\partial\sigma_{HT}}\frac{\partial\sigma_{HT}}{\partial HoV} + \frac{\partial\eta_b}{\partial\eta_{ideal}}\frac{\partial\eta_{ideal}}{\partial\gamma}\frac{\partial\gamma}{\partial HoV} + \frac{\partial\eta_b}{\partial\sigma_{ideal}}\frac{\partial\sigma_{ideal}}{\partial HoV}\right)\right] \tag{21}$$

Evaluating the first group of terms on the right-hand side using values for the terms as they are defined above results in the following expression: $\left[\frac{1}{\eta_b}\frac{\partial\eta_b}{\partial OI}\frac{\partial OI}{\partial HoV}\frac{\partial HoV}{\partial HoV_{AFM}}\right] = 8.5(0.01)\left(\frac{1}{\eta_b}\frac{\partial\eta_b}{\partial OI}\right) = 0.085\left(\frac{1}{\eta_b}\frac{\partial\eta_b}{\partial OI}\right)$. Substituing $\frac{1}{\eta_b}\frac{\partial\eta_b}{\partial OI}$ from Section 3.1 yields Eq. 22.

$$\left[\frac{1}{\eta_b}\frac{\partial\eta_b}{\partial OI}\frac{\partial OI}{\partial HoV}\frac{\partial HoV}{\partial HoV_{AFM}}\right] = \frac{0.085\left(\frac{HoV/(AFR+1) - HoV_{ref}}{AFR_{ref}+1}\right)}{1.6} \tag{22}$$

Jung *et al.* provided an empirical estimate for the second group of terms in Eq. 21 and found that, overall, vaporization cooling increased the thermal efficiency of a throttled DI engine by about 4.2% between E0 and E85 or 1% for an increase in HoV of ~130 kJ/kg [214]. The estimate is likely conservative due to the relatively large displacement of the test engine compared to the displacement expected for a downsized engine. Thus, an estimate for the second group of terms in Eq. 21 is given by

$$\frac{1}{\eta_b}\frac{\partial HoV}{\partial HoV_{AFM}}\frac{\partial\eta_b}{\partial HoV} = \frac{8.5}{130}\frac{\%\ \eta_b\ increase}{kJ/kgAFM} = \frac{1}{15.3}\frac{\%\ \eta_b\ increase}{kJ/kgAFM} \tag{23}$$

Although considerations in this analysis are limited as to how HoV affects engine efficiency, HoV can also have other important impacts on engine operation, such as cold-start behavior and differences in the degree of enrichment needed for catalyst protection. Both Szybist and Splitter [192] and Stein *et al.* [208] demonstrate that fuels with differences in high HoV and advanced combustion phasing can result in reduced exhaust temperature that can result in significant changes to the need for catalyst protection at conditions near peak torque. This effect is difficult to incorporate into the merit function because it strongly depends on the engine hardware system and the calibration. Some engines might not regularly operate at conditions where the HoV will mean the difference between enrichment and stoichiometric conditions, but other engine configurations could operate there frequently. It therefore is recommended that this factor be taken into account when individual systems are being modeled with greater fidelity.

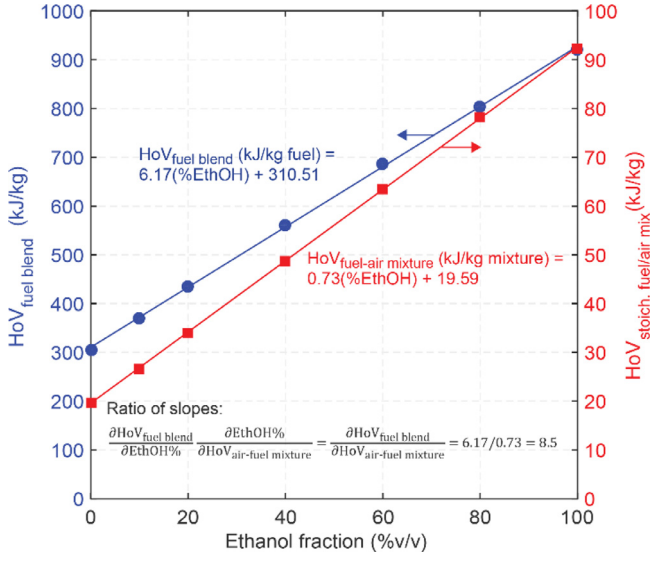

Fig. 30. Heat of vaporization for ethanol-gasoline fuel blends (blue) and for stoichiometric ethanol-gasoline-air mixtures (red). The ratio of the slopes of these curves provides an estimate of $\frac{\partial HoV}{\partial HoV_{AFM}}$.

3.3. The effects of flame speed

3.3.1. Thermodynamic effects of flame speed on engine efficiency

A higher S_L can shorten the total burn duration and this has the potential to increase the thermal efficiency if a more ideal

constant-volume combustion process can be achieved. However, for conventional non-dilute stoichiometric operation, the burn duration is normally sufficiently short that very little gain is expected. Instead, it is considered here that the primary impact of increased S_L on engine efficiency in stoichiometric SI engines is to increase the EGR dilution tolerance. The overall efficiency advantages for high-EGR conditions are described in detail in a thermodynamic modeling study by Caton [79]. First, additional mass from the EGR causes the manifold pressure to increase without increasing the intake oxygen flow, which at part-load conditions can decrease engine pumping losses and increase engine efficiency. Second, the peak in-cylinder temperature decreases with EGR, causing the in-cylinder heat transfer to decrease. Third, due to a combined thermal and composition effect, the γ increases with EGR relative to a stoichiometric mixture due to the dilution of the very low γ fuel components.

Increasing S_L increases EGR dilution tolerance by decreasing the cycle-to-cycle variability of the combustion event [84,218]. Combustion stability and cycle-to-cycle variability in SI engines have been the subjects of extensive research over multiple decades, and Ozdor *et al.* [86] performed a comprehensive literature review in1994 that remains relevant. They characterize the initial flame kernel development, which is typically about a third of the total combustion duration, as being the most crucial to cycle-to-cycle variation because of its high sensitivity to a large number of factors. During flame kernel development, the laminar flame speed of the mixture dominates the combustion rate; the turbulent flame propagation stage dominates only after the flame kernel is sufficiently large to be influenced by multiple turbulent eddies simultaneously. Fuels with high flame speed complete the early flame kernel development process more quickly, making them less susceptible to the stochastic cycle-to-cycle differences in turbulence and ultimately provide more stable combustion.

The aforementioned reduction in throttling losses with EGR acts to increase η_{GE}. The γ of EGR is different from that of fresh air, so η_{ideal} and σ_{ideal} may change with EGR addition. Assuming EGR dilution tolerance depends only on laminar flame speed, the effect of the S_L on brake thermal efficiency is given as

$$\frac{1}{\eta_b}\frac{\partial \eta_b}{\partial S_L} = \frac{1}{\eta_b}\frac{d\eta_b}{dEGR}\frac{dEGR}{dS_L} \tag{24}$$

$\frac{d\eta_b}{dEGR}$, the change in brake thermal efficiency with respect to EGR rate, is calculated using the chain rule to account for the effects described above (refer to section 2.1 for definitions of the variables):

$$\frac{d\eta_b}{dEGR} = \frac{\partial \eta_b}{\partial \eta_{GE}}\frac{\partial \eta_{GE}}{\partial EGR} + \frac{\partial \eta_b}{\partial \sigma_{HT}}\frac{\partial \sigma_{HT}}{\partial EGR} + \frac{\partial \eta_b}{\partial \eta_{ideal}}\frac{\partial \eta_{ideal}}{\partial \gamma}\frac{\partial \gamma}{\partial EGR} + \frac{\partial \eta_b}{\partial \sigma_{ideal}}\frac{\partial \sigma_{ideal}}{\partial \gamma}\frac{\partial \gamma}{\partial EGR} \tag{25}$$

Data available in the literature do not provide a means to evaluate all of the individual terms in Eq. 25, but they are sufficient for an empirical estimate of the right-hand side of Eq. 24.

3.3.2. Determination of laminar flame speed

Difficulties and uncertainties in determining S_L complicate the use of this fuel property in a merit function. S_L is dependent on pressure, temperature, and dilution, but measuring S_L at elevated pressures representative engine conditions at spark timing precludes the use of most flat-flame burners, which is the most common way to measure S_L. Using a constant volume vessel has the advantage of reproducing pressure and temperature conditions that are relevant to engines [219,220], but these vessels produce spherical flames and burning rates that can differ substantially from flat flame burners due to flame stretch, or varying degrees of flame curvature and aerodynamic strain in the experimental devices [221–224]. While there are well-established theoretical methods to extrapolate the unstretched S_L from spherical flames using the stretch rate, Markstein Length, and flame area [225], there is a significant amount of uncertainty and disagreement with how to perform this extrapolation in-practice [219,226–234].

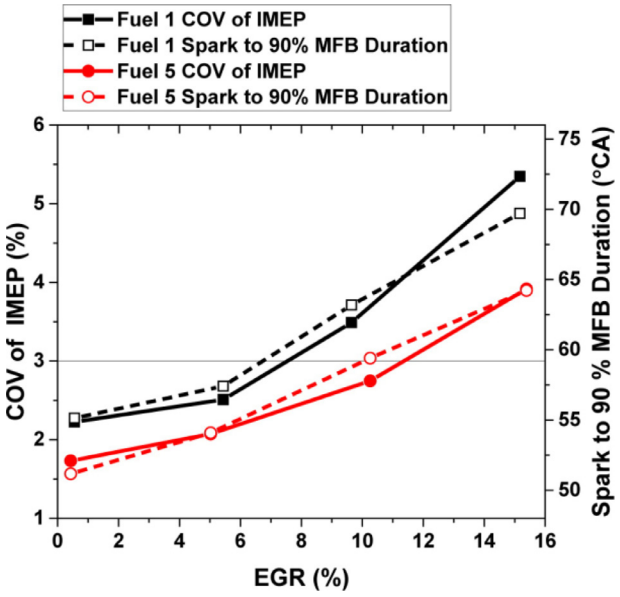

Fig. 31. Increased dilution tolerance with higher S_L fuels at 2000 rpm and 3.5 bar gross $IMEP_g$. Fuel 1 has S_L of 45 cm/s and Fuel 5 has S_L of 50.3 cm/s. Reprinted from Szybist and Splitter [84] with permission of SAE International.

As a result of these complications, it is recommended that unstretched S_L measurements from flat flame burners be used for merit function evaluation. Even for flat flame burners, S_L measurements can be found in the literature at a variety of temperature and pressure conditions. Thus, the S_L will be considered at a standard condition of 1 atm and 353 K. In order to use S_L data measured at other pressure-temperature found in literature, a power-law scaling correlation (e.g., Metghalchi and Keck [235]) can be adopted. Such a relationship scales the typical behavior of flame speed to increase with temperature and decrease with pressure, allowing the flame speed to be estimated over a broad range of conditions.

3.3.3. Quantifying the effect of flame speed

Two studies have quantified the extended dilution tolerance of stoichiometric SI combustion using fuels with a known range of S_L [84, 218]. The increased dilution tolerance was assessed at 3% COV of $IMEP_g$ [84] or $IMEP_n$ [218] for low- and high-S_L fuels composed of pure components (iso-octane, n-heptane, toluene, and ethanol). Values for S_L have been calculated both using a Le Chatelier energy and the molar-weighted mixing law [236] at peak S_L ($\Phi = 1.1$) and stoichiometric chemical kinetic modeling in Chemkin, at initial conditions of 1 atm and 358 K.

In the first of these studies, Szybist and Splitter [84] observed that, at 2000 rpm and 3.5 bar $IMEP_g$, there was a 50% relative increase (8% to 12%) in EGR dilution tolerance (Fig. 31) when fuel S_L increased from 45 cm/s (Fuel 1) to 50.3 cm/s (Fuel 5); each percentage point (p.p.) increase of EGR indicated a rise in thermal efficiency (ITE) of 0.064 p.p. In the second study, at 1500 rpm and 5.6 bar $IMEP_n$, Kolodziej *et al.* [218] also observed a 4% increase in EGR dilution tolerance (18.6% to 22.8%) when fuel S_L increased from 45.7 cm/s (Fuel 2) to 52.1 cm/s (Fuel 4), as shown in Fig. 32. For this study, each p.p. increase of EGR raised ITE by 0.11% for a total absolute efficiency gain of 0.3% (from 39.5% to 39.8%).

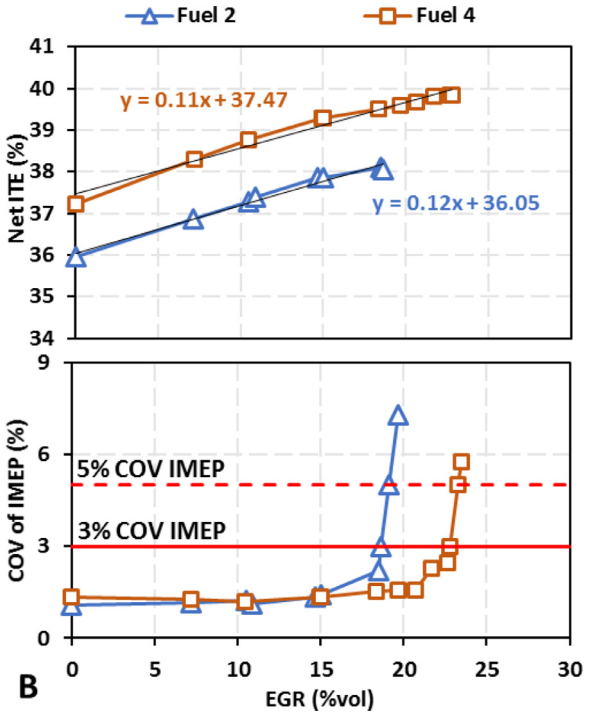

Fig. 32. . Increased dilution tolerance with higher S_L fuels at 1500 rpm and 5.6 net gross $IMEP_n$. Fuel 2 has S_L of 45.7 cm/s and Fuel 5 has S_L of 52.1 cm/s. Reprinted from Kolodziej *et al.* [218] with permission of SAE International.

These estimates of efficiency gain per p.p. of EGR, 0.064 from Szybist and Splitter [84] and 0.11 from Kolodziej *et al.* [218], equate to an ITE increase of 1.3 to 2.2 p.p. for a 20% EGR condition relative to a baseline engine operating condition. This estimate is largely in line with the efficiency gains of 1 to 1.5 p.p. ITE increase at 20% EGR found by Chang and Szybist [83], Caton [79,237], and Alger *et al.* [80].

Eq. 25 can be evaluated with the underlying assumption that a relative increase in indicated thermal efficiency is equal to the corresponding relative increase in η_b. The measurements by Szybist and Splitter [84] provide one estimate:

$$\frac{1}{\eta_b}\frac{\partial \eta_b}{\partial S_L} = \frac{1}{\eta_b}\left(\frac{\partial \eta_b}{\partial EGR}\frac{\partial EGR}{\partial S_L}\right) = \frac{1}{\eta_b}\left(\frac{0.064\ p.p.\ ITE}{\%\ EGR} * \frac{4\%\ EGR\ Increase}{5.3\ \frac{cm}{s}\ flame\ speed\ increase}\right) = \frac{0.05}{\eta_b}\frac{p.p.\ ITE}{\frac{cm}{s}\ flame\ speed\ increase} \tag{26}$$

The same analysis is performed on the data obtained by Kolodziej *et al.* [218] to provide a second estimate:

$$\frac{1}{\eta_b}\frac{\partial \eta_b}{\partial S_L} = \frac{1}{\eta_b}\left(\frac{\partial \eta_b}{\partial EGR}\frac{\partial EGR}{\partial S_L}\right) = \frac{1}{\eta_b}\left(\frac{0.11\ p.p.\ ITE}{\%\ EGR} * \frac{4.1\%\ EGR\ Increase}{6.45\ \frac{cm}{s}\ flame\ speed\ increase}\right) = \frac{0.07}{\eta_b}\frac{p.p.\ ITE}{\frac{cm}{s}\ flame\ speed\ increase} \tag{27}$$

Since these calculations are in terms of absolute increased engine efficiency, it is necessary to convert to relative efficiency gains, by dividing by the efficiency of the base 0% EGR condition. For the data from Szybist and Splitter [84], dividing by a base ITE of 27% and converting to relative percent (multiplying by 100) provides 0.179% relative ITE increase per centimeter per second increase in S_L. Applying this same approach to the data by Kolodziej *et al.* (2017) [218], which had a base ITE of 37.2%, provides 0.190% relative ITE increase per centimeter per second increase in S_L Eq. 25 can now be estimated in full:

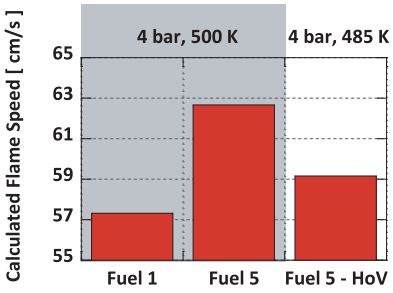

Fig. 33. Flame speed for Fuel 1 (no ethanol content) and Fuel 5 (30 vol % ethanol) at 4 bar, 500 K, and for Fuel 5 at 4 bar at a reduced temperature of 485 K after taking into account the HoV of ethanol. Reprinted from Szybist and Splitter [84] with permission of SAE International.

$$\left.\frac{1}{\eta_b}\frac{\partial \eta_b}{\partial S_L}\right|_{Szybist\ and\ Splitter} = 0.179\frac{\%}{cm/s} \tag{28}$$

$$\left.\frac{1}{\eta_b}\frac{\partial \eta_b}{\partial S_L}\right|_{Kolodziej} = 0.190\frac{\%}{cm/s} \tag{29}$$

The reciprocals of these terms are used to define the laminar flame speed term in the merit function, and the average of the two values is used. This yields the following:

$$\frac{1}{\eta_b}\frac{\partial \eta_b}{\partial S_L} = \frac{1}{\frac{1}{2}\left(\frac{1}{0.179}+\frac{1}{0.190}\right)} \approx \frac{1}{5.4}\frac{\%}{cm/s} \tag{30}$$

3.3.4. Additional laminar flame speed effects

While strong evidence has been presented that increased fuel S_L allows increased SI dilution tolerance and therefore increased engine ITE, it is not clear whether the effects of fuel S_L are measurable for nondilute stoichiometric SI combustion. For example, Heese *et al.* modeled flame speed impacts on efficiency under nondilute operation for conditions that were both knock-limited and not knock-limited and found only minor differences (<0.2 %) with large changes in flame speed (> 20%) [238]. Remmert *et al.* demonstrated that there was an efficiency benefit for higher-S_L fuels at a constant spark timing, but it was not clear whether it could be adjusted for by matching combustion phasing through different spark timing [239]. For experimental studies, it is not possible to change the flame speed in isolation from other fuel properties, which makes it difficult to deconvolute the effects of individual fuel properties. For example, it is well known that adding ethanol to a fuel blend increases its S_L (see Broustail *et al.*) [240]. However, ethanol addition also increases the fuel's HoV. Increased fuel evaporative cooling reduces in-cylinder gas temperatures and therefore also a fuel's S_L, as demonstrated by Szybist and Splitter [84] and illustrated in Fig. 33.

In addition to lean stratified-charge conditions, Sjöberg and Reuss investigated nondilute SI combustion with E0 gasoline and E85 gasoline [241]. The results show that the increased HoV of ethanol can counteract the inherent tendency of ethanol to increase S_L for a given charge temperature. Rockstroh *et al.* [193] found that the cooler temperature with a high HoV fuel (E50, approximately 90 K lower than the non-ethanol fuel) caused the combustion duration to be slower despite the higher S_L when compared at the same temperature. This phenomenon is demonstrated in Fig. 34, with fundamental flame measurements by Zhao shown in Fig. 34(a), and corresponding temperature and heat-release traces for engine experiments with the same fuels shown in Fig. 34(b) and (c). Fig. 34(a) illustrates that going from a regular grade of gasoline without ethanol (RD3–87) to E85 increases S_L by roughly 14% for stoichiometric conditions, yet Fig. 34(c) reveals that the heat-release rate is invariant with fuel type.

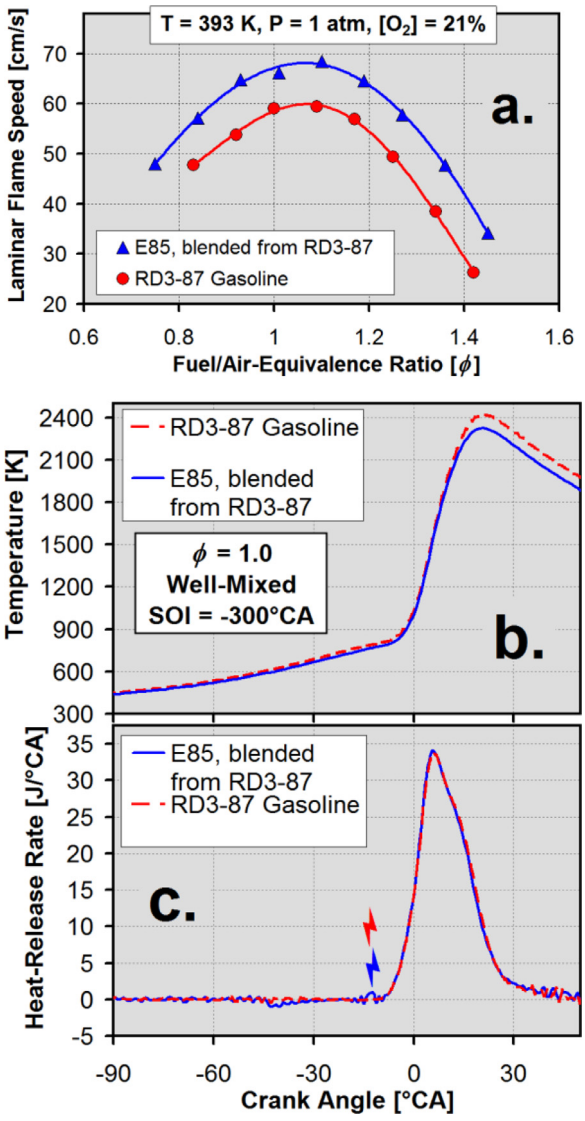

Fig. 34. (a) S_L for regular-grade gasoline without ethanol (RD3–87) and E85 (blended from RD3–87) over a range of Φ, as measured by Runhua Zhao, USC, following the procedures outlined in Li *et al.* [242]. (b) Reduction of charge temperature with increased HoV of E85. (c) Heat-release rate for gasoline and E85. Fuel properties are given in Sjöberg and Reuss [241].

Farrell *et al.* [226] claimed that increased fuel S_L caused increased engine ITE. However, the magnitude of the ITE increase is difficult to see solely through a comparison of the rates of heat release between the fuels. Ayala and Heywood [243] investigated significant increases to mixture S_L by introducing hydrogen. However, no gain in ITE was detected for stoichiometric nondilute SI engine operation. This may be explained by the relatively short 10–90% burn duration of 20°CA for the baseline gasoline, providing near ideal constant-volume combustion even without hydrogen addition.

Thus, for the purposes of quantifying the impact of S_L on efficiency unrelated to dilution tolerance, no conclusive relationships could be established based on the examined literature.

3.4. Low-speed preignition

Downsized and boosted SI engines are one of the main approaches being used by engine manufacturers to improve vehicle efficiency and to reduce CO_2 emissions (see Section 1.2.1)

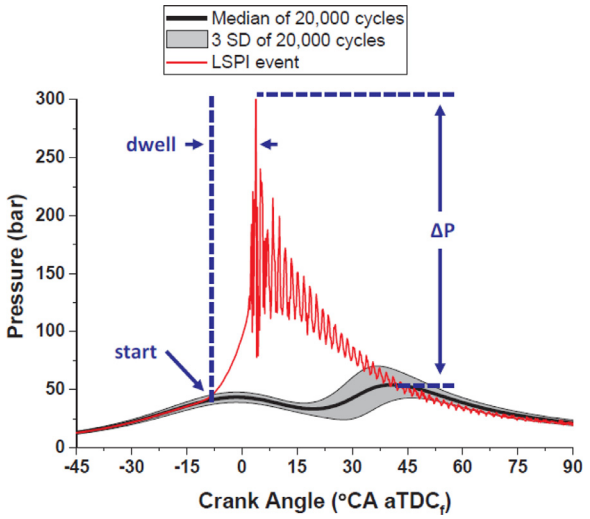

Fig. 35. Example showing the cylinder pressure of an LSPI cycle in comparison to the average cylinder pressure. Reprinted from Jatana *et al.* [246] with permission of Elsevier.

[1,37,190]. Although boosted HPD engines are effective at improving fuel economy, their increased power density makes them more prone to damaging preignition phenomena followed by superknock, which is a very high-pressure knocking event that can cause engine damage. Preignition is a phenomena in which the premixed fuel-air mixture is ignited unintentionally prior to the firing of the spark plug and can have a number of different causes. In many instances, preignition is not destructive [244]. However, in downsized boosted engines, the high-load and typically low-speed operating conditions result in preignition coupled to intense superknock events referred to as low-speed preignition (LSPI). Despite its name, LSPI and superknock have recently been reported during an on-road study at engine speeds in excess of 3000 RPM [245]. LSPI can be detrimental to engine hardware as the early ignition of the fuel-air mixture can lead to heavy knocking or detonation events resulting in very high peak pressures and pressure oscillations. Fig. 35 provides an illustration of the magnitude of an LSPI superknock event that exceeds 300 bar during an engine operating condition that normally has a peak pressure of about 50 bar [246]. LSPI effectively limits vehicle efficiency because it is a barrier to further engine downsizing and downspeeding; manufacturers size and calibrate engines and transmission combinations for vehicle powertrains to avoid engine operation that is prone to LSPI.

3.4.1. Causes of low speed preignition

Chapman *et al.* [244] explain that, for these damaging events to occur, there is a multi-step sequence where each step is required but not sufficient on its own, as illustrated in Fig. 36. The first step is initiation, where an ignition source deposits energy into the fuel and air mixture. If this ignition source transfers sufficient energy, it leads to a preignition where there is flame propagation in the combustion chamber prior to spark ignition. The preignition event causes compression heating of the end gas, leading to end gas autoignition. Wang *et al.* [247] conclude that preignition can result in a full spectrum of outcomes, including non-knocking cycles, mild knock that does not require mitigation, or heavy knock can damage the engine. It is only if there is sufficient coupling of the energy release rate with the surrounding thermodynamic conditions that will result in a developing detonation to produce superknock [248].

While the LSPI event and the resulting superknock event are related, they are distinct phenomena, and not all LSPI cycles exhibit superknock [247]. LSPI occurs stochastically and, under appropri-

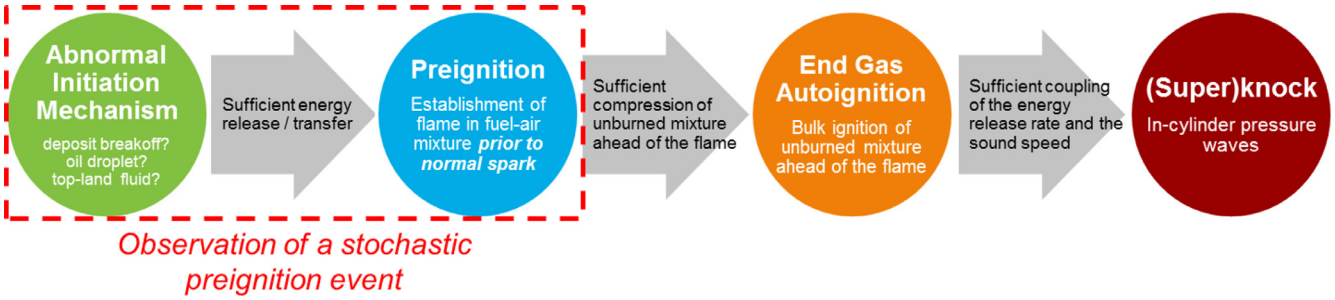

Fig. 36. Sequence of steps required for a damaging LSPI superkock event. Reprinted from Chapman and Costanzo [244] with permission of SAE International.

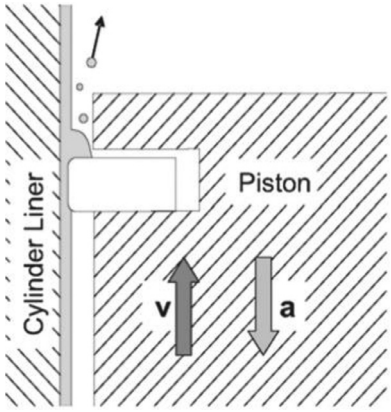

Fig. 37. The droplet ejection mechanism from the top-ring land that leads to LSPI, as proposed by Dahnz *et al.* [255]. Reprinted from Dahnz *et al.* [255] with permission of SAE International.

ate operating conditions, will typically occur within every 10,000 cycles [249]. However, LSPI can also manifest as a cluster of many events that occur in an alternating pattern; wherein, every-other-cycle exhibits LSPI behavior. Additionally, though rare, the occurrence of consecutive LSPI cycles has also been reported [249].

3.4.2. Fuel-related causes of LSPI initiation

Fuel interactions with LSPI and superknock are complex because fuel properties can act to either promote or mitigate any of the events in the sequence shown in Fig. 36, with many studies focusing on fuel effects associated with preignition initiation. As explained by Zaccardi and Escudie [250], there can be a number of distinct initiation steps for LSPI, such as autoignition in the gaseous phase and the ignition of the fuel-air mixture due to either liquid droplets or solid particles. While a number of researchers have shown that flaking deposits or other solids can initiate LSPI events [251–253], Gupta *et al.* [254] concluded that it would be improbable for those sources to persist over multiple cycles, making this cause an unlikely cause of clustered LSPI events.

A more probable initiation mechanism is droplets of fuel or lubricant ejected from the top-ring land of a piston, as shown in Fig. 37 [249,255]. A significant amount of recent LSPI research on the droplet ejection theory has focused on understanding the effects of fuel [256–259] and lubricant [260–267] properties as well as the interaction of fuel sprays and lubricating oil in the top crevice region [249,268,269]. Kalghatgi *et al.* [270,271] noted that the ignition source must be highly reactive, more so than n-heptane, to successfully produce a preignition event. In addition, the stochastic nature of LSPI has also partially been attributed to variations in piston ring motion [249] and cycle-to-cycle turbulence variations [272].

Zahdeh *et al.* [249] evaluated an engine's LSPI frequency with hardware configuration (e.g. injector targeting, piston top-ring geometry). The results illustrated the sensitivities of LSPI to different operating conditions, resulting in strategies to reduce the frequency of preignition events: use of a high-volatility fuel, fuel sprays that target the piston top rather than the cylinder liner, and using multiple fuel injections. Fig. 38 illustrates some of the findings of that work that highlight instances where increased fuel-wall impingement correlated with increased LSPI event count.

Further studies on fuel properties show that physical properties that minimize fuel-wall impingement, specifically reduced distillation temperatures, correlate with reduced LSPI frequency and support the fuel-oil ejection theory. For example, Chapman *et al.* illustrate in Fig. 39 that LSPI frequency is correlated with distillation T50 (temperature at which 50% of the fuel evaporated) [257]. A number of other researchers also showed a linear dependency of LSPI frequency on the fraction of fuel that boiled above 150°C [273–275].

In addition to the distillation curve, Mansfield *et al.* noted that fuels with high aromatic content were particularly prone to LSPI [249,259]. Since the high temperature fraction of gasoline distillation tends to contain an increased fraction of aromatics, it is difficult to separate the difference between distillation and aromatic content on LSPI. It is noteworthy, though, that, in a study where liquid sample was collected from the crevice region and speciated, the aromatic content at the heavy end of the distillation curve preferentially remained in this area [276]. Further, Splitter *et al.* recently showed that nitro compounds, which can be readily formed from liquid phase aromatics with elevated temperature and pressure and the presence of NOx, are a possible LSPI ignition source [277]. Thus, there is evidence supporting that both distillation curve and aromatics promote preignition tendency.

3.4.3. Additional LSPI fuel-effects

The previous section specifically focused on fuel effects of LSPI initiation, but Fig. 36 illustrates that LSPI is a sequential process, and fuel effects can occur at multiple steps in the process. First, both Zaccardi and Escudie [250] and Splitter *et al.* [278] noted the importance of the thermodynamic state of the fuel-air mixture. Splitter *et al.* [278] showed that fuel-air mixtures that undergo pre-spark heat release due to LTHR are highly kinetically active and increase LSPI tendency.

Kalghatgi *et al.* [270,271] investigated the magnitude of energy input necessary to cause LSPI using a series of surrogate fuel formulations and found that fuels with higher S_L had more LSPI events. From this, Kalghatgi and Bradley [270] developed a preignition rating (PR), where a high PR indicates that a fuel is resistant to LSPI. Fig. 40 illustrates that PR increases with the inverse of flame speed. Kalghatgi and Bradley attributed this effect to the flame thickness: fuels with increased flame speed will have decreased flame thickness, allowing the flame to more reliably propagate, similar to flame propagation under dilute combustion discussed in Section 3.3. Rudloff *et al.* [279] expanded upon this work in a modeling study and showed the possibility of high S_L fuels

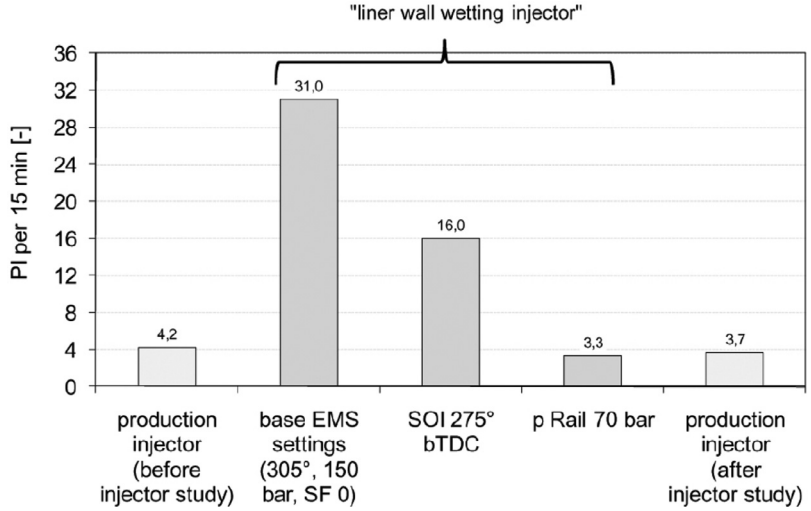

Fig. 38. Preignition tendency of fuel injection timing and delivery settings, increased fuel-linear interaction correlated with increased preignition count. Reprinted from Zahdeh, *et al.* [249] with permission of SAE International.

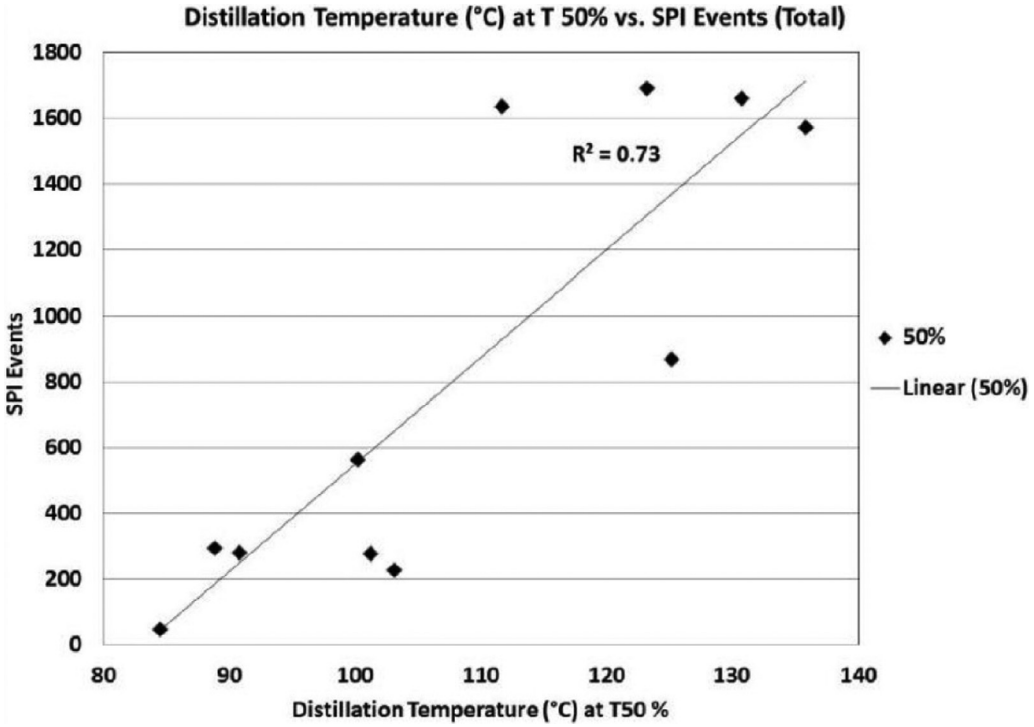

Fig. 39. Preignition tendency as a function of T50. Reprinted from Chapman *et al.* [257] with permission of SAE International.

leading to developing detonations in strong LSPI events. This work showed that fuels with high S_L are more prone to high intensity superknock events and not just increased preignition frequency.

Jatana *et al.* [246] studied the frequency and severity of LSPI as part of the Co-Optima initiative by changing the composition of the fuel components to vary S_L while holding the distillation curve constant. To accomplish this, three blendstocks were blended into a baseline gasoline at 25% mass fraction, with the blendstocks having a similar RON (99.5 ± 1.5) and boiling point (131 ± 5°C). This boiling point range was chosen to increase the distillation T50 temperature relative to the baseline gasoline, which was identified by Chapman *et al.* as correlating strongly with LSPI frequency [257]. The three blendstocks included a ketone (cyclopentanone), an alcohol (2-methyl-1-butanol), and an aromatic (ethylbenzene). The study found that, relative to the baseline fuel, all the fuel candidates investigated in this study increase LSPI events significantly. However, despite having a similar number of LSPI events, there was a large difference in LSPI intensity, as is shown by the pressure rise associated with the LSPI event in Fig. 41. Specifically, the fuel components with the higher S_L, cyclopentanone and 2-methyl-1-butanol, resulted in the most severe LSPI events, and the fuel component with the lowest S_L, ethylbenezene, resulted in the lowest magnitude LSPI events.

3.4.4. Quantification of the fuel-related causes of low-speed preignition

While it is clear from Section 3.4.3 that there are fuel effects that extend beyond preignition initiation, the fuel properties that affect initiation, discussed in Section 3.4.2, are the best understood and will form the basis for the quantification of efficiency im-

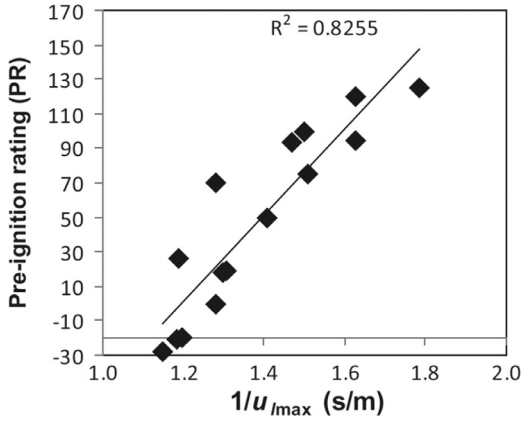

Fig. 40. Preignition rating as a function of the inverse flame speed of the fuel. Reprinted from Kalghatgi and Bradley [270] with permission of Sage Publishing.

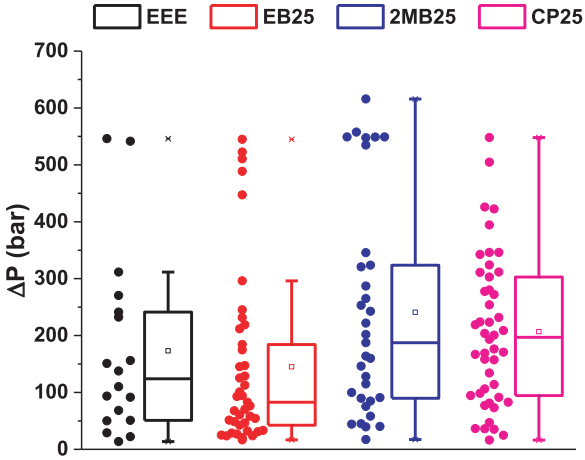

Fig. 41. Pressure rise for each preignition event relative to mean cylinder pressure for certification gasoline (EEE), a 25 mass % blend of ethylbenzene (EB25), a 25 mass % of 2-methyl-1-butanol (2MB25), and a 25 mass % blend with cyclopentanone (CP25). Reprinted from Jatana *et al.* [246] with permission of Elsevier.

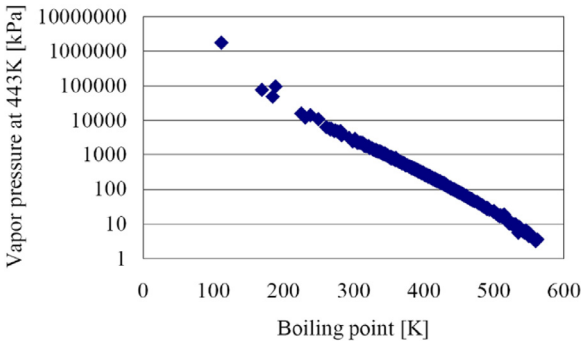

Fig. 42. Correlation between vapor pressure and boiling point. Reprinted from Aikawa *et al.* [280] with permission of SAE International.

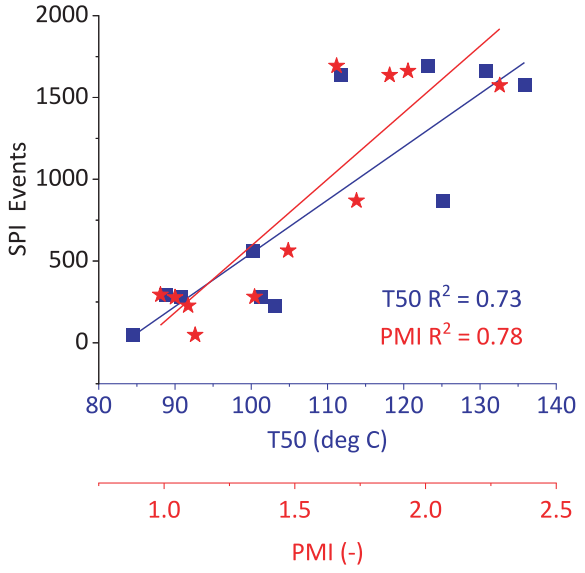

Fig. 43. Re-evaluation of SPI data from Chapman *et al.* [257] including both T50 and PMI.

pacts discussed here. This section illustrated that LSPI frequency increases with both higher aromatic content [249,259] and with higher distillation temperature [257,273–275]. While not originally intended to apply to LSPI fuel effects, the particulate matter index (PMI), which was developed by Aikawa *et al.* [280] to predict the PM formation tendencies of a fuel, is a fuel property metric that accounts for both distillation temperature and aromatic content, as shown in Eq. 31

$$PMI = \sum_{i=1}^{n}\left[\frac{(DBE_i + 1)}{VP(443K)_i} \times Wt_i\right] \quad (31)$$

where DBE (double bond equivalent) is a structural descriptor of each component's unsaturation (i.e., rings and double bonds) and VP is the vapor pressure. Aikawa *et al.* [280] further explain that the vapor pressure and boiling point for the higher boiling point species are closely correlated, as shown in Fig. 42.

While PMI was not developed to be predictive of LSPI frequency, there is evidence to suggest that this fuel property provides a superior indication of LSPI frequency than distillation curve alone. While PMI data were not originally published by Chapman *et al.* [257], the LSPI data were obtained from the authors and re-evaluated, as shown in Fig. 43. The correlation between SPI events using PMI marginally improved relative to the T50 correlation, increasing the R^2 correlation coefficient from 0.73 to 0.78. An additional study by Swarts *et al.* [281] investigating LSPI frequency for 17 different fuels again showed a strong correlation to PMI, but the PMI correlation only held for LSPI frequency and not severity.

Thus, for the purpose of attempting to quantify the effects of LSPI on engine efficiency, PMI will be used as a fuel property indicator of LSPI frequency. As shown in Fig. 43, this is an imperfect indicator, but this is to be expected given that LSPI occurrence, and ultimately superknock, is a series of events where fuel properties can affect the outcome in multiple different ways in the sequence, as was shown in Fig. 36.

The next step is to quantify the impact of LSPI frequency on engine efficiency. As noted at the beginning of Section 3.4, LSPI limits the degree of engine downsizing. Downsizing and downspeeding with high power density engines has been a widespread trend in the automotive industry, as evidenced by the trend since 2005 towards engines with fewer cylinders as shown in Fig. 4. Further, in Section 3.1.5, the engine efficiency increase associated with an increase in OI incorporated a downsizing multiplier, which was then extended to the first HoV term associated with knock mitigation. For the purposes of quantifying the effects of LSPI on efficiency with the merit function, this downsizing multiplier will be eliminated above a critical threshold PMI ($PMI_{LSPI,crit}$) value where LSPI is prone to occur.

Thus, the terms in Eqs. (15) and (22) can be combined into Eq. 32 to show the net impact of improved knock resistance on engine efficiency. This Eq. also incorporates the limitation on downsizing imposed by LSPI for fuels with PMI > $PMI_{LSPI,crit}$. This control

term is based on the Heaviside function, $H(x)$, which is a form of step function between zero and one. In this case, the presumptions are that below $PMI_{LSPI,crit}$, the downsizing efficiency multiplier applies, but above this value, LSPI is too prevalent and prevents further downsizing.. While this analysis provides a structure of how this term will be incorporated, the quantification of $PMI_{LSPI,crit}$ for LSPI to occur still needs to be done, and it may be different for different engine designs.

$$\frac{1}{\eta_b}\frac{\partial \eta_b}{\partial OI}\left(OI - OI_{ref}\right) = \frac{\left(RON - RON_{Ref}\right)}{1.6 + 0.3 * H(PMI - PMI_{LSPI,crit})} - K\frac{\left(S_{octane} - S_{octane,Ref}\right)}{1.6 + 0.3 * H(PMI - PMI_{LSPI,crit})} + \frac{0.085\left(\frac{HoV/(AFR+1)-415}{14.0+1}\right)}{1.6 + 0.3 * H(PMI - PMI_{LSPI,crit})}. \quad (32)$$

4. How fuels influence efficiency through emission controls

Section 3 focused on in-cylinder impacts, which are the most direct ways fuel properties affect engine efficiency, and ultimately vehicle fuel consumption. However, all vehicles sold must meet emissions standards, and fuels can influence the emissions produced by the engine in either a positive or negative way. In this section, the ways in which fuel properties affect emissions from stoichiometric SI engines are discussed, and then the effect of differences in emissions on fuel efficiency is quantified. This is done first for gaseous emissions in Section 4.1 and then for particulate matter (PM) emissions in Section 4.2.

4.1. Gaseous emissions

4.1.1. Derivation of the gaseous emissions merit function term

The motivation and derivation for the gaseous emissions merit function term, including detailed discussions of the assumptions and data analysis methods used in numerical evaluation of the merit function term, have been described elsewhere [282]. A brief summary of that work is included in this section. Note that some of the variables used in that analysis have been updated from reference [282] to match the conventions used in other parts of this review.

All vehicles sold in the United States must comply with US EPA emissions regulations for three classes of gaseous emissions: CO, NOx, and nonmethane organic gases (NMOG). To comply with these regulations, all modern SI vehicle engines sold in the United States operate with a nominally stoichiometric AFR to enable the use of TWCs for exhaust aftertreatment. As discussed in Section 1, TWCs are extremely effective at removing CO, NOx, and NMOG from the exhaust of a properly calibrated engine/emissions control system at typical SI engine exhaust temperatures. However, TWCs do not work effectively when they are at ambient temperatures. The TWC temperature must be above a certain threshold, commonly referred to as the "light-off temperature," before the catalytic oxidation/reduction reactions required to convert the regulated pollutants to N_2, CO_2, and H_2O become active. Thus, the majority of the regulated pollutants emitted by modern vehicles equipped with SI engines are released during the cold start period immediately after the engine is turned on [282]. This can be observed in emissions data collected during the US EPA Federal Test Procedure (FTP) city driving cycle, such as in Fig. 44. Most emissions (60% of CO; 80% of HCs, equivalent to NMOG in this case, and 60% of NOx) occur during the first 120 s of the cycle, before the catalyst achieves light-off. Once the catalyst is hot, the gaseous emissions are quite low for the remainder of the FTP cycle.

To comply with emissions standards, engine operation during cold start must be carefully controlled to heat the TWC above the light-off temperature as quickly as possible. Methods for catalyst heating include operation with excess fuel and air and delayed spark timing, creating hot chemically reactive exhaust to rapidly increase TWC temperature [283–285]. While such strategies are necessary to meet emissions regulations, they also incur a fuel penalty since the engine is purposefully operated at abnormally low-efficiency conditions during the cold start process [283–286]. The magnitude of the fuel penalty will depend on how long it takes for the catalyst to achieve light-off: higher light-off temperatures will require more time under the cold-start strategy, resulting in a larger fuel penalty. The cold-start fuel penalty provides a means for linking emissions with engine efficiency.

Data from the EPA FTP city driving cycle provides one method for estimating the fuel penalty associated with catalyst heating during cold-start operation. The FTP is broken into three sections, also known as "bags" 1, 2 and 3, as shown in Fig. 44. Since the engine and emissions control catalysts are at ambient temperature at the beginning of the test, the first section begins with a cold start. The third section is identical to the first, except for one important detail: the engine and emissions control catalysts begin at elevated temperatures since it is run shortly after the second section is completed. The third section is therefore considered a "hot" start. The calculations for fuel economy and emissions measurements actually include a fourth section with the same speed and load profile as the second, but since the fuel consumption and emissions for the second and fourth sections are so similar, in practice fuel economy calculations multiply the second section fuel consumption by two to reduce testing time. The total fuel energy consumed is calculated according to the following formula:

$$Q_{tot} = Q_1 + 2Q_2 + Q_3 \quad (33)$$

Note that this formula is not strictly accurate, as the US EPA regulations in fact weight the fuel consumed during Sections 3 and 4 slightly higher than the fuel from Sections 1 and 2. However, the relative weighting factors are not large enough to significantly impact the analysis laid out in this section.

Comparing the total fuel consumed during the first and third sections of the FTP allows for calculation of ΔQ_{LO}, the fuel penalty during cold start:

$$\Delta Q_{LO} = Q_1 - Q_3 \quad (34)$$

The increased fuel consumption during cold start is not entirely caused by the catalyst heating strategy; higher friction due to cold vehicle components and lubricants also contributes to the cold start fuel penalty [282]. However, there have not been detailed analyses of the relative contributions of catalyst heating and friction published in the open literature, so for this analysis it is assumed that all of the cold start fuel penalty prior to catalyst light-off (roughly 120 sec) is due to the catalyst heating strategy [282]. Substituting the expression for cold start penalty into the formula for total fuel consumed during the FTP cycle gives:

$$Q_{tot} = \Delta Q_{LO} + 2Q_2 + 2Q_3 \quad (35)$$

Next, $\overline{\Delta q}_{LO}$ is defined as the average difference between the cold-start fuel consumption rate and the hot-start fuel consumption rate, which is calculated by dividing the total fuel penalty during cold start (ΔQ_{LO}) by the time to achieve catalyst light-off (t_{LO}):

$$\overline{\Delta q}_{LO} = \frac{\Delta Q_{LO}}{t_{LO}} \quad (36)$$

Changing the fuel composition will change the composition and concentration of the unburned and partially burned organic gases emitted from the engine. Since different organic gases can have different catalytic reactivities, changing fuel composition can raise or lower the light-off temperature of the TWC. Shifting the light-off temperature would change the time required to reach light-off,

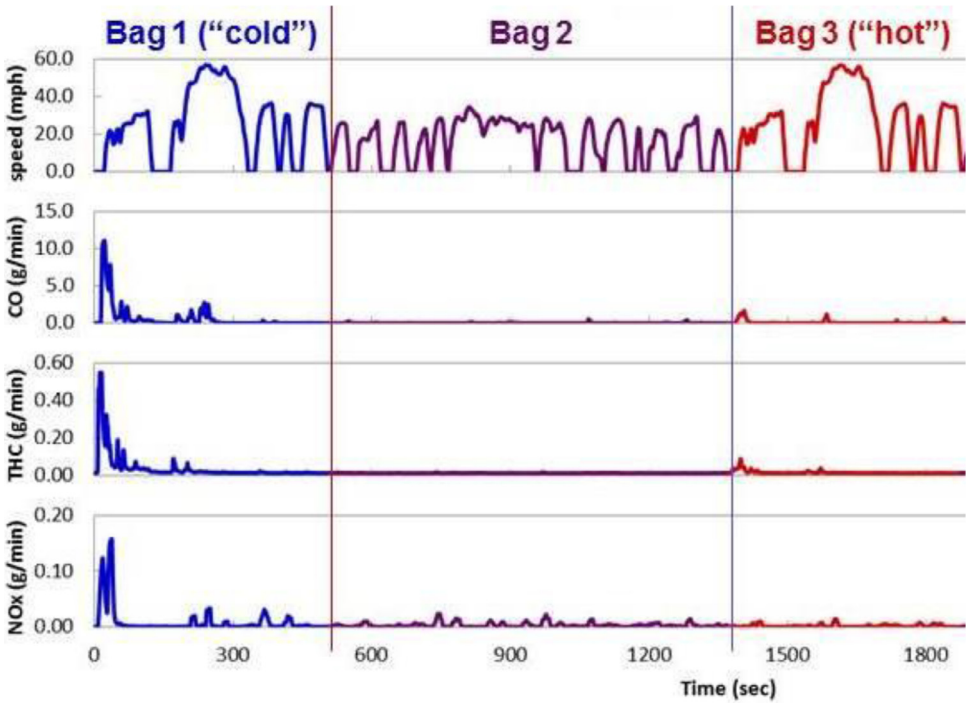

Fig. 44. FTP time traces for vehicle speed and regulated gaseous emissions. Data were collected with a 2013 Ford Focus ST on a chassis dynamometer. Reprinted from Pihl *et al.* [282] with permission of SAE International.

and, therefore, the fuel penalty associated with catalyst heating. Note that a reduced light-off temperature could be leveraged to provide several different benefits to an automaker: the aforementioned reduced catalyst heating fuel penalty, lower overall emissions, lower cost emissions control catalysts, or some combination of all of these benefits. Predicting how automakers would actually make use of a lower light-off temperature is beyond the scope of this analysis. Since the intent of this section is to link emissions control performance back to the merit function, which is based on fuel efficiency, it is assumed that a reduced light-off temperature would be used to decrease the fuel penalty for catalyst heating.

To obtain an expression relating the time to light-off with the light-off temperature, we start with the observation that the catalyst temperature continuously increases with time during cold start[284] from ambient temperature, T_{amb}, to the light-off temperature $T_{c,90}$. If α is defined as the average catalyst heating rate:

$$\alpha = \frac{T_{c,90} - T_{amb}}{t_{LO}} \tag{37}$$

then the time to light-off can be calculated from the catalyst light-off temperature:

$$t_{LO} = \frac{1}{\alpha}(T_{c,90} - T_{amb}) \tag{38}$$

Substituting Eq. 38 into Eq. 36 yields the following expression for the light-off fuel penalty:

$$\Delta Q_{LO} = \overline{\Delta q}_{LO}\frac{1}{\alpha}(T_{c,90} - T_{amb}) \tag{39}$$

and the total fuel consumed during the FTP can be calculated from:

$$Q_{tot} = \overline{\Delta q}_{LO}\frac{1}{\alpha}(T_{c,90} - T_{amb}) + 2Q_2 + 2Q_3 \tag{40}$$

To place the cold start fuel penalty in the same functional form as the other merit function terms, it must be translated to an engine efficiency. Since exhaust emissions are measured on a drive cycle, one way to define efficiency is the ratio between the total amount of work done over the drive cycle and the total fuel energy consumed over the drive cycle:

$$\eta = \frac{w_{tot}}{Q_{tot}} \tag{41}$$

The change in efficiency due to a change in catalyst light-off temperature can be expressed as:

$$\frac{1}{\eta}\frac{\partial \eta}{\partial T_{c,90}} = \frac{1}{\eta}\frac{\partial}{\partial T_{c,90}}\frac{w_{tot}}{Q_{tot}} = \frac{Q_{tot}}{w_{tot}}w_{tot}\frac{\partial}{\partial T_{c,90}}\frac{1}{Q_{tot}} = -\frac{1}{Q_{tot}}\frac{\partial Q_{tot}}{\partial T_{c,90}} \tag{42}$$

Note that this derivation relies on the fact that the total amount of work done over the FTP cycle is always the same for a given vehicle, as the test protocol defines the speed/load profile. Substituting the expression for Q_{tot} that was derived above yields:

$$\begin{aligned}\frac{1}{\eta}\frac{\partial \eta}{\partial T_{c,90}} &= -\frac{1}{Q_{tot}}\frac{\partial}{\partial T_{c,90}}\left(\overline{\Delta q}_{LO}\frac{1}{\alpha}(T_{c,90} - T_{amb}) + 2Q_2 + 2Q_3\right) \\ &= \frac{-\overline{\Delta q}_{LO}}{Q_{tot}}\frac{1}{\alpha}\frac{\partial}{\partial T_{c,90}}(T_{c,90} - T_{amb})\end{aligned} \tag{43}$$

Since catalyst light-off temperature will depend on the catalyst formulation and catalyst age in addition to the fuel composition, it is important to normalize for these effects. Thus, the change in efficiency with catalyst light-off temperature for a new fuel mixture should be evaluated relative to the light-off temperature of a baseline fuel over the same catalyst. Evaluation of Eq. 43 for two fuels (designated as "conv" for conventional and "mix" for a new fuel mixture) yields the final Eq. for the catalyst light-off merit function term:

$$\frac{1}{\eta}\frac{\partial \eta}{\partial T_{c,90}} = \frac{\overline{\Delta q}_{LO}}{Q_{tot}}\frac{1}{\alpha}(T_{c,90,conv} - T_{c,90,mix}) \tag{44}$$

4.1.2. Evaluation of the gaseous emissions merit function term

There are two constant parameters in the merit function term: the fractional increase in fuel consumption rate during cold start, $\overline{\Delta q}_{LO}/Q_{tot}$, and the catalyst heating rate, α. Both of these terms can

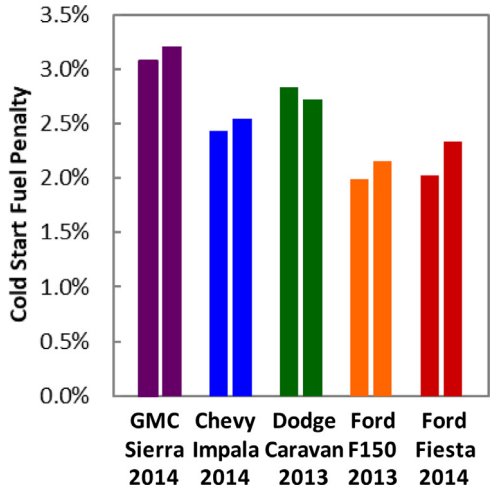

Fig. 45. Duplicate tests of the calculated cold start fuel penalty for several vehicles. Reprinted from Pihl *et al.* [282] with permission of SAE International.

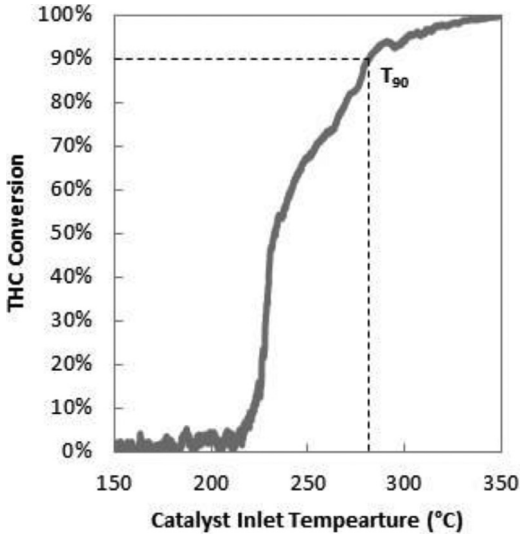

Fig. 46. Light-off curve for an E10 surrogate fuel mixture (10% ethanol, 25% toluene, 65% iso-octane by volume) measured over an aged TWC in a synthetic exhaust flow reactor according to a protocol [287] developed by the U.S. DRIVE Advanced Combustion and Emission Control Technical Team. Reprintedfrom Pihl *et al.* [282] with permission of SAE International.

be extracted from FTP data; detailed analysis can be found in Pihl *et al.* [282]. Briefly, the fractional increase in fuel consumption rate during cold start can be evaluated through the definition of $\overline{\Delta q_{LO}}$ in Eq. 45:

$$\frac{\overline{\Delta q_{LO}}}{Q_{tot}} = \frac{1}{t_{LO}} \frac{\Delta Q_{LO}}{Q_{tot}} = \frac{1}{120\ s} 2\% \tag{45}$$

where $\Delta Q_{LO}/Q_{tot}$ is the total cold start fuel penalty and t_{LO} is the light-off time. A typical light-off time is 120 s; Fig. 45 shows that an average cold start fuel penalty is roughly 2%.

Evaluation of the heating rate term requires the light-off time (120 s) as well as the difference between the light-off temperature and ambient temperature. Ambient temperature for the FTP test is 25 °C. TWC light-off temperature will depend on catalyst formulation, catalyst age, and fuel composition. Typical gasoline constituents light-off between 250 °C and 300 °C under realistic exhaust mixtures over commercially relevant TWCs. The light-off curve for an E10 surrogate measured in a synthetic exhaust flow reactor over an aged commercial TWC is shown in Fig. 46.

The $T_{c,90}$, or temperature at which 90% of organic gases are converted, of roughly 275°C is consistent with light-off temperatures measured with other gasoline constituents over relevant TWCs [288]. Combining this light-off temperature with the time to achieve light-off from the vehicle FTP data sets allows estimation of the catalyst heating rate. Evaluating Eq. 37:

$$\alpha = \frac{T_{c,90} - T_{amb}}{t_{LO}} = \frac{275\ C - 25\ C}{120\ s} = \frac{250\ C}{120\ s} \tag{46}$$

Inserting the estimated values in Eqs. 45 and 46 into Eq. 44 and multiplying the constants yields the final form of the gaseous emission control term for the merit function:

$$\frac{1}{\eta}\frac{\partial \eta}{\partial T_{c,90}} = \frac{2\%}{120\ s}\frac{120\ s}{250\ C}(T_{c,90,conv} - T_{c,90,mix})$$
$$= 0.008\frac{\%}{C}(T_{c,90,conv} - T_{c,90,mix}) \tag{47}$$

Based on the analysis and assumptions described above, and detailed by Pihl *et al.* [282], the merit function term associated with gaseous emissions control simplifies to a difference between the catalytic light-off temperatures of a candidate fuel ($T_{c,90,mix}$) and a conventional fuel ($T_{c,90,conv}$). The light-off temperatures for candidate fuels can be measured through several different methods. A method using synthetic exhaust flow reactor experiments is described by Majumdar et al. [289]. Fig. 47 shows the light-off temperatures for a wide range of both conventional and potential high-performance biomass-derived fuel constituents. Measurements such as these can be used to evaluate the gaseous emissions merit function term.

4.2. Particulate Emissions

The combustion of fuel in engines produces PM, a regulated pollutant that can be both physically and chemically heterogeneous material. It may consist of soot (i.e. black carbon or elemental carbon, which is referred to here as PM_{soot}), unburned or partially oxidized hydrocarbons (i.e. organic carbon), and/or ash (inorganic material) [290].

4.2.1. PM emissions regulations

Light-duty gasoline DI vehicles have been in commercial production since the late 1990s [188,291] and, in 2016, reached 50% of new market share for passenger cars in the US fleet. Gasoline DI engines tend to produce more PM on a mass basis than their PFI counterparts [292–296]; PM levels of early gasoline DI vehicles exceeded those of diesels equipped with diesel particulate filters and conventional PFI vehicles [297]. Because of the impact of mobile sources on air quality, any large-scale change in engine technology and fuel may have far-reaching effects. As ambient air standards for fine PM decrease, direct emissions of PM from gasoline DI vehicles may affect the air quality attainment status of some regions.

Regulation of PM from US mobile sources began in the 1980s as part of the Tier 0 emission standards and continued with stricter emission standards under the Tier 1 regulation, which started phase-in with model year 1994 [298]. While both Tier 0 and Tier 1 passenger vehicle emission standards were applied to all light-duty vehicles regardless of fuel, there was an exclusion in which the PM emission standard was only applicable to diesel vehicles [298]. However, this was not the case with the Tier 2 PM emission standards for passenger vehicles that were phased in between model years 2004 and 2009. All Tier 2 gasoline light-duty vehicles were required to meet a 10 mg/mile PM standard over the FTP drive cycle, at a full useful life of 120,000 miles, and on an individual vehicle basis rather than a fleet average basis [299,300]. Limited data are available on PM emissions from vehicles certified under the Tier 2 standards due to a waiver of PM emission testing

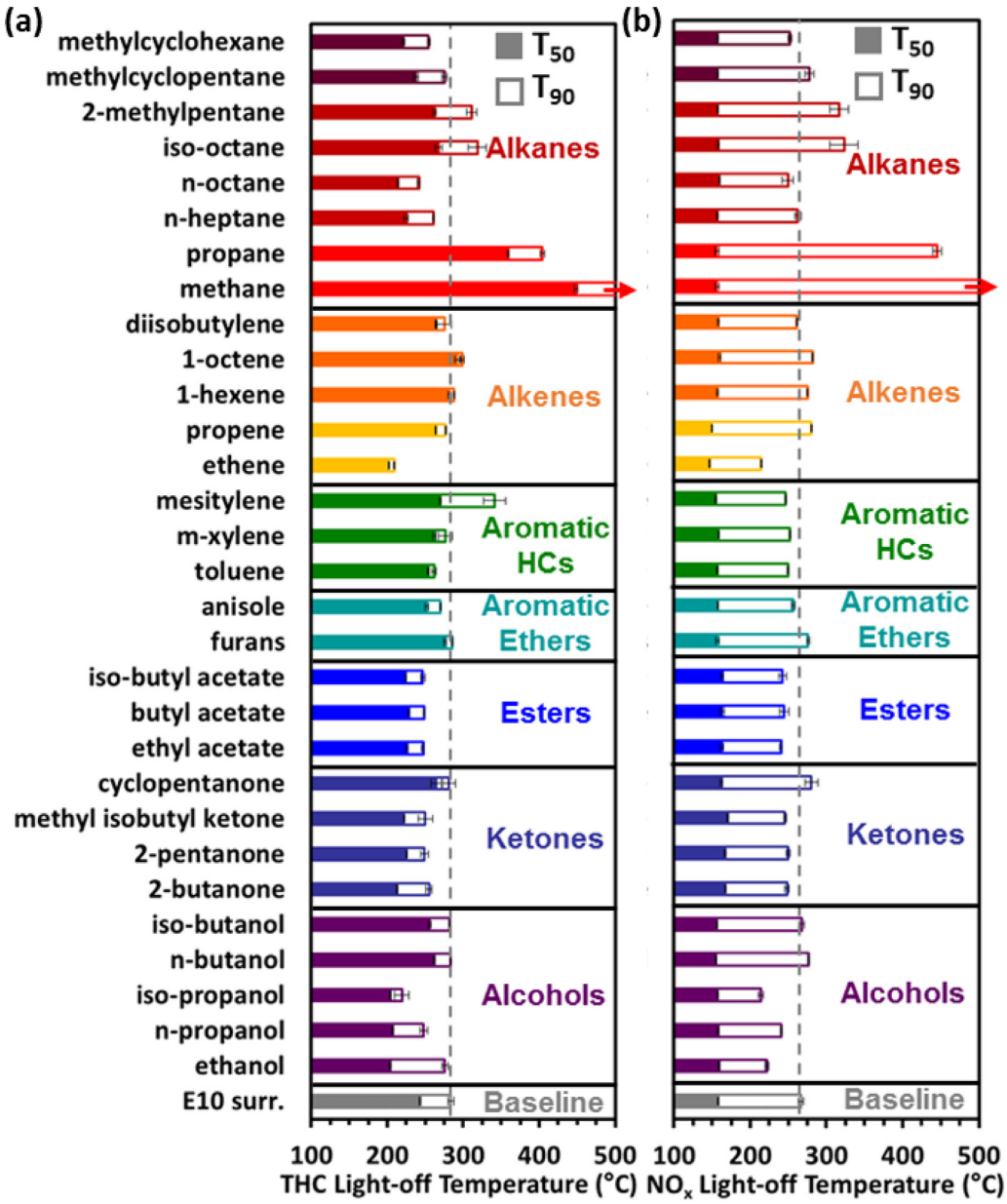

Fig. 47. Comparison of T_{50} and T_{90} catalyst light-off temperature for (a) hydrocarbons (THC) and (b) NOx. Feed conditions: 13% CO_2, 13% H_2O, 5000 ppm CO, 1000 ppm NO, 1670 ppm H_2, 3000 ppm C1, O_2 to achieve $\lambda = 0.999$. Reprinted from Majumdar *et al.* [289] with permission of Elsevier.

requirements [299]. This testing waiver was not extended to EPA's Tier 3 PM regulation, which applies to all vehicles, phases in between 2017 and 2020, and has a limit of 3 mg/mile over the FTP drive cycle [301]. California's Air Resources Board (CARB) plans to phase in a stricter LEV III regulation of 1 mg/mile between model years 2025 and 2028 [302]. Historically, EPA often follows CARB's lead on emission regulations. Therefore, if PM regulations follow historical trends, the EPA may adopt the 1 mg/mile standard sometime after 2025. Thus, the 1 mg/mile PM standard will be used as a basis for evaluating the PM Control term for the merit function.

In Europe, there has been additional concern about particle number (PN) emissions from mobile sources. The Euro 6 standards, which were implemented beginning in 2015 [303], were widely regarded as a technology-forcing regulation for diesel vehicles due to the incorporation of a PN standard. Previously, many heavy-duty and light-duty diesel vehicles had used in-cylinder methods such as advanced timing and high-pressure injection to control PM to below the standard and then applied aftertreatment to meet the NOx standard. The Euro 6b regulation specified that PN emissions > 23 nm in diameter must be below 6×10^{12} particle #/km as measured by the Particulate Measurement Protocol by 2016, and then 6×10^{11} #/km by 2019 (Euro 6c) [303]. Of particular interest to this analysis, the PN standard only applies to diesel-fueled vehicles and gasoline-fueled vehicles equipped with DI engines. Researchers [304–306] have seen a strong correlation between PN and PM mass for solid particles (e.g. 2×10^{12} #/mg [306]) and found that the newest Euro 6 b, c, and d PN standard of 6×10^{11} #/km represents about one order-of-magnitude lower PM mass emissions than the Euro 6 b, c, and d PM mass standard requires (0.3 vs. 4.5 mg/km). Therefore, for a vehicle to meet the PN standard, its PM mass must be an order-of-magnitude less than is required by the current PM mass standard.

4.2.2. Methods for controlling PM Emissions from gasoline DI Engines

There are two predominant pathways to complying with PM and/or PN emissions regulations: using a gasoline particulate filter (GPF) and reducing the generation of particles in-cylinder. PM filtration technology has proven to be an effective means to remove particles from the exhaust for diesel engines, with Platt *et al.* reported that the PM emissions from diesel vehicles equipped with PM filters are significantly lower than gasoline DI vehicles that do not use GPFs. GPF technologies are currently being deployed in both Europe and China as a way to reduce PM emissions from SI engines, and vehicles using GPFs to comply with PN regulations emit orders of magnitude lower particles than allowed by the regulations [307]. Thus, it is clear that GPFs are a highly effective technology that is rapidly maturing, and will continue to be considered as a method to achieve PM mass and PN emissions compliance with the increasingly stringent standards motivated by PM health concerns [308]. However, as will be discussed and quantified in Section 4.2.4, a GPF introduces backpressure on the engine, creating a thermodynamic penalty. Thus, if it can be avoided, a GPF is not the preferred route for PM emissions control.

A second way to control PM emissions is to improve combustion system performance through better fuel-air mixture preparation. PFI engines generally have lower PM emissions than gasoline DI engines because more time is available for evaporation. Furthermore, the DI spray can contact combustion chamber surfaces under some conditions, which inhibits fuel evaporation, whereas PFI spray typically has reduced interaction with the combustion chamber surfaces. Continued development of gasoline DI combustion systems is reducing PM emissions, and the improvements will probably allow most vehicle manufacturers to meet EPA's PM regulation of 3 mg/mile without a GPF. A recent technology assessment by CARB predicts that vehicle manufacturers will meet their 1 mg/mile PM regulation primarily through improved combustion systems [309]. Minimizing PM formation in gasoline DI engines depends primarily on avoiding liquid fuel deposition on combustion chamber surfaces and on achieving rapid spray breakup, evaporation and air mixing. Examples of technology improvements toward these objectives include:

- piezoelectric injectors that allow multiple, shorter injections, which reduce spray penetration length and spray impingement on combustion chamber surfaces [310];
- intake ports and combustion chambers designed for better mixing that further reduce spray impingement;
- higher fuel pressures coupled with injector nozzles that improve spray breakup and resist deposit formation [311,312]; and
- dual injection systems that feature both direct and port injectors, which enable more flexible engine calibrations to reduce PM emissions under conditions where DI injectors alone are challenged, such as cold start and acceleration [313–315].

Higher injection pressures may reduce PM formation, but they can also reduce engine efficiency due to increased parasitic losses. For instance, Husted *et al.* [316] estimated an associated fuel-economy penalty of roughly 0.4% on the new European driving cycle if the injection pressure was increased from 100 bar to 400 bar across the speed and load range. However, for a more optimal implementation (and to reduce the fuel penalty), the fuel pressure would be modulated for operating conditions that do not require high fuel mass flow rates and/or enhanced spray breakup.

4.2.3. Fuel effects on PM emissions

A third way to reduce PM emissions is through improved fuel properties and fuel chemistry. The PMI of gasoline, previously shown in Eq. 31, has been shown to correlate well with PM mass and PN emissions trends in PFI engines as well as DI engines [280,317]. Depending on the regulatory transient drive cycle, PM emissions can increase several times over for a unit increase in PMI. PMI is based on the detailed hydrocarbon analysis of the gasoline, from which two properties of the individual components (DBE and VP) are applied and summed to calculate PMI [280]. It is noteworthy that, since PMI was first developed, a modification to the detailed hydrocarbon analysis method has been developed as a way to provide more resolution to the heavy end of the gasoline boiling range to provide more accurate PMI numbers [318].

DBE is intended to capture the tendency of highly unsaturated compounds such as aromatics to form more soot than saturated compounds such as alkanes. In the PMI calculation, shown in Eq. 31, DBE+1 is used as the intrinsic chemical sooting tendency of the molecule – arbitrarily assigning a value of 1 to all normal and iso-alkanes. The VP, computed at 443 K for each component, represents the tendency of less volatile compounds to resist evaporation and therefore experience rich combustion that forms soot. However, while PMI has shown good correlation with PM emissions for a range of commercial gasolines [293], the presence of oxygen in the fuel can affect the tendency of the fuel to make PM.

A recent study by Barrientos *et al.* [319] compared PMI with other indices of fuel PM potential. These included Threshold Sooting Index and Oxygen Extended Sooting Index, using one set of fuels reported by Aikawa *et al.* [280], as well as a series of gasoline blends with ethanol, n-butanol, and isobutanol. The general finding was that none of the alternative indices improved upon PMI for the prediction of PM emissions over various vehicle test cycles. Another study, by Ratcliff *et al.* [320], used a wider range of oxygenates blended into gasoline and showed that the PMI model can break-down in cases of (1) oxygenates with facile routes to soot not available to hydrocarbons (underpredicted PM_{soot}) and (2) oxygenates with very low vapor pressure (overpredicted PM_{soot}). Combustion of low-vapor-pressure hydrocarbons may similarly lead to overpredicted PM, and the hypothesized mechanism would involve substantially incomplete evaporation, leading to dissolution into the lube oil, or potentially carbonaceous deposits in the combustion chamber.

Research with a single-cylinder gasoline DI engine using a full factorial design fuel matrix [321] suggests there is a vapor pressure threshold for aromatic hydrocarbons, below which they can produce significant increases in PM emissions when the fuel blend also contains ethanol and at injection timing intended to cause spray impingement on the piston. However, ethanol blending also dilutes aromatics in gasoline on a molar basis, even when aromatics are held volumetrically constant, as was the case in reference [321]. Molar dilution occurs because ethanol's molecular weight (46) is approximately half the averaged molecular weight of gasoline, and only 31% to 38% that of the aromatics used in this study. Thus, the effects on aromatic vapor pressure and aromatic dilution from ethanol blending are in competition. For example, Fig. 48 shows that, at 2500 rpm and 13 bar $IMEP_n$, blends of E30 containing 10 or 20 vol % of low-vapor-pressure 4-t-butyltoluene (VP @ 443 K = 58 kPa) in gasoline produced significant increases in PM_{soot} relative to the matching blends having no ethanol. In contrast, for similar blends containing 10 or 20 vol % of the more volatile aromatic cumene (iso-propylbenzene; VP @ 443 K = 152 kPa), the dilution effect of ethanol prevailed, resulting in slightly lower or equivalent PM_{soot} emissions from the E30 blends. Thus, cumene appears to be above the vapor pressure threshold for ethanol to negatively affect PM_{soot}, while 4-t-butyltoluene is below the vapor pressure threshold. PM mass in Fig. 48 is PM_{soot}, as measured by an AVL Microsoot Sensor (MSS).

Across the designed fuel matrix, PMI was poorly predictive of PM emissions with an adjusted R^2 ranging from 0.53 to 0.74 for different engine test conditions. Characterization of the fuel blends by the advanced distillation curve method [322] revealed that ethanol blending suppressed the evaporation of aromatic hy-

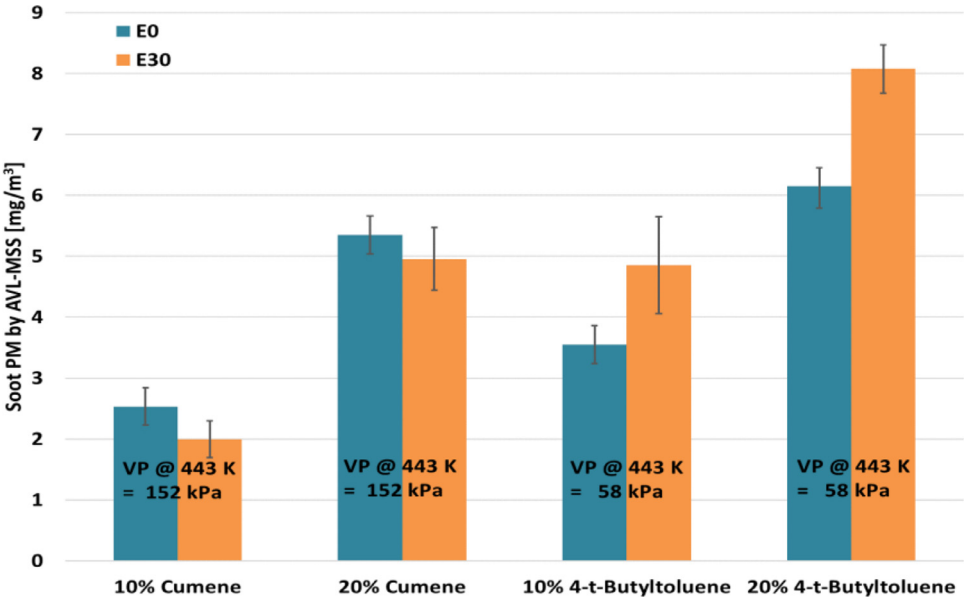

Fig. 48. Comparison of PM_{soot} emissions at 2500 rpm and 13 bar $IMEP_n$ from blends of aromatic hydrocarbons gasoline, with and without ethanol using data from Ratcliff *et al.* [321]. PM_{soot} measured by an AVL Microsoot sensor (MSS).

drocarbons in gasoline until all the ethanol evaporated [323,324]. The aromatic concentration effect was also observed in fuel spray droplet evaporation simulations under engine-relevant temperature and pressure conditions. The models also demonstrated that ethanol blending significantly reduced the droplet temperature because of ethanol's higher HoV, prolonging droplet lifetime. The increased PM emissions that were observed for the E30 + 4-t-butyltoluene blends can be attributed to the combined effects of suppression of aromatic vaporization and longer droplet lifetimes, in conjunction with postulated increased fuel spray impingement. These distillation and droplet evaporation results suggested some nonlinear interactions between ethanol and the aromatics. The LASSO method [325] was used to identify two predominant combined variable terms, shown in this Eq.:

$$PM = X1 + X2 * [(EtOH\% * Aro\%)/AroVP@443K] + X3 * [(AroYSI * Aro\%)/AroMW] \quad (48)$$

where ethanol (*EtOH*) and aromatic (*Aro*) concentrations are in mole percent,

VP@443 K is the vapor pressure at 443 K,

YSI is the yield sooting index, and

MW is the molecular weight.

YSI is a metric for the intrinsic soot-forming tendency of individual fuel molecules, as measured by color pyrometry for low concentration, constant-mole-fraction blends of the molecules in a methane/air flame [326]. The first combined variable term in Eq. 48 represents the delaying effects on aromatic evaporation caused by ethanol blending and aromatic vapor pressure; the second combined variable term reflects the kinetic tendency of the aromatic to form soot. Using this regularized regression model results in an adjusted R^2 of 0.96 for predicting PM from the fuel matrix [321]. More research is required to incorporate these improved terms into a generalized model such as PMI. Therefore, the merit function developed in this work continues to rely upon the PMI model as the most established approach currently available.

The PM emissions from several different fuel blends, including the Co-Optima core fuels described in Section 3 [144], were measured as part of the Co-Optima initiative. Steady-state conditions were employed, and exhaust PM_{soot} was measured with an AVL model 415S smoke-meter, which reports both native Filter Smoke Number as well as PM_{soot} concentrations calculated from the filter blackening using a built-in correlation that assumes a constant relationship between optical properties and PM_{soot} regardless of the fuel used. The emissions trends, both in terms of PM_{soot} and smoke, are plotted in Fig. 49. To first order, the data show a linear relationship between PMI and PM_{soot} for these steady-state conditions.

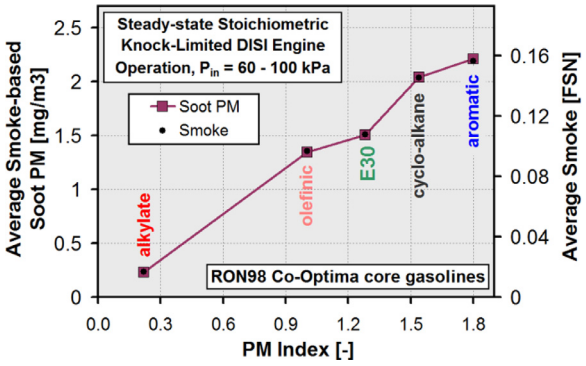

Fig. 49. Steady-state engine-out PM data for Co-Optima Core Fuels (FSN: AVL Filter Smoke Number) corresponding to the engine tests reported in Vuilleumier *et al.* [171].

Because cold start accounts for much of the total PM emitted by gasoline DI vehicles during the FTP [297, 327], cold-start PM emissions were examined as part of the Co-Optima initiative for a fuel matrix that included the Co-Optima core fuels discussed in Section 3 [144] as well as six blends based on the same blendstock for oxygenate blending (BOB) that was used to make $E30_{Co\text{-}Optima}$. The six blends based on the $E30_{Co\text{-}Optima}$ BOB included the BOB by itself, the BOB with 10 vol % EtOH (E10), $E30_{Co\text{-}Optima}$, and three blends that contained the BOB with 10 vol % EtOH + 20 vol % of other oxygenates (total 30 vol % oxygenate). Fig. 50 shows the formulation of each fuel and the chemical structures of the oxygenates studied. For comparison, a US Tier III regular grade certification E10 fuel was also studied.

Cold-start behavior was studied using a reproducible 90 s cold-start idle transient run on an engine start-cart that included a 2012

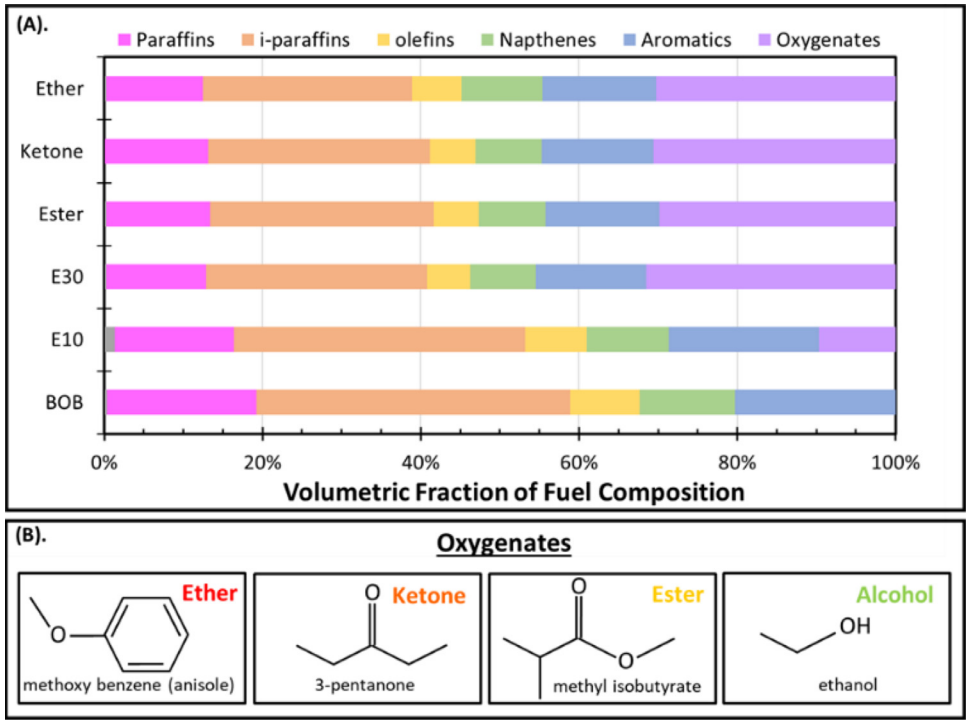

Fig. 50. (A). The volumetric composition of the five oxygenated fuels blended with the BOB (also shown) used to mix the Co-Optima E30 core fuel. (B). Chemical structures of the four oxygenate compounds used in the fuel blends. Oxygenate used in both $E30_{Co\text{-}Optima}$ and E10 fuels is the alcohol, ethanol from Moses-DeBusk *et al.* [328].

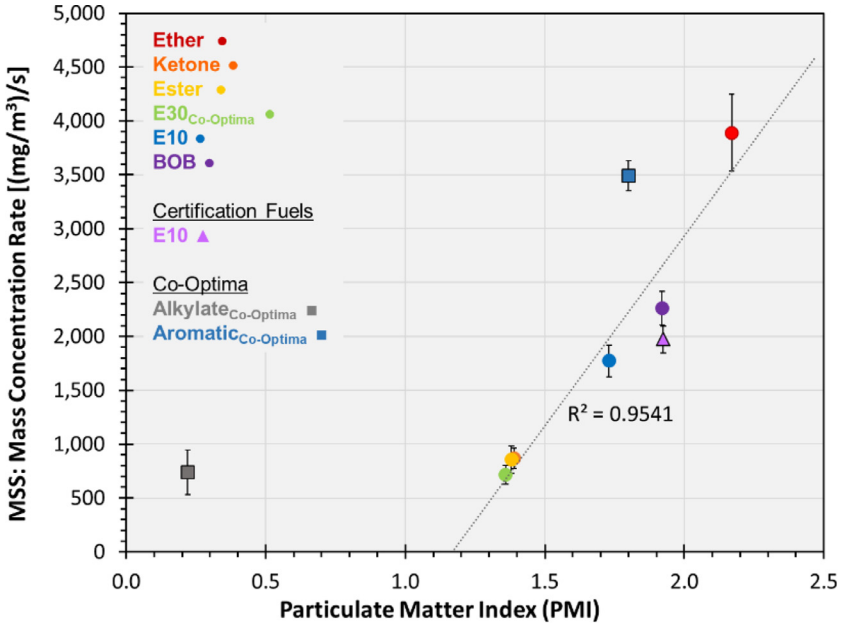

Fig. 51. Graph showing the correlation of fuel PMI value with the mass concentration rate of PM_{soot} generated during a cold start idle transient. The average value calculated from AVL- Microsoot Sensor data collected for six cold starts per fuel is plotted with error bars representing standard deviation of the six starts. The legend shows the fuel data color coding. The trend line and its R^2 value are for the six fuels described in Fig. 50 and omits $Co\text{-}Optima_{Alkylate}$, $Co\text{-}Optima_{Aromatic}$, and the Tier III regular grade certification E10. Error bars represent the standard deviation calculated from 18 cold-start idle transients from data presented by Moses DeBusk *et al.* [328].

2.0 L Ford Ecoboost engine, modified with forced cooling to enable multiple cold starts per day [328]. An AVL Microsoot Sensor was used to monitor the PM_{soot} emissions during the first 90 s of a cold start and idle transient. The results are plotted in Fig. 51 in terms of the mass concentration rate of PM_{soot} over the cold start idle transient. The correlation of PMI with cold start PM_{soot} emissions for the five blends and the BOB is quite good, although the PM_{soot} for $aromatic_{Co\text{-}Optima}$ and $alkylate_{Co\text{-}Optima}$ fuels appear to be higher than expected, indicating that other factors may be at work during cold start.

4.2.4. Particulate matter impact on engine thermodynamics

Adding a GPF to the exhaust system can degrade SI engine efficiency because a GPF increases back pressure, which increases pumping work. Increased back pressure could also require spark retard or lower r_c, both of which would decrease efficiency, to compensate for an increased knock propensity due to an increase

in trapped residuals. However, recent studies indicate that the impact of a GPF on vehicle fuel consumption over regulatory drive cycles is minor [329–332]. Yang *et al.* showed that there was no statistically significant difference [333]. Thus, the effects of increased back pressure and more frequent application of spark retard may be tempered by the fact that most drive cycles include substantial operating time at conditions of low exhaust flow rate that are not knock-limited.

As discussed in Section 4.2.2, there is currently a significant amount of uncertainty whether compliance with PM emissions regulations will necessitate using a GPF. There could be different regional outcomes, where they are used in some countries or regions and not others, depending on regulations. As discussed in Section 4.2.3, Eq. 48 improved PM emissions predictions compared to PMI (Eq. 31) by including terms for YSI and the interactions between ethanol and aromatics. However, Eq. 48 is based on a study with single specific aromatics blended into an otherwise highly paraffinic gasoline and were investigated under a specific set of engine operating conditions. Therefore, its present form does not have the general utility of PMI, which sums relevant property values from each gasoline component. Consequently, PMI is used here to predict PM effect on engine efficiency in the merit function. This section develops a framework to account for the effect of fuel properties, specifically PMI (Eq. 31), on engine thermodynamics and assumes that there is a threshold value of PMI over which a GPF will be required.

The presence of a GPF—as well as the degree to which it is loaded with PM—increases the exhaust back pressure and thereby decreases η_{GE}. The increased back pressure also increases the mass of hot residual gas retained in the cylinder after the exhaust stroke. The increased hot residual gas increases the engine's propensity for knocking, which would likely require retarded spark timing (decreased σ_{ideal}) or, in extreme cases, a decrease in r_c (decreased η_{ideal}). The trend of the PM_{soot} generation propensity for a given set of fuels is reasonably well captured by PMI [280], although more robust properties are being developed. Since the effect of PM on efficiency depends on whether a GPF is installed on the engine, it is assumed that a GPF will be necessary when the fuel's PMI exceeds some threshold value. These effects and relationships are described by the following Eq.:

$$\frac{1}{\eta_b}\frac{\partial \eta_b}{\partial PMI_{mix}} = -H(PMI_{mix} - PMI_{threshold})\frac{1}{\eta_b}\left(\frac{\partial \eta_b}{\partial \eta_{GE}}\frac{\partial \eta_{GE}}{\partial P_{ex}}\frac{\partial P_{ex}}{\partial PMI_{mix}} + \frac{\partial \eta_b}{\partial \sigma_{ideal}}\frac{\partial \sigma_{ideal}}{\partial P_{ex}}\frac{\partial P_{ex}}{\partial PMI_{mix}} + \frac{\partial \eta_b}{\partial \eta_{ideal}}\frac{\partial \eta_{ideal}}{\partial r_c}\frac{\partial r_c}{\partial P_{ex}}\frac{\partial P_{ex}}{\partial PMI_{mix}}\right) \quad (49)$$

where H is the Heaviside step function: $H(x) = \begin{cases} 0, & x < 0 \\ 1, & x \geq 0 \end{cases}$

Eq. 49 does not consider any fuel economy penalty associated with engine operation to regenerate the particulate filter.

At this time, no definitive study has been identified from which we can conclude or deduce that current technology DI vehicles, tested with gasoline having a PMI greater than a given threshold, will require a GPF to meet a given emission regulation. The limited data available [280,317] suggest that a very low PMI of about 1 is required for a DI vehicle to meet 1 mg/mile of PM without a GPF with current production technology. Given that almost no retail gasolines have PMI values that low [280], we might conclude that all vehicles will require a GPF. However, the referenced studies used early DI technology and engine manufacturers are continuing to improve the combustion systems to minimize PM formation.

Similar to the fuel effect on LSPI, the PM Control term in the merit function is also based on the Heaviside function, $H(x)$. In this case, the presumptions are that, given a PM emission regulatory target and some state of DI combustion system development to control PM, a fuel property that quantifies soot-forming potential can be used to trigger the step function. The PM Control merit function term is

$$\frac{1}{\eta_b}\frac{\partial \eta_b}{\partial PMI_{mix}} = -H(PMI - 1.6)\left[0.7 + 0.5\left(PMI - PMI_{Ref}\right)\right] \quad (50)$$

where the fuel property *PMI* is the step function trigger. If $PMI < 1.6$, then $H(x) = 0$, meaning that no GPF is required and engine efficiency is not degraded. If $PMI \geq 1.6$, then $H(x) = 1$ and engine efficiency is degraded by the amount dictated by the other factors in the PM Control term. Because certification gasoline is used to determine compliance with emission regulations, the literature was surveyed for PMI data of these fuels. PMI values for certification gasolines range from about 1.4–1.8 [280,309,317], from which the mid-point value of 1.6 was selected. Furthermore, 1.6 is in the same PMI range for the soot measurements from the Co-Optima cold-start idle transient study that correlates to an EPA FTP equivalent of 1 mg/mile (see Table 4) [328]. However, there is a significant amount of uncertainty about both future emissions regulations around the world and the potential of future engine technologies to reduce PM emissions. Thus, it is best to consider the PM control merit function term in Eq. 50 as a framework where the threshold value of 1.6 can be updated based on PM emission regulations and engine technology. Note that the value of PMI_{Ref} in Eq. 50 refers to the PMI of the merit function's baseline gasoline (shown in Section 5, Table 5) and is distinct from the PMI value that is the Heaviside step function trigger.

The other factors in the PM control term represent a 0.7% engine efficiency loss from increased back pressure of the GPF (including some lifetime averaged loading of ash) and an additional 0.5% efficiency loss per unit increase in PMI from increased back pressure arising from fuels with PMIs higher than that of the merit function's baseline fuel, which has the value of 1.4 (see Table 5). The analysis of Mamakos *et al.* [332] concluded that, over a vehicle's lifetime, higher back pressure from the GPF increases fuel consumption by 0.5% to 1.5%, plus 0.17% for GPF regeneration, summing to a 0.67% increase in fuel consumption. A study by Mikulic *et al.* [334] reported fuel consumption increases of 2% to 3% at high vehicle speeds. A more recent report by Lambert *et al.* showed that exhaust flow rates of 600 kg/h resulted in back pressures ranging from ~12 to 42 kPa over a variety of fresh and dyno-aged GPFs during clean filtration; however, engine efficiencies were not reported as part of that study [335]. Until more data and analyses are available, we attempt to make a conservative assumption that ash-loaded GPF back pressure will reduce engine efficiency by 0.7% [336]. An efficiency loss for GPF regeneration is not explicitly included because previous studies have shown that regeneration occurs passively during periods of deceleration, when fuel cutoff and throttle control can be used to elevate the oxygen concentration for burning out soot in the GPF [337].

5. The merit function

The purpose of the merit function is to assess the combined ability of a set of fuel properties to improve efficiency relative to a baseline fuel representative of a current "regular" grade gasoline. Initially presented in a US Department of Energy report [139], the merit function is the summation of the individual fuel property effects on efficiency, as discussed in the previous sections, normalized to a relative efficiency improvement. That is, a merit function score of 10 indicates the potential for 10% more work output for a given amount of fuel energy in an optimized engine relative to the baseline fuel (or, an 9.1% decrease in fuel consumption for a given

Table 4
Total mass of soot measured by an AVL microsoot sensor during a 90 s cold-start idle transient test using a start-cart for a series of fuels.

Fuel	*Fuel PMI*	*Flow Corrected Mass*[*] *(mg, PM_{soot})*	*FTP Cold-Start Equivalent*[‡] *(mg/mile)*
E30	1.36	9.09	0.52
Ketone	1.39	10.70	0.62
Ester	1.38	10.95	0.63
E10	1.73	21.83	1.26
E10-cert	1.92	23.59	1.36
BOB	1.92	25.69	1.48
Ether	2.17	39.06	2.25
			y = 1.87x-2.01
			if y =1.0 mg/mile; x = 1.6 PMI

[*] The microsoot sensor mass concentration data was converted to total mass during transient using the fuel flow rate and lambda sensor data.
[‡] An FTP mg/mile was calculated assuming the PM_{soot} measured by the microsoot sensor was the only PM produced during the cold-start portion of the cycle (mg Soot/7.47miles)*0.43.

Table 5
Fuel properties of the baseline E10 gasoline for use in the merit function.

RON	91
MON	83
S_{octane}	8
AKI	87
Ethanol	10 vol %
HoV	415 kJ/kg
S_L	46 cm/s
LHV	42 MJ/kg
PMI	1.4
AFR_{stoich}	14.0
$T_{c,90}$	276°C

Table 6
Realistic fuel property variability for merit function sensitivity analysis.

	Realistic Low Value	Realistic High Value	E85 value
RON [-]	89	102	107
S [-]	0	15	17
HoV [kJ/kg]	350	550	800
SL [cm/s]	43.7	48	52
PMI [-]	0.0	4.0	N/A
TC,90 [°C]	261	291	N/A

work output requirement). The baseline fuel is intended to be representative of a US regular grade gasoline containing 10% ethanol, with baseline fuel properties shown in Table 5.

The complete merit function is expressed in Eq. 51, where units for each term are consistent with Table 5.

$$Merit = 100 * \frac{\eta-\eta_{ref}}{\eta_{ref}} = \frac{(RON[-]-91)}{1.6+0.3*H(PMI-PMI_{LSPI,crit})} - K[-]\frac{(S_{Octane}[-]-8)}{1.6+0.3*H(PMI-PMI_{LSPI,crit})} + \frac{0.085\left[\frac{kJ}{kg}\right]^{-1}\cdot\left(\frac{HoV\left[\frac{kJ}{kg}\right]/(AFR[-]+1)-415[kJ/kg]}{14.0[-]+1}\right)}{1.6+0.3*H(PMI-PMI_{LSPI,crit})} + \frac{HoV[kJ/kg]/(AFR[-]+1)-(415\left[\frac{kJ}{kg}\right]/14.0[-]+1)}{15.3\left[\frac{kJ}{kg}\right]} + \frac{(S_L[cm/s]-46[cm/s])}{5.4\left[\frac{cm}{s}\right]} - H(PMI-1.6)[0.7+0.5(PMI-1.4)] + 0.008[^\circ C]^{-1}(T_{c,90,conv}[^\circ C]-T_{c,90,mix}[^\circ C]) \quad (51)$$

Simplifying Eq. 51 to remove units and combine constants yields:

$$Merit = 100 * \frac{\eta-\eta_{ref}}{\eta_{ref}} = \frac{(RON-91)}{1.6+0.3*H(PMI-PMI_{LSPI,crit})} - K\frac{(S_{Octane}-8)}{1.6+0.3*H(PMI-PMI_{LSPI,crit})} + \frac{0.085\cdot\left(\frac{HoV}{(AFR+1)}-\frac{415}{15.0}\right)}{1.6+0.3*H(PMI-PMI_{LSPI,crit})} + \frac{HoV/(AFR+1)-27.67}{15.3} + \frac{(S_L-46)}{5.4} - H(PMI-1.6)[0.7+0.5(PMI-1.4)] + 0.008\cdot(T_{c,90,conv}-T_{c,90,mix}) \quad (52)$$

While the merit function provides a tool to assess the efficiency potential of individual fuel properties in an SI engine, the merit function needs to be exercised to provide insights about which fuel properties have the largest effect on efficiency and which fuels provide those properties. In this section, the fuel properties will be assessed first through a sensitivity analysis over realistic fuel property ranges, and then with blends with potential alternative gasoline-range fuel components.

5.1. Realistic fuel property ranges for the sensitivity analysis

In order to assess the ranges of fuel properties of interest, we must first quantify realistic ranges of fuel property variability. For the purposes of the sensitivity analysis, the ranges of properties considered primarily consist of limiting the blend concentration of any particular component to 30 vol %, where the balance of the fuel blend would be a petroleum-derived blendstock. It is noteworthy that these assumptions exclude E85, which contains more than 30 vol % ethanol. In the United States, the exact ratio of fuel ethanol to hydrocarbon may vary according to ASTM 5798 that specifies the allowable ethanol content in E85 as ranging from 51 to 83 vol %. For a point of comparison, a separate data point on the sensitivity plots for "E85" is included, assuming the ethanol concentration is 75 vol %. The ranges for each of the ranges are summarized in Table 6, and the justification for each of the fuel property ranges selected is discussed in Section 5.1.1 to 5.1.6.

5.1.1. Realistic range of RON

The lower limit of RON for the sensitivity analysis was selected to be 89, a value that marginally expands the lower limit compared to the value of 89.5 from a market survey of 459 regular-grade gasolines [198]. The upper limit of RON was selected at 102, which is a value that was investigated in a refinery economics study but was found to be marginally beyond what is economically feasible for blending with ethanol at 30 vol % [338]. By comparison, the

RON value for a 75 vol % ethanol blend fuel can be as high as 107 [339].

5.1.2. Realistic range of S_{octane}

The lower limit of S_{octane} for the sensitivity analysis is zero, which is the S_{octane} value of iso-octane. Near-zero S_{octane} can also be found in refinery streams that are primarily alkanes, such as the alkylate refinery stream. An upper limit of 15 is used for this sensitivity analysis. That limit is marginally higher than would be expected for a 30 vol % ethanol blend [208]. By comparison, S_{octane} for a 75 vol % ethanol blend can be as high as 17 [339].

The S_{octane} is also dependent on K value, and for the purpose of this sensitivity analysis, three K values are used in determining the merit function score. The significance of the K factor to the pressure-temperature domain was discussed in Section 3.1.2. While Figs. 16 and 17 illustrated that the pressure-temperature trajectory changes with engine operating condition, thereby changing the K value within a given engine, this analysis is only concerned with the K value at the most knock-limited conditions. This is because the knock-limited engine operating conditions effectively limit r_c and engine efficiency. The upper boundary of K for naturally aspirated engines is K = 0 [185], where the knock-limited cases follow a pressure-temperature trajectory that is close to that of the RON test. Next, lightly boosted engines are represented by K = -0.5, and highly boosted downsized engines are represented by K = -1.25.

5.1.3. Realistic range of HoV

The lower limit of HoV can be assumed to be a petroleum-derived gasoline stream that does not contain any oxygenates, which Chupka *et al.* [207] report to be 350 kJ/kg. The most effective way to vary the HoV over wide ranges, however, is by using an alcohol, such as ethanol. The upper limit can be assumed to be a blended fuel that contains 30 vol % ethanol, which has an HoV of approximately 530 kJ/kg [207]. By comparison, the HoV for 75% ethanol blends is reported to be 800 kJ/kg [339]. When exercising the HoV term in the merit function, the stoichiometric air-fuel ratio can also change and needs to be accounted for, as explained in Section 3.2.1.

5.1.4. Realistic range of flame speed

The selection of upper and lower limits of S_L was done in a three-step manner. First, the fuels that bound the upper and lower flame speed limits were identified by Farrell *et al.* [234], who measured the S_L of a wide variety of chemical structures and identified ethanol as having the fastest flame speed and 1,3,5-trimethylbenzene as having the slowest. However, the quantitative results from that study cannot be used directly because they were collected at elevated pressure and temperature in a spherical combustion vessel. Thus, the second step was to determine S_L of these components at the reference condition of 1 atm and 353 K. For ethanol, which is the upper-bound fuel, an S_L value of 55 cm/s was used [236], and for 1,3,5-trimethylbenzene, an S_L value of 39 cm/s was used [340]. The final step was to assume that the high and low S_L components are blended with the baseline gasoline at a maximum of 30 vol %. Using the methodology from Sileghem *et al.* [236], S_L of the blends were estimated using an energy fraction mixing rule, where flame speed is a linear function of the blend energy of the components. From that we can assume an upper S_L limit of 48.0 cm/s for 30 vol % ethanol and a lower flame S_L of 43.7 cm/s for 30 vol % for 1,3,5-trimethylbenzene. By comparison, using the same methodology, the S_L for a blend containing 75 vol % ethanol is significantly higher at 52.0 cm/s.

5.1.5. Realistic range of PMI

The selection of a lower limit for the PMI term is not required since the merit function term uses a Heaviside function, making fuels with a PMI < 1.6 not contribute to the merit function term. An upper limit to PMI of 4.0 will be used for the merit function sensitivity analysis, which is marginally higher than PMI = 3.86 reported by Aikawa *et al.* [280] as the maximum PMI observed in a global sample of 1445 gasolines. Since the PMI for ethanol as a pure substance is 0.06, E85 will not contribute to an increase in PMI relative to the base fuel. However, as described in Section 4.2, using PMI has shortcomings associated with the sooting tendency of oxygenated fuels.

5.1.6. Realistic range of Tc,90

For the catalyst light-off term of the merit function, the reference fuel has a $T_{c,90}$ of 276 °C. $T_{c,90}$ for liquid-phase pure hydrocarbons and alcohols ranges between 219 °C for iso-propanol to 342 °C for mesitylene [289]. However, follow-on work [341] by the same authors shows that, at a 30 vol % blend level, the light-off behavior of the petroleum-derived blendstock dominates, and addition of up to 30 vol % of other components only varies the light-off behavior within a ± 15 °C range. For the purposes of this sensitivity analysis, we will assume that the $T_{c,90}$ can vary by as much as 20 °C from the baseline fuel, providing low and high limits of 256 °C and 296 °C, respectively. No data are available for the $T_{c,90}$ of a blend of 75 vol % ethanol.

5.2. Merit function sensitivity analysis

Fig. 52 shows the sensitivity of the merit function score as a function of each individual property over their individual ranges and includes data points for E85 when available. This examines variations of each individual term of the merit function in Eq. 51 without considering the contributions from other merit function terms. As described in Section 3.4.4 (Eq.s 32), there is a $PMI_{LSPI,crit}$ threshold above which LSPI becomes too severe and the engine can no longer be downsized. This is represented in Fig. 52 through the use of dashed lines in the first three terms. Additionally, the form used in the merit function assumes a constant linear response for each term. However, there will likely be some degree of diminishing returns for large values, thus the uncertainty in the merit function response increases for large changes in fuel properties relative to the reference fuel. Observations for each fuel property follow in Sections 5.2.1 through 5.2.6.

5.2.1. RON impact on merit function

RON has the largest impact on the merit function of all the fuel properties, with the potential to increase the merit function score by 7.5 points at RON = 102 from this fuel property alone. The dashed line, which represents the RON impact on the merit function if LSPI prevents the downsizing efficiency multiplier from being used, is a minor relative change to the overall RON effect, but is substantial relative to some of the other fuel properties considered. Using E85, the RON component of the merit function is increased by 10 points.

5.2.2. S_{octane} impact on merit function

As was discussed in Section 5.1.2, the impact of S_{octane} was evaluated at three K values for this sensitivity analysis to represent naturally-aspirated engines, lightly boosted engines, and highly boosted engines. Naturally-aspirated engines are represented with K = 0, and for these conditions, S_{octane} does not change the merit function score. Next, lightly boosted engines are represented by K = -0.5, and highly boosted downsized engines are represented by K = -1.25. For conditions where K is negative, a high S_{octane} improves the merit function score. As a result, high S_{octane} benefits highly boosted and downsized engines more than it benefits lightly boosted engines because of their lower K values. For cases where K is negative, S_{octane} represents the second-biggest impact on the

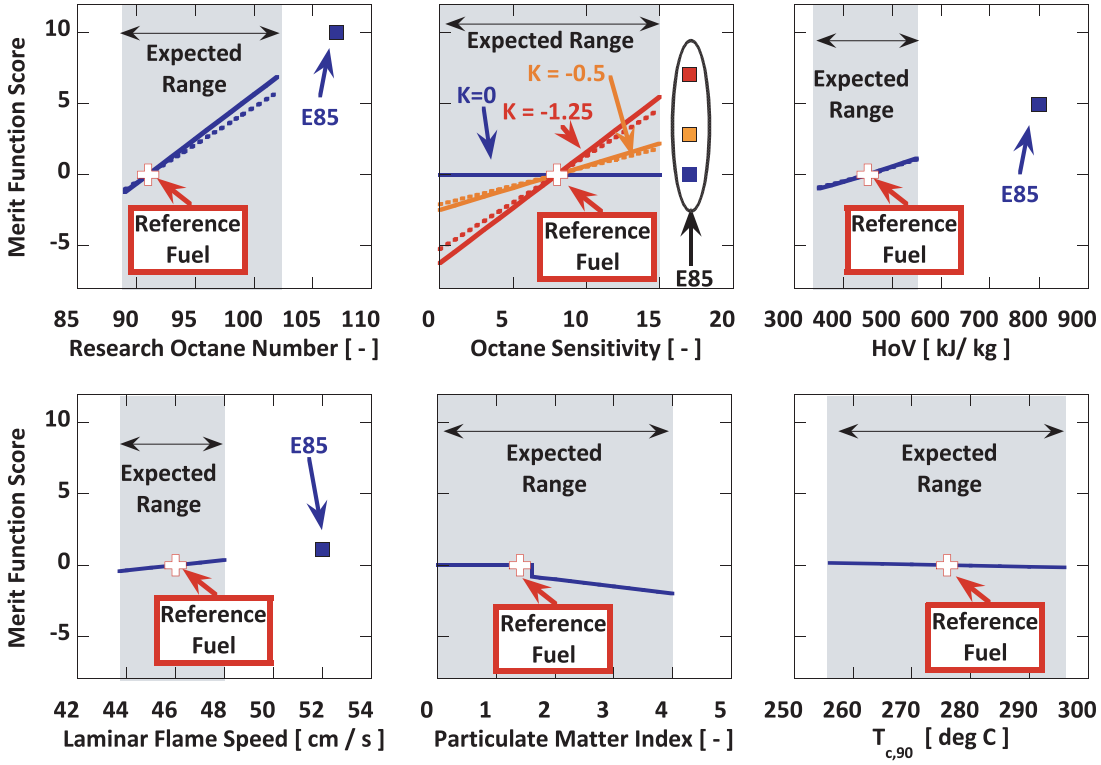

Fig. 52. Sensitivity analysis of the merit function to each fuel property over an expected range of possible variation.

merit function score behind RON. The S_{octane} for the baseline fuel in the merit function score is 8, and S_{octane} values lower than that of the baseline fuel have a substantially detrimental impact on the merit function score when K < 0. The dashed line, which represents the S_{octane} impact on the merit function if LSPI prevents the downsizing efficiency multiplier from being used, is a minor change relative to the overall S_{octane} effect, but increases in importance with lower K values. The very high S_{octane} value of 17 for E85 means that this fuel would provide more of a benefit than any of the fuels where fuel components would be blended at 30 vol %.

5.2.3. HoV impact on merit function

The impact of HoV on the merit function is less significant than that of either RON or S_{octane} for boosted engines, providing an increase in the merit function of up to 1.1 for the expected range of values. The dashed line, which represents the HoV impact on the merit function if LSPI prevents the downsizing efficiency multiplier from being used, is such a small change that it is difficult to see the difference between the lines on the scale used. It is also interesting that E85 derives a substantially higher change in merit function score from HoV, reaching nearly 5, because of both its high HoV and its low stoichiometric air-fuel ratio.

5.2.4. Flame speed impact on merit function

The impact of flame speed variation on the merit function score over the expected range is small, ±0.4, for fuels up to the expected blend level of 30 vol %. Similarly, the merit function score for E85 is also smaller than for RON, S_{octane}, and HoV, increasing the merit function score by 1.1.

5.2.5. PMI impact on merit function

The PMI term cannot provide a positive contribution to the merit function. Rather, it provides a penalty for fuels with too much sooting propensity because they will require that a particulate filter be used, as discussed in Section 4.2. As a result, fuels with a PMI that is less than the 1.6 threshold do not contribute to the merit function score. For fuels with higher PMI, the merit function penalty can be significant, as much as −2 for a PMI of 4.

5.2.6. Catalyst light-off temperature impact on merit function

In comparison to the other terms in the merit function, the catalyst light-off term has a small influence (± 0.2) on the overall merit function score.

5.3. Exercising the merit function

In order to exercise the merit function for a variety of potential fuel candidates, representing a condition where the engine has been optimized for each fuel candidate with a conventional SI combustion strategy, the properties of the fuel candidates must be evaluated. However, many of the fuel properties, such as RON and MON, do not blend linearly. The nonlinear blending behavior of RON and MON with numerous blendstocks being considered by the Co-Optima initiative was reported by McCormick *et al.* [342]. Some fuels, such as ethanol and methanol, exhibit a convex curve in Fig. 53, which indicates synergistic blending behavior in which the octane number of the mixture is higher than would be expected. Other fuels exhibit a straight line, indicating linear blending, or a concave curve which indicates antagonistic blending where the octane number of the blend is lower than expected based on a linear by volume or mole model. The nonlinearity of octane response with ethanol is more linear on a molar basis than on a volumetric basis [339,343], but there has also been research that shows a nonlinearity on a molar blending basis [344].

To account for this nonlinearity, the blending research octane numbers ($RON_{blending}$) and blending motor octane numbers ($MON_{blending}$) approach was adopted, as described by Gary and Handwerk [345]. Blending octane numbers describe what the octane number of the pure component would need to be if the blend exhibited linear behavior. For the purposes of this analysis,

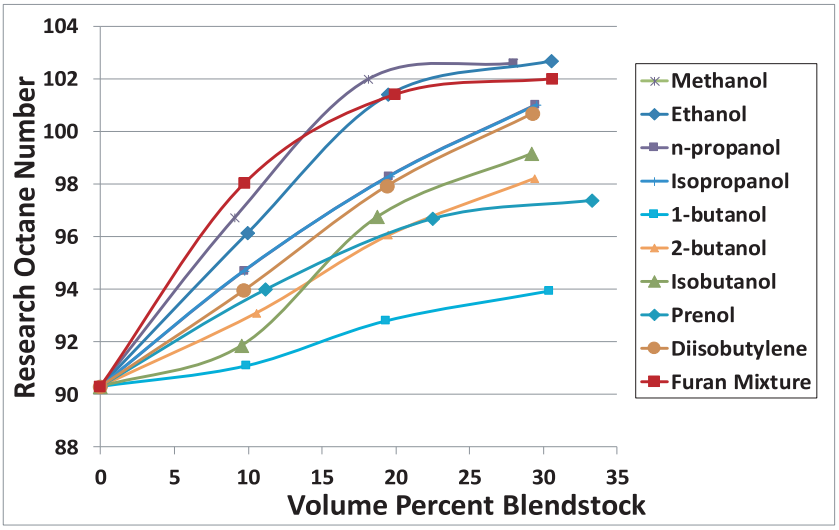

Fig. 53. Research octane number as a function of volume percent blended for 10 potential bio-blendstocks. Reprinted from McCormick *et al.* [342] with permission of SAE International.

Table 7
Values of $RON_{blending}$ and $MON_{blending}$ for various blendstocks considered by the Co-Optima initiative [346].

Blendstock	$RON_{blending}$ 10 vol %	20 vol %	30 vol %	$MON_{blending}$ 10 vol %	20 vol %	30 vol %
2-Methylfuran	166	142	127	125	108	102
Methanol	161	155	134	126	111	105
Ethanol	149	147	131	119	112	107
Di-isobutylene	128	130	126	108	101	97
Ethyl acetate	112	116	117	114	110	111
Isobutanol	107	125	121	100	100	96

Table 8
Fuel properties of BOB used to calculate merit function scores for fuel candidates shown in Table 7.

RON	85.5
MON	80.5
HoV	340.3
Stoichiometric AFR	14.76
PMI	< 1.6

$RON_{blending}$ and $MON_{blending}$ for each fuel component were calculated from the nonlinear blending relationships reported by McCormick *et al.* [342]. The $RON_{blending}$ and $MON_{blending}$ change as the blending concentration changes. Thus, these values were calculated for concentrations of 10, 20, and 30 vol % for a relatively small set of fuel components intended to represent a range of fuel chemistries (alcohols, furans, olefins, and acetates); these data are shown in Table 7. A more comprehensive list of the fuel merit function scores and blending properties for the fuel blends considered within the Co-Optima initiative, including the lifecycle environmental benefits for these specific fuel blends, is provided by Gaspar *et al.* [346].

The other properties needed to calculate the merit function are HoV, S_L, PMI, and $T_{c,90}$. Both S_L and $T_{c,90}$ have very small impacts on the expected merit function score, as shown in Fig. 52, and therefore will be neglected for this analysis. HoV blends nearly linearly on a mass basis [207], and therefore is readily accounted for if the HoV as the pure component or blending stream values were taken from McCormick *et al.* [342]. Similarly, while PMI blends linearly on a molar basis by definition [280] and PMI for any fuel blend can be readily calculated, all of the components considered for this analysis have PMI < 1.6, which prevents the Heaviside function for this term from being activated. Additionally, since the PMI < 1.6 for all components of interest, we assume that this is below the $PMI_{LSPI,crit}$ threshold value, thus the downsizing efficiency multiplier is active.

The fuel properties for the selected bioblendstocks shown in Table 7 were calculated at blends of 0, 10, 20, 30, and 100 vol% using the BOB properties shown in shown in Table 7. These BOB properties are based on data from Chupka *et al.* [207] and can be considered typical properties for the BOB that is used to produce a regular grade E10 gasoline. The merit function scores are shown in Fig. 54, and note that the data for 100 vol% is presented using a different y-axis scaling. The results show that methanol and ethanol have the highest potential to increase efficiency for boosted SI engines of the candidates considered here. Methyl furan also scores high at 20 and 30 vol% while diisobutylene scores high at 30 vol%. Interestingly, because of the non-linear blending of RON and MON, methanol, ethanol, and methyl furan provide nearly the same merit function score at 20 vol% as they do at 30 vol%. In contrast, both iso-butanol and diisobutylene exhibit a much more linear blending behavior, with a substantial merit function increase between 20 and 30 vol%. Finally, despite ethyl acetate having a very high RON (118), its low S_{octane} (−2.3) and antagonistic blending behavior make it a very low value blendstock.

The merit function scores for this subset of fuel candidates is not a comprehensive assessment of the efficiency potential for all fuels. Rather, it is a demonstration of the technique to estimate the efficiency improvement potential of a fuel if the engine is optimized for the fuel. Further, the merit function produces reasonable results when compared with values published in the literature. For

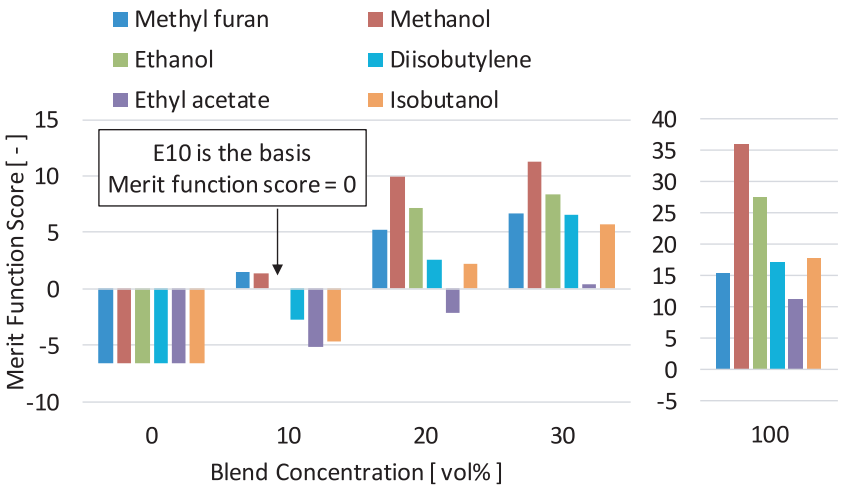

Fig. 54. Calculated merit function score for select components at 0, 10, 20, 30, and 100 vol %. Note that the 0 vol % concentrations represents a sub-octane BOB and thus has a negative merit function score relative to the baseline gasoline.

instance, for a blend of 30 vol % ethanol, the merit function score is 10, or a 10% relative improvement compared to a baseline regular grade gasoline. In a paper from Leone *et al.* [209], a fuel blend containing 30 vol % ethanol combined with a compression ratio increase from 10:1 to 13:1 produced a relative efficiency increase of 8.6% over the baseline regular grade gasoline. Similarly, Splitter and Szybist [347] reported a relative efficiency gain of 7% compared to the base gasoline at a lower compression ratio, but also showed that a higher load was achievable with the E30, meaning that the compression ratio and efficiency could likely have been increased further, or the engine could have been downsized, to achieve a matched engine power density.

The merit function was developed as a tool to determine the efficiency potential of a fuel blend in an SI engine based on its fuel properties, representing a condition where the engine has been optimized for each fuel candidate with a conventional SI combustion strategy. However, there are other potential criteria for the merit of a particular fuel or blending component, such as criteria emissions compliance, lifecycle greenhouse gas emissions, or production cost. Thus, fuel properties that are not included in the merit function, or that produce a negligible efficiency difference in the merit function, can still be significant in other contexts.

6. Future prospects

The analysis presented in this paper provides a systematic methodology to assess the efficiency potential of a particular fuel blend on the basis of its fuel properties in a chemistry-agnostic manner, according to the CFPH. While much of the information that contributed to the development of this methodology was previously known, this all-encompassing approach is new. As a result, in most instances, the merit function was based on fuel-property studies that were not specifically designed to quantify the impact of an isolated fuel property on efficiency. Thus, research can be recommended for each term in the merit function with the objective of reducing uncertainty and/or including fuel effects that are not yet accounted for in the current merit function form. This is described for each of the fuel properties below.

6.1. Improvements to antiknock properties

In this analysis, measures of fuel antiknock properties were accounted for using OI, which is superior to RON, MON, or AKI, as described in Section 3.1. However, OI is an extrapolation of RON and MON tests that do not represent modern engines. These tests do not use stoichiometric AFR, operate at engine speeds that are slower than modern engines, have long combustion duration due to the low turbulence levels, use advanced spark timing and combustion phasing, and test for knock at light loads with ambient pressure intake manifolds. Further, the knock sensing technology in these engines is different from the accelerometer that is used in modern engines.

Thus, potential future work for improving the merit function would center on developing an improved antiknock fuel property metric that is more representative of knock in modern engines, both for boosted HPD and naturally aspirated LPD engines. Such a development program should consider the fundamental kinetic basis for the knock event, such that the K factor isn't a required input since the uncertainty of OI increases as the K factor decreases below zero [171].

6.2. Improvements to heat of vaporization impact

Despite significant progress in decoupling the effects of HoV from S_{octane}, as described in Section 3.2, the isolated effect of HoV still is not clear. This is partially due to the different ways that HoV can impact the RON and MON tests, which, as described by Kolodziej *et al.* [211] and shown in Fig. 29, can lead to a factor of 4 difference in the impact of HoV on the knock propensity. Thus, in order to better quantify the effect of HoV on knock propensity in an unambiguous manner, we recommend that HoV be considered in the development of the new antiknock metric proposed in Section 6.1 in a way that the HoV effect can be isolated.

6.3. Improvements to flame speed impact

Despite it being well-known to fuels and engine combustion engineers that high flame speed is important for engines, this literature review, which focused on stoichiometric combustion, did not find clear evidence that flame speed could provide an efficiency benefit in stoichiometric SI engines beyond the ability to extend the dilution limit. Instead, it was found that slow flame speed could degrade efficiency in the absence of modifications to engine operation, and it was not clear that the degradation would persist in an optimized engine when, for example, combustion timing could be optimized with advanced spark timing. Thus, it is recommended that the effect of flame speed on engine efficiency be studied to determine what flame speed impacts exist under non-dilute operating conditions.

6.4. Improved quantification of LSPI fuel impacts

Our understanding of fuel impacts on LSPI is still very much under development. In order to attempt to quantify the effects of LSPI on engine efficiency, PMI was used as a fuel property basis because is increases with high distillation temperatures and with aromatics. However, linking PMI with LSPI is a relatively new concept. Thus, it is recommended that this proposed fuel property basis for LSPI be validated across several different engine platforms and for a wide range of fuels. Further, it is recommended that the efficiency penalty associated with LSPI be further developed. In this review, it was hypothesized that LSPI prevented further downsizing of the engine, thereby precluding the use of the downsizing efficiency multiplier, but this hypothesis has not yet been validated.

Lastly, because LSPI is a multi-step sequence where each step is required but not sufficient on its own, as described by Chapman *et al.* [247] and shown in Fig. 36, it is recommended that non-initiation LSPI fuel effects be further developed. A number of these were described in Section 3.4.3, but they are at an early stage of development and cannot yet be quanified in the merit function.

6.5. Improved particulate matter impacts

Although presently PMI (a fuel property) appears to be the best available model for predicting PM emissions from gasoline composition, the literature has demonstrated PMI's shortcomings regarding effects on PM from blending oxygenates into gasoline. Therefore, continued development of better models is warranted. However, because ethanol is the dominant oxygenate currently in the gasoline market, and C3-C4 alcohols appear to have similar potential, near term PM model improvements might be constrained to account for alcohol-aromatic interaction effects.

In addition to being able to predict PM in a more accurate manner, developing a better understanding of how PM can affect efficiency is necessary. Specifically, the impact of PMI was quantified with a Heaviside function that assumed that a GPF would be necessary above a certain threshold value. There is a significant amount of uncertainty about the development of engine technologies and emissions standards, such that identifying such a threshold value is challenging. Thus, it is recommended that studies be conducted to quantify the threshold value of PMI (or an improved PMI replacement) such that the threshold value can be identified. Further investigations into the efficiency impacts of GPFs are also warranted.

6.6. Improved understanding of catalyst light-off

Section 5.2 illustrated that the catalyst light-off temperature is expected to only have a minor impact on engine efficiency. However, it remains true that all engines must meet applicable emissions standards to be sold. Further, allowable emissions of criteria pollutants continue to decrease such that meeting these emissions standards at the full useful life of the engine is becoming more challenging. Thus, it is recommended that a different merit function be developed that quantifies how fuel properties and chemistry impact the ability to achieve criteria emissions.

7. Summary/conclusions

As a part of the US Department of Energy Co-Optima initiative, which aims to provide the fundamental knowledge needed to co-develop fuels and engines to simultaneously maximize energy efficiency and maximize the utilization of renewable fuels, this review identified and quantified the efficiency potential of fuels in SI engines based on their fuel properties. This effort started by adopting a thermodynamic expression of brake engine efficiency as the product of several component efficiencies that include:

- mechanical efficiency
- combustion efficiency
- gas exchange efficiency
- proportion of total heat release available after wall heat losses
- ideal cycle efficiency
- degree to which the actual heat release profile resembles the ideal profile.

Using this framework, the incremental efficiency potentials of individual fuel properties were quantified by their ability to incrementally change one or more of the component efficiency terms identified in the thermodynamic analysis through in-cylinder processes. Specifically, the fuel properties quantified were: the ability to resist knock, as described by OI which includes both RON and S_{octane}; the combined effects of HoV; and the effect of S_L on the EGR dilution tolerance. Note that the efficiency improvements were considered for an optimized engine where, for instance, if a fuel property enhanced the knock resistance of the fuel, the quantified efficiency improvement considers a corresponding r_c increase. Significant fuel effects on LSPI were also reviewed, and a framework on how fuel properties affecting LSPI can limit engine efficiency by preventing downsizing was proposed. The fuel property threshold at which this downsizing limit is met has yet to be quantified.

Additionally, this study considered the effect of fuel properties on the use of exhaust aftertreatment, which is needed to meet emission standards. For gaseous emissions, this was done through quantifying the difference in fuel consumption, relative to a baseline fuel, to achieve three-way catalyst light-off, where the temperature at which light-off occurred was fuel-specific. For particle emissions, it was done by assuming there was a threshold sooting tendency, quantified by PMI, over which a GPF would be required to achieve emissions compliance. Under this PMI threshold, no efficiency penalty would be incurred, but above the threshold the penalty would continuously increase.

Each of these individual terms was normalized on the basis of a relative efficiency improvement and combined into a merit function. Performing a sensitivity analysis of the merit function over the expected ranges of fuel properties, it is apparent that RON and S_{octane} have the most potential to improve efficiency, and that HoV can also provide a significant benefit. However, S_L, PMI, and the catalyst light-off temperature were found to have small effects on efficiency.

As constructed, the merit function provides a tool for comparing the advantages and disadvantages of different fuel properties as they relate to efficiency for different fuel blends. The merit function is applicable, to the first order, to both conventional petroleum-derived fuels, bio-based fuels, or blends of the two. Further, the merit function applies to all types of stoichiometric SI engine architectures that use a fixed r_c, including both boosted and naturally aspirated engines. As a result, this is a tool that can be used to guide producers of alternative fuels towards formulations that can enable the highest efficiency engine operation.

Declaration of Competing Interest

None.

Acknowledgements

This research was conducted as part of the Co-Optimization of Fuels and Engines (Co-Optima) initiative sponsored by the US Department of Energy Office of Energy Efficiency and Renewable Energy and Bioenergy Technologies and Vehicle Technologies Offices. Co-Optima is a collaborative project of multiple national lab-

oratories initiated to simultaneously accelerate the introduction of affordable, scalable, and sustainable biofuels and high-efficiency, low-emission vehicle engines. Special thanks to the Vehicle Technologies Office program managers Kevin Stork, Gurpreet Singh, Leo Breton, and Mike Weismiller, as well as the Bioenergy Technology Office Program manager Alicia Lindauer.

We would also like to thank the Co-Optima Leadership Team comprised of John Farrell, Robert Wagner, John Holladay, Art Pontau, Dan Gaspar, Chris Moen, Bob McCormick, and Paul Bryan. We would also like to thank the entire Co-Optima team.

Finally, we would like to thank Runhua Zhao of USC for allowing us to include unpublished flame speed measurements (Fig. 34) that were made as part of a collaboration between Sandia National Laboratories and USC, as well as Darko Kozarac of the University of Zagreb for providing assistance calibrating the friction model used in the assessment of factors which increase SI engine efficiency (Section 2).

Supplementary materials

Supplementary material associated with this article can be found, in the online version, at doi:10.1016/j.pecs.2020.100876.

References

[1] Splitter DA, Pawlowski AE, Wagner RM. A historical analysis of the co-evolution of gasoline octane number and spark-ignition engines. *Front Mech Eng* 2016;**1**:1–22.
[2] Wang Z, Liu H, Reitz RD. Knocking combustion in spark-ignition engines. *Prog Energ Combust* 2017;**61**:78–112.
[3] ASTM D2699-18a. *Standard test method for research octane number of spark-ignition engine fuel*. West Conshohocken, PA: ASTM International; 2018.
[4] ASTM D2700-18a. *Standard test method for motor octane number of spark-ignition engine fuel*. West Conshohocken, PA: ASTM International; 2018.
[5] Boyd TA. Pathfinding in fuels and engines. *SAE Techn Paper 500175* 1950.
[6] Leake JP, Kolb L, Howell WH, Chesley AJ, Edsall DL, Hunt R, et al. *The use of tetraethyl lead gasoline in its relation to public health*. Government Report OCLC 37184326, G.P.O.; 1926.
[7] Needleman HL. Childhood lead poisoning: The promise and abandonment of primary prevention. *Am J Public Health* 1998;**88**:1871–7.
[8] Nevin R. How lead exposure relates to temporal changes in IQ, violent crime, and unwed pregnancy. *Environ Res* 2000;**83**:1–22.
[9] United States Public Health Service. *Proceedings of a conference to determine whether or not there is a public health question in the manufacture, distribution, or use of tetraethyl lead gasoline*. Government Report OCLC 18596366, G.P.O.; 1925.
[10] United States Public Health Service. Public health aspects of increasing tetraethyl lead content in motor fuel. a report [of the] advisory committee on tetrathyl lead to surgeon general of public health service, U.S. dept. of health, education, and welfare, public health service, bureau of state services, division of special health services, occupational health program; 1959.
[11] Shelton EM, Whisman ML, Woodward PW. *Trends in motor gasolines: 1942-1981*; 1982. DOE Report DOE/BETC/RI-82/4.
[12] Kohl GA. Passenger car performance trends. *SAE Tech Paper 690211* 1969.
[13] Balouet JC, Oudijk G, Smith KT, Petrisor L, Grudd H, Stocklassa B. Applied dendroecology and environmental forensics. Characterizing and age dating environmental releases: fundamentals and case studies. *Environ Forensics* 2007;**8**:1–17.
[14] Canfield RL, Henderson CR, Cory-Slechta DA, Cox C, Jusko TA, Lanphear BP. Intellectual impairment in children with blood lead concentrations below 10 mu g per deciliter. *New Engl J Med* 2003;**348**:1517–26.
[15] Needleman HL. The removal of lead from gasoline: historical and personal reflections. *Environ Res* 2000;**84**:20–35.
[16] Nriagu JO. The rise and fall of leaded gasoline. *Sci Total Environ* 1990;**92**:13–28.
[17] Oudijk G. Fingerprinting and age-dating of gasoline releases - a case study. *Environ Forensics* 2005;**6**:91–9.
[18] Patterson C. Age of meteorites and the Earth. *Geochim Cosmochim Ac* 1956;**10**:230–7.
[19] Patterson CC. Contaminated and natural lead environments of man. *Arch Environ Health* 1965;**11**:344–60.
[20] Gibbs LM. Gasoline additives - when and why. *SAE Tech Paper 902104* 1990.
[21] Gibbs LM. How gasoline has changed. *SAE Tech Paper 932828* 1993.
[22] US EPA. Regulation of fuels and fuel additives: notice of proposed rule making. *Fed. Reg. Session* 1973;**38**:1258–61.
[23] Kummer JT. Catalysts for automobile emission control. *Prog Energ Combust* 1980;**6**:177–99.
[24] Campau RM. Low emission concept vehicles. *SAE Tech Paper 710294* 1971.
[25] Dickson CL, Woodward PW, Bjugstad PL. *Trends of petroleum fuels. National institute for petroleum and energy research technical report NIPER-224*; 1987. ON:DE87001237.
[26] Neligan RE, Mader PP, Chambers LA. Exhaust composition in relation to fuel composition. *J. Air Pollution Control Ass.* 1961;**11**:178–86.
[27] US EPA: Office of Mobile Sources Air and radiation. *History Reducing Tailpipe Emissions* 1999. http://www3.epa.gov/otaq/consumer/f99017.pdf.
[28] Caris DF, Nelson EE. a new look at high compression engines. *SAE Tech Paper 590019* 1959.
[29] Energy Policy and Conservation Act 42 USC 6201, Public law 94-163. 1975.
[30] Dahl D, Andersson M, Denbratt I. The origin of pressure waves in high load hcci combustion: a high-speed video analysis. *Combust. Sci. Technol.* 2011;**183**:1266–81.
[31] Kraus BJ, Godici PE, King WH. Reduction of octane requirement by knock sensor spark retard system. *SAE Tech Paper 780155* 1978.
[32] Holl WH. Air-fuel control to reduce emissions i. engine-emissions relationships. *SAE Tech Paper 800051* 1980.
[33] Rivard JG. Closed-loop electronic fuel injection control of the internal combustion engine. *SAE Tech Paper 730005* 1973.
[34] Zechnall R, Baumann G, Eisele H. Closed-loop exhaust emission control system with electronic fuel injection. *SAE Tech Paper 730566* 1973.
[35] Hegedus LL, Summers JC, Schlatter JC, Baron K. Poison-resistant catalysts for the simultaneous control of hydrocarbon, carbon monoxide, and nitrogen oxide emissions. *J. Catalysis* 1979;**56**:321–35.
[36] Kaneko Y, Kobayashi H, Komagome R, Hirako O, Nakayama O. Effect of air-fuel ratio modulation on conversion efficiency of three-way catalysts. *SAE Tech Paper 780607* 1978.
[37] Pawlowski A, Splitter D. SI engine trends: a historical analysis with future projections. *SAE Tech Paper 2015-01-0972* 2015.
[38] US EPA. *US EPA Report EPA-420-R-19-002*; 2019.
[39] Lubetsky J. *History of fuel economy: one decade of innovation, two decades of inaction*. The Pew Environmental Group; 2011 *https://www.pewtrusts.org/~/media/assets/2011/04/history-of-fuel-economy-clean-energy-factsheet.pdf*.
[40] Xu X, Dong P, Liu Y, Zhang H. Progress in automotive transmission technology. *Automotive Innovation* 2018;**1**:187–210.
[41] Virzi Mariotti G. *Engine/transmission matching: encyclopedia of automotive engineering*. Wiley & Sons; 2014.
[42] Tucker R. Trends in automotive lightweighting. *Metal Finishing* 2013;**111**:23–5.
[43] Thomas J. Vehicle efficiency and tractive work: rate of change for the past decade and accelerated progress required for U.S. fuel economy and CO2 regulations. *SAE Int J Fuels Lubr* 2016;**9**:290–305.
[44] Basshuysen V. Ottomotor mit Direkteinspritzung Verfahren, Systeme, Entwicklung. *Potenzial* 2007.
[45] Golloch R, P, Merker G. Downsizing bei verbrennungsmotoren. *MTZ – Motortechnische Zeitschrift* 2005;**66**:126–34.
[46] Schumann F, Sarikoc F, Buri S, Kubach H, Spicher U. Potential of spray-guided gasoline direct injection for reduction of fuel consumption and simultaneous compliance with stricter emissions regulations. *Int J Engine Res* 2013;**14**:80–91.
[47] Attard WP, Toulson E, Watson H, Hamori F. Abnormal combustion including mega knock in a 60% downsized highly turbocharged PFI engine. *SAE Tech Paper 2010-01-1456* 2010.
[48] Boretti A. Towards 40% efficiency with BMEP exceeding 30bar in directly injected, turbocharged, spark ignition ethanol engines. *Energ Convers Manage* 2012;**57**:154–66.
[49] Cruff L, Kaiser M, Krause S, Harris R, Krueger U, Williams M. EBDI® - application of a fully flexible high BMEP downsized spark ignited engine. *SAE Tech Paper 2010-01-0587* 2010.
[50] Hancock D, Fraser N, Jeremy M, Sykes R, Blaxill H. A new 3 cylinder 1.2l advanced downsizing technology demonstrator engine. *SAE Tech Paper 2008-01-0611* 2008.
[51] Martin S, Beidl C, Mueller R. Responsiveness of a 30 Bar BMEP 3-cylinder engine: opportunities and limits of turbocharged downsizing. *SAE Tech Paper 2014-01-1646* 2014.
[52] Turner JWG, Popplewell A, Patel R, Johnson TR, Darnton NJ, Richardson S, et al. Ultra boost for economy: extending the limits of extreme engine downsizing. *SAE Tech Paper 2014-01-1185* 2014.
[53] Schenk C, Butters K. *2014 Mazda 2.0L SKYACTIV-G Engine Tested with Tier 2 Test Fuel – Test Data Package*. U.S. Environmental Protection Agency: National Vehicle and Fuel Emissions Laboratory; 2018. Version 2018-02.
[54] Hwang K, Hwang I, Lee H, Park H, Choi H, Lee K, et al. Development of new high-efficiency kappa 1.6L GDI engine. *SAE Tech Paper 2016-01-0667* 2016.
[55] Matsuo S, Ikeda E, Ito Y, Nishiura H. The new Toyota inline 4 cylinder 1.8L ESTEC 2ZR-FXE gasoline engine for hybrid car. *SAE Tech Paper 2016-01-0684* 2016.
[56] Hakariya M, Toda T, Sakai M. The new Toyota inline 4-cylinder 2.5l gasoline engine. *SAE Tech Paper 2017-01-1021* 2017.
[57] Kargul J, Stuhldreher M, Barba D, Schenk C, Bohac S, McDonald J, et al. Benchmarking a 2018 Toyota Camry 2.5-liter atkinson cycle engine with cooled-EGR. *SAE Tech Paper 2019-01-0249* 2019.
[58] Newman KA, Doorlag M, Barba D. Modeling of a conventional mid-size car with CVT using ALPHA and comparable powertrain technologies. *SAE Tech Paper 2016-01-1141* 2016.
[59] Dugdale PH, Rademacher RJ, Price BR, Subhedar JW, Duguay RL. Ecotec 2.4L VVT: A variant of GM's global 4-cylinder engine. *SAE Tech Paper 2005-01-1942* 2005.

[60] Stuhldreher M. *2016 Honda 1.5L L15B7 Engine Tested with Tier 2 Fuel – NCAT Test Report*. US EPA, National Vehicle and Fuel Emissions Laboratory, National Center for Advanced Technology: US EPA, National Vehicle and Fuel Emissions Laboratory, National Center for Advanced Technology; 2018. Version 2018-05.
[61] Sluder CS, Smith DE, Wissink ML, Anderson JE, Leone TG, Shelby MH. Effects of octane number, sensitivity, ethanol content, and engine compression ratio on GTDI engine efficiency, fuel economy, and CO2 emissions. *CRC AVFL-20* 2017:1–117.
[62] Szybist JP, West BH. The impact of low octane hydrocarbon blending streams on the knock limit of "E85". *SAE Int J Fuels Lubricants* 2013;**6**:44–54.
[63] Heywood J. *Internal Combustion Engine Fundamentals 2E*. McGraw-Hill Education; 2018.
[64] King J, Barker L, Turner J, Martin J. SuperGen - a novel low costs electro-mechanical mild hybrid and boosting system for engine efficiency enhancements. *SAE Tech Paper 2016-01-0682* 2016.
[65] Chow EW, Heywood JB, Speth RL. Benefits of a higher octane standard gasoline for the U.S. light-duty vehicle fleet. *SAE Tech Paper 2014-01-1961* 2014.
[66] Wirth M, Mayerhofer U, Piock WF, Fraidl GK. Turbocharging the DI Gasoline Engine. *SAE Tech Paper 2000-01-0251* 2000.
[67] Zhao F, Lai MC, Harrington DL. Automotive spark-ignited direct-injection gasoline engines. *Prog Energ Combust* 1999;**25**:437–562.
[68] Zhao H. *Advanced direct injection combustion engine technologies and development: gasoline and gas engines*. Woodhead Publishing; 2009.
[69] Spicher U, Reissing J, Kech JM, Gindele J. Gasoline direct injection (GDI) engines - development potentialities. *SAE Tech Paper 1999-01-2938* 1999.
[70] Iyer CO, Yi J. Spray pattern optimization for the duratec 3.5L ecoboost engine. *SAE Int J Engines* 2009;**2**:1679–89.
[71] Bandel W, Fraidl GK, Kapus PE, Sikinger H, Cowland CN. The turbocharged GDI engine: boosted synergies for high fuel economy plus ultra-low emission. *SAE Tech Paper 2006-01-1266* 2006.
[72] Ranini A, Monnier G. Turbocharging a gasoline direct injection engine. *SAE Tech Paper 2001-01-0736* 2001.
[73] Heywood JB. *Internal Combustion Engine Fundamentals*. New York: New York: McGraw-Hill; 1988.
[74] Szybist JP, Youngquist AD, Barone TL, Storey JM, Moore WR, Foster M, et al. Ethanol blends and engine operating strategy effects on light-duty spark-ignition engine particle emissions. *Energ Fuel* 2011;**25**:4977–85.
[75] Sellnau M, Rask E. Two-step variable valve actuation for fuel economy, emissions, and performance. *SAE Tech Paper 2003-01-0029* 2003.
[76] Sellnau M, Kunz T, Sinnamon J, Burkhard J. 2-step variable valve actuation: system optimization and integration on an SI engine. *SAE Tech Paper 2006-01-0040* 2006.
[77] Taylor J, Fraser N, Dingelstadt R, Hoffmann H. Benefits of late inlet valve timing strategies afforded through the use of intake cam in cam applied to a gasoline turbocharged downsized engine. *SAE Tech Paper 2011-01-0360* 2011.
[78] Osborne R, Downes T, O'Brien S, Pendlebury K, Christie M. A miller cycle engine without compromise - the magma concept. *SAE Tech Paper 2017-01-0642* 2017.
[79] Caton JA. A Comparison of lean operation and exhaust gas recirculation: thermodynamic reasons for the increases of efficiency. *SAE Tech Paper 2013-01-0266* 2013.
[80] Alger T, Mangold B, Roberts C, Gingrich J. The interaction of fuel anti-knock index and cooled egr on engine performance and efficiency. *SAE Int J Eng* 2012;**5**:1229–41.
[81] Splitter DA, Szybist JP. Experimental Investigation of spark-ignited combustion with high-octane biofuels and EGR. 2. Fuel and EGR effects on knock-limited load and speed. *Energ Fuel* 2014;**28**:1432–45.
[82] Splitter DA, Szybist JP. Experimental investigation of spark-ignited combustion with high-octane biofuels and EGR. 1. engine load range and downsize downspeed opportunity. *Energ Fuel* 2014;**28**:1418–31.
[83] Chang Y, Szybist JP. Fuel effects on combustion with EGR dilution in spark ignited engines. *The 2016 spring technical meeting of the central states section of the combustion institute (CSSCI 2016) Technical Paper 145IC-0082*; 2016.
[84] Szybist JP, Splitter D. Effects of fuel composition on EGR dilution tolerance in spark ignited engines. *Sae Int J Eng.* 2016;**9**:819–31.
[85] Alger T, Chauvet T, Dimitrova Z. Synergies between High EGR operation and GDI systems. *SAE Int. J. Eng.* 2008;**1**:101–14.
[86] Ozdor N, Dulger M, Sher E. Cyclic variability in spark ignition engines a literature survey. *SAE Tech Paper 940987* 1994.
[87] Van Basshuysen R, Schaefer F. *Internal Combustion Engine Handbook*. 2nd English Edition. SAE International; 2016.
[88] Dale JD, Checkel MD, Smy PR. Application of high energy ignition systems to engines. *Prog Energ Combust* 1997;**23**:379–98.
[89] Lee B, Oh H, Han S, Woo S, Son J. Development of high efficiency gasoline engine with thermal efficiency over 42%. *SAE Tech Paper 2017-01-2229* 2017.
[90] Harrington JA, Shishu RC, Asik JR. A study of ignition system effects on power, emissions, lean misfire limit, and EGR tolerance of a single-cylinder engine-multiple spark versus conventional single spark ignition. *SAE Tech Paper 740188* 1974.
[91] Asik JR, Bates B. The ferroresonant capacitor discharge ignition (FCDI) system: a multiple firing CD ignition with spark discharge sustaining between firings. *SAE Tech Paper 760266* 1976.
[92] Alger T, Gingrich J, Mangold B, Roberts C. A continuous discharge ignition system for EGR limit extension in SI engines. *SAE Tech Paper 2011-01-0661* 2011.
[93] Modien RM, Checkel MD, Dale JD. The effect of enhanced ignition systems on early flame development in quiescent and turbulent conditions. *SAE Tech Paper 910564* 1991.
[94] Cho YS, Santavicca DA, Sonntag RM. The effect of spark power on spark-ignited flame kernel growth. *SAE Tech Paper 922168* 1992.
[95] Nakai M, Nakagawa Y, Hamai K, Sone M. Stabilized combustion in a spark ignited engine through a long spark duration. *SAE Tech Paper 850075* 1985.
[96] Pischinger S, Heywood JB. A study of flame development and engine performance with breakdown ignition systems in a visualization engine. *SAE Tech Paper 880518* 1988.
[97] Dale JD, Smy PR, Clements RM. Laser ignited internal combustion engine - an experimental study. *SAE Tech Paper 780329* 1978.
[98] Cimarello A, Grimaldi CN, Mariani F, Battistoni M, Dal Re M. Analysis of RF corona ignition in lean operating conditions using an optical access engine. *SAE Tech Paper 2017-01-0673* 2017.
[99] Burrows J, Lykowski J, Mixell K. Corona ignition system for highly efficient gasoline engines. *MTZ worldwide* 2013;**74**:38–41.
[100] Oppenheim AK, Teichman K, Hom K, Stewart HE. Jet Ignition of an ultra-lean mixture. *SAE Tech Paper 780637* 1978.
[101] Cetegen B, Teichman KY, Weinberg FJ, Oppenheim AK. Performance of a plasma jet igniter. *SAE Tech Paper 800042* 1980.
[102] Murase E, Ono S, Hanada K, Nakahara S. Plasma jet ignition in turbulent lean mixtures. *SAE Tech Paper 890155* 1989.
[103] Asik JR, Piatkowski P, Foucher MJ, Rado WG. Design of a plasma jet ignition system for automotive application. *SAE Tech Paper 770355* 1977.
[104] Edwards CF, Oppenheim AK, Dale JD. A comparative study of plasma Ignition systems. *SAE Tech Paper 830479* 1983.
[105] Karim GA, Al-Himyary TJ, Dale JD. An examination of the combustion processes of a methane fuelled engine when employing plasma jet ignition. *SAE Tech Paper 891639* 1989.
[106] Kupe J, Wilhelmi H, Adams W. Operational characteristics of a lean burn SI-engine: comparison between plasma-jet and conventional ignition system. *SAE Tech Paper 870608* 1987.
[107] Sevik J, Wallner T, Pamminger M, Scarcelli R, Singleton D, Sanders J. Extending Lean and EGR-dilute operating limits of a modern GDI engine using a low-energy transient plasma ignition system. *ASME ICEF2015-1048* 2015.
[108] Wolk BM, Ekoto I. Calorimetry and imaging of plasma produced by a pulsed nanosecond discharge igniter in EGR gases at engine-relevant densities. *SAE Tech Paper 2017-01-0674* 2017.
[109] Shiraishi T, Urushihara T. Fundamental analysis of combustion initiation characteristics of low temperature plasma ignition for internal combustion gasoline engine. *SAE Tech Paper 2011-01-0660* 2011.
[110] Sjöberg M, Zeng W, Singleton D, Sanders JM, Gundersen MA. Combined effects of multi-pulse transient plasma ignition and intake heating on lean limits of well-mixed E85 DISI engine operation. *SAE Tech Paper 2014-01-2615* 2014.
[111] Gussak LA, Karpov VP, Tikhonov YV. The application of lag-process in prechamber engines. *SAE Tech Paper 790692* 1979.
[112] Gussak LA, Turkish MC, Siegla DC. High chemical activity of incomplete combustion products and a method of prechamber torch ignition for avalanche activation of combustion in internal combustion engines. *SAE Tech Paper 750890* 1975.
[113] Oppenheim AK, Beltramo J, Faris DW, Maxson JA, Hom K, Stewart HE. Combustion by pulsed jet plumes - key to controlled combustion engines. *SAE Tech Paper 890153* 1989.
[114] Maxson JA, Hensinger DM, Hom K, Oppenheim AK. Performance of multiple stream pulsed jet combustion systems. *SAE Tech Paper 910565* 1991.
[115] Hensinger DM, Maxson JA, Hom K, Oppenheim AK. Jet plume injection and combustion. *SAE Tech Paper 920414* 1992.
[116] Attard WP, Fraser N, Parsons P, Toulson E. A turbulent jet ignition pre-chamber combustion system for large fuel economy improvements in a modern vehicle powertrain. *SAE Tech Paper 2010-01-1457* 2010.
[117] Bunce M, Blaxill H. Sub-200g/kWh BSFC on a light duty gasoline engine. *SAE Tech Paper 2016-01-0709* 2016.
[118] Benajes J, Novella R, Gomez-Soriano J, Martinez-Hernandiz PJ, Libert C, Dabiri M. Evaluation of the passive pre-chamber ignition concept for future high compression ratio turbocharged spark-ignition engines. *Appl Energy* 2019;**248**:576–88.
[119] Mendler C, Gravel R. Variable compression ratio engine. *SAE Tech Paper 2002-01-1940* 2002.
[120] Kleeberg H, Tomazic D, Dohmen J, Wittek K, Balazs A. Increasing efficiency in gasoline powertrains with a two-stage variable compression ratio (VCR) system. *SAE Tech Paper 2013-01-0288* 2013.
[121] Wittek K, Tiemann C, Pischinger S. Two-stage variable compression ratio with eccentric piston pin and exploitation of crank train forces. *SAE Int J Eng* 2009;**2**:1304–13.
[122] Wolfgang S, Sorger H, Loesch S, Unzeitig W, Huettner T, Fuerhapter A. The 2-step VCR conrod system - modular system for high efficiency and reduced CO2. *SAE Tech Paper 2017-01-0634* 2017.
[123] Kojima S, Kiga S, Moteki K, Takahashi E, Matsuoka K. Development of a new 2L gasoline VC-turbo engine with the world's first variable compression ratio technology. *SAE Tech Paper 2018-01-0371* 2018.
[124] Sugiyama T, Hiyoshi R, Takemura S, Aoyama S. Technology for improving engine performance using variable mechanisms. *SAE Tech Paper 2007-01-1290* 2007.
[125] Tanaka Y, Hiyoshi R, Takemura S, Ikeda Y, Sugawara M. A study of a compres-

sion ratio control mechanism for a multiple-link variable compression ratio engine. *SAE Tech Paper 2007-01-3547* 2007.
[126] IAV Engineering Variable compression ratio for reduced fuel consumption and lower emissions. *Automotion* 2015.
[127] Drangel H, Olofsson E, Reinmann R. The variable compression (SVC) and the combustion control (SCC) - two ways to improve fuel economy and still comply with world-wide emission requirements. *SAE Tech Paper 2002-01-0996* 2002.
[128] Christensen M, Hultqvist A, Johansson B. Demonstrating the multi fuel capability of a homogeneous charge compression ignition engine with variable compression ratio. *SAE Tech Paper 1999-01-3679* 1999.
[129] Harne V, Marathe SR. Variable compression ratio two-stroke engine. *SAE Tech Paper 891750* 1989.
[130] Ishikawa S, Kadota M, Yoshida K, Takahashi K, Kawajiri S. Advanced design of variable compression ratio engine with dual piston mechanism. *SAE Int J Eng* 2009;**2**:982–90.
[131] Kadota M, Ishikawa S, Yamamoto K, Kato M, Kawajiri S. Advanced control system of variable compression ratio (VCR) engine with dual piston mechanism. *SAE Int J Eng* 2009;**2**:1009–18.
[132] Turner JWG, Blundell DW, Pearson RJ, Patel R, Larkman DB, Burke P, et al. Project omnivore: a variable compression ratio ATAC 2-stroke engine for ultra-wide-range HCCI operation on a variety of fuels. *SAE Int J Eng* 2010;**3**:938–55.
[133] Wirbeleit FG, Binder K, Gwinner D. Development of pistons with variable compression height for increasing efficiency and specific power output of combustion engines. *SAE Tech Paper 900229* 1990.
[134] Shelby MH, Leone TG, Byrd KD, Wong FK. Fuel economy potential of variable compression ratio for light duty vehicles. *SAE Int J Eng* 2017;**10**:817–31.
[135] Leone TG, Pozar M. Fuel economy benefit of cylinder deactivation - sensitivity to vehicle application and operating constraints. *SAE Tech Paper 2001-01-3591* 2001.
[136] Wilcutts M, Switkes J, Shost M, Tripathi A. Design and benefits of dynamic skip fire strategies for cylinder deactivated engines. *SAE Tech Paper 2013-01-0359* 2013.
[137] Serrano J, Routledge G, Lo N, Shost M, Srinivasan V, Ghosh B. Methods of evaluating and mitigating nvh when operating an engine in dynamic skip fire. *SAE Tech Paper 2014-01-1675* 2014.
[138] Stuhldreher M. Fuel efficiency mapping of a 2014 6-cylinder GM EcoTec 4.3L engine with cylinder deactivation. *SAE Tech Paper 2016-01-0662* 2016.
[139] Miles P. *U.S. Department of Energy Technical Report*; 2018. DOE/GO-102018-5041.
[140] ASTM D4814-19. *Standard specification for automotive spark-ignition engine fuel*. West Conshohocken, PA: ASTM International; 2019.
[141] CARB. The California reformulated gasoline regulations. *California Code of Regulations* Title 13,; 2014. Sections 2250-2273.5.
[142] Dunn JB, Biddy M, Jones S, Cai H, Benavides PT, Markham J, et al. Environmental, economic, and scalability considerations and trends of selected fuel economy-enhancing biomass-derived blendstocks. *ACS Sustain Chem Eng* 2018;**6**:561–9.
[143] Farrell JT, Holladay J, Wagner RM. Fuel Blendstocks with the Potential to Optimize Future Gasoline Engine Performance. *Identification of five chemical families for detailed evaluation*; 2018. DOE/GO-102018-4970.
[144] Fouts L, Fioroni G, Christensen E, Ratcliff MA, McCormick R, Zigler BT, et al. *National renewable energy laboratory technical report NREL/TP-5400-71341*; 2018.
[145] Nicolaus Langen A. August Otto: der Schöpfer des Verbrennungsmotors. *Stuttgart: Franksche Verlagshandlung* 1949.
[146] Ricardo H. The Progress of the internal combustion engine and its fuel. *Engineer* 1935.
[147]] Clerk D. Investigations on gaseous explosions. Part 2. Explosive reactions considered in reference to internal combustion engines. Introductory survey. *Trans. Farady Soc* 1926;**22**:338–40.
[148] Ricardo H. Recent research work on the internal-combustion engine. *SAE Tech Paper 220001* 1922.
[149] Midgley T, Boyd TA. Methods of measuring detonation in engines. *SAE Tech Paper 220004* 1922.
[150] Coull NM. Methods of measuring detonation. *SAE Tech Paper 280007* 1928.
[151] Cummings HK. Methods of measuring the antiknock value of fuels. *SAE Tech Paper 270003* 1927.
[152] Graham E. Detonation specifications for automotive fuels. *SAE Tech Paper 270006* 1927.
[153] Horning HL. Effect of compression on detonation and its control. *SAE Tech Paper 230033* 1923.
[154] Campbell JM, Lovell WG, Boyd TA. Detonation characteristics of some of the fuels suggested as standards of antiknock quality. *SAE Tech Paper 300018* 1930.
[155] Graham E. Comparison of methods of measuring knock characteristics of fuels. *SAE Tech Paper 280008* 1928.
[156] Boyd TA. 1937 road knock tests. *SAE Tech Paper 380145* 1938.
[157] Campbell JM, Greenshields RJ, Holaday WM. 1940 road detonation tests - (compiled from report1 of the cooperative fuel research committee). *SAE Tech Paper 410107* 1941.
[158] Veal CB. C.F.R. committee report on 1934 detonation road tests. *SAE Tech Paper 350094* 1935.
[159] Veal CB, Best HW, Campbell JM, Holaday WM. Antiknock research coordinates laboratory and road tests. *SAE Tech Paper 330015* 1933.
[160] Swarts A, Yates A, Viljoen C, Coetzer R. Standard knock intensity revisited: atypical burn rate characteristics identified in the CFR octane rating engine. *SAE Tech Paper 2004-01-1850* 2004.
[161] Swarts A, Yates A, Viljoen C, Coetzer R. A further study of inconsistencies between autoignition and knock intensity in the CFR octane rating engine. *SAE Tech Paper 2005-01-2081* 2005.
[162] Arrigoni V, Cornetti GM, Spallanzani G, Calvi F, Tontodonati A. High speed knock in S.I. engines. *SAE Tech Paper 741056* 1974.
[163] Broeze JJ. Combustion in piston engines: spark-ignition and compression-ignition: H. *Stam* 1963.
[164] Taylor CF. *The internal combustion engine in theory and practice Volume 2: Combustion, fuels, materials, design*. The MIT press; 1985.
[165] Rockstroh T, Kolodziej CP, Jespersen MC, Goldsborough SS, Wallner T. Insights into engine knock: comparison of knock metrics across ranges of intake temperature and pressure in the CFR engine. *SAE Tech Paper 2018-01-0210* 2018.
[166] Leppard WR. The chemical origin of fuel octane sensitivity. *SAE Tech Paper 902137* 1990.
[167] Curran HJ, Gaffuri P, Pitz WJ, Westbrook CK. A comprehensive modeling study of n-heptane oxidation. *Combust Flame* 1998;**114**:149–77.
[168] Curran HJ, Gaffuri P, Pitz WJ, Westbrook CK. A comprehensive modeling study of iso-octane oxidation. *Combust Flame* 2002;**129**:253–80.
[169] Splitter DA, Gilliam A, Szybist J, Ghandhi J. Effects of pre-spark heat release on engine knock limit. *P Combust Inst* 2019;**37**:4893–900.
[170] Mittal V, Heywood JB, Green WH. The underlying physics and chemistry behind fuel sensitivity. *SAE Int J Fuels Lubricants* 2010;**3**:256–65.
[171] Vuilleumier D, Huan X, Casey T, Sjöberg M. Uncertainty assessment of octane index framework for stoichiometric knock limits of co-optima gasoline fuel blends. *SAE Int J Fuels Lubr* 2018;**11**:247–69.
[172] Szybist JP, Splitter DA. Pressure and temperature effects on fuels with varying octane sensitivity at high load in SI engines. *Combust Flame* 2017;**177**:49–66.
[173] Westbrook CK, Mehl M, Pitz WJ, Sjöberg M. Chemical kinetics of octane sensitivity in a spark-ignition engine. *Combust Flame* 2017;**175**:2–15.
[174] Yates ADB, Swarts A, Viljoen CL. Correlating auto-ignition delays and knock--limited spark-advance data for different types of fuel. *SAE Tech Paper 2005-01-2083* 2005.
[175] Mehl M, Faravelli T, Giavazzi F, Ranzi E, Scorletti P, Tardani A, et al. Detailed chemistry promotes understanding of octane numbers and gasoline sensitivity. *Energ Fuel* 2006;**20**:2391–8.
[176] Kalghatgi GT. Fuel anti-knock quality - part I. engine studies. *SAE Tech Paper 2001-01-3584* 2001.
[177] Kalghatgi GT. Fuel anti-knock quality- part II. vehicle studies - how relevant is motor octane number (MON) in modern engines? *SAE Tech Paper 2001-01-3585* 2001 v.
[178] Kalghatgi GT, Nakata K, Mogi K. Octane appetite studies in direct injection spark ignition (DISI) engines. *SAE Tech Paper 2005-01-0244* 2005.
[179] Mittal V, Heywood JB. The relevance of fuel RON and MON to knock onset in modern SI engines. *SAE Tech Paper 2008-01-2414* 2008.
[180] Kalghatgi GT. Auto-ignition quality of practical fuels and implications for fuel requirements of future SI and HCCI engines. *SAE Tech Paper 2005-01-0239* 2005.
[181] Davies T, Cracknell R, Lovett G, Cruff L, Fowler J. Fuel effects in a boosted DISI engine. *SAE Tech Paper 2011-01-1985* 2011.
[182] Remmert S, Campbell S, Cracknell R, Schuetze A, Lewis A, Giles K, et al. Octane appetite: the relevance of a lower limit to the MON specification in a downsized, highly boosted DISI engine. *SAE Int J Fuels Lubricants* 2014;**7**:743–55.
[183] Zhou Z, Yang Y, Brear M, Lacey J, Leone TG, Anderson JE, et al. A comparison of four methods for determining the octane index and K on a modern engine with upstream, port or direct injection. *SAE Tech Paper 2017-01-0666* 2017.
[184] Amer A, Babiker H, Chang J, Kalghatgi G, Adomeit P, Brassat A, et al. Fuel effects on knock in a highly boosted direct injection spark ignition engine. *SAE Int J Fuels Lubricants* 2012;**5**:1048–65.
[185] Prakash A, Cracknell R, Natarajan V, Doyle D, Jones A, Jo YS, et al. Understanding the octane appetite of modern vehicles. *SAE Int J Fuels Lubricants* 2016;**9**:345–57.
[186] Kalghatgi G, Risberg P, Ångstrom H-E. A method of defining ignition quality of fuels in HCCI engines. *SAE Tech Paper 2003-01-1816* 2003.
[187] Kalghatgi GT, Head RA. The available and required autoignition quality of gasoline - like fuels in HCCI engines at high temperatures. *SAE Tech Paper 2004-01-1969* 2004.
[188] Risberg P, Kalghatgi G, Ångstrom H-E. Auto-ignition quality of gasoline-like fuels in HCCI engines. *SAE Tech Paper 2003-01-3215* 2003.
[189] Szybist JP, Wagnon SW, Splitter D, Pitz WJ, Mehl M. The reduced effectiveness of EGR to mitigate knock at high loads in boosted SI engines. *SAE Int J Eng* 2017;**10**:2305–18.
[190] Szybist JP, Splitter DA. Understanding chemistry-specific fuel differences at a constant RON in a boosted SI engine. *Fuel* 2018;**217**:370–81.
[191] Ratcliff MA, Burton J, Sindler P, Christensen E, Fouts L, McCormick RL. Effects of heat of vaporization and octane sensitivity on knock-limited spark ignition engine performance. *SAE Tech Paper 2018-01-0218* 2018.
[192] Szybist J, Foster M, Moore WR, Confer K, Youngquist A, Wagner R. Investigation of knock limited compression ratio of ethanol gasoline blends. *SAE Tech Paper 2010-01-0619* 2010.
[193] Rockstroh T, Floweday G, Yates A. Optimisation of synthetic gasoline blend recipes for use in modern charge boosted GDI engines. *Fuel* 2016;**186**:800–20.
[194] Risberg P, Kalghatgi G, Ångstrom H-E. The influence of EGR on auto-ignition

quality of gasoline-like fuels in HCCI engines. *SAE Tech Paper 2004-01-2952* 2004.
[195] Shibata G, Urushihara T. Auto-ignition characteristics of hydrocarbons and development of HCCI fuel index. *SAE Tech Paper 2007-01-0220* 2007.
[196] Vuilleumier D, Sjöberg M. Significance of RON, MON, and LTHR for knock limits of compositionally dissimilar gasoline fuels in a DISI engine. *SAE Int J Eng* 2017;**10**:938–50.
[197] Vuilleumier D, Sjöberg M. The use of transient operation to evaluate fuel effects on knock limits well beyond RON conditions in spark-ignition engines. *SAE Tech Paper 2017-01-2234* 2017.
[198] Leone TG, Anderson JE, Davis RS, Iqbal A, Reese RA, Shelby MH, et al. The effect of compression ratio, fuel octane rating, and ethanol content on spark-ignition engine efficiency. *Environ Sci Technol* 2015;**49**:10778–89.
[199] Yokoo N, Nakata K, Chapman B, Joseph D, Sabio N, Farenback-Brateman J, et al. Effect of high RON fuels on engine thermal efficiency and greenhouse gas emissions. *SAE Tech Paper 2019-01-0629* 2019.
[200] Smith P, Heywood J, Cheng W. Effects of compression ratio on spark-ignited engine efficiency. *SAE Tech Paper 2014-01-2599* 2014.
[201] Anderson W, Yang J, Brehob DD, Vallance JK, Whiteaker RM. Understanding the thermodynamics of direct injection spark ignition (DISI) combustion systems: an analytical and experimental investigation. *SAE Tech Paper 962018* 1996.
[202] Kasseris E, Heywood JB. Charge cooling effects on knock limits in SI DI engines using gasoline/ethanol blends: part 1-quantifying charge cooling. *SAE Tech Paper 2012-01-1275* 2012.
[203] Kasseris E, Heywood JB. Charge cooling effects on knock limits in SI DI engines using gasoline/ethanol blends: part 2-effective octane numbers. *SAE Int J Fuels Lubricants* 2012;**5**:844–54.
[204] Okamoto K, Ichikawa T, Saitoh K, Oyama K, Hiraya K, Urushihara T. Study of antiknock performance under various octane numbers and compression ratios in a DISI engine. *SAE Tech Paper 2003-01-1804* 2003.
[205] Wyszynski LP, Stone CR, Kalghatgi GT. The volumetric efficiency of direct and port injection gasoline engines with different fuels. *SAE Tech Paper 2002-01-0839* 2002.
[206] Russ S. A review of the effect of engine operating conditions on borderline knock. *SAE Tech Paper* 1996;**960497**.
[207] Chupka GM, Christensen E, Fouts L, Alleman TL, Ratcliff MA, McCormick RL. Heat of vaporization measurements for ethanol blends up to 50 volume percent in several hydrocarbon blendstocks and implications for knock in SI engines. *SAE Int J Fuels Lubricants* 2015;**8**:251–63.
[208] Stein RA, Polovina D, Roth K, Foster M, Lynskey M, Whiting T, et al. Effect of heat of vaporization, chemical octane, and sensitivity on knock limit for ethanol - gasoline blends. *SAE Int J Fuels Lubricants* 2012;**5**:823–43.
[209] Leone TG, Olin ED, Anderson JE, Jung HH, Shelby MH, Stein RA. Effects of fuel octane rating and ethanol content on knock, fuel economy, and CO2 for a turbocharged DI engine. *SAE Int J Fuels Lubricants* 2014;**7**:9–28.
[210] Foong TM, Morganti KJ, Brear MJ, da Silva G, Yang Y, Dryer FL. The effect of charge cooling on the RON of ethanol/gasoline blends. *SAE Int J Fuels Lubricants* 2013;**6**:34–43.
[211] U.S. Department of Energy. Office of EERE Vehicle Technologies Office: Advanced Combustion Systems and Fuels 2017 Annual Progress Report. 2017.
[212] Sluder CS, Szybist JP, McCormick RL, Ratcliff MA, Zigler BT. Exploring the relationship between octane sensitivity and heat-of-vaporization. *SAE Int J Fuels Lubricants* 2016;**9**:80–90.
[213] Thewes M, Kupper C, Rezaei R, Pischinger S. Future fuels for modern DISI engines. *19th Aachen colloquium automobile and engine technology Aachen, Germany*; 2010.
[214] Jung HH, Leone TG, Shelby MH, Anderson JE, Collings T. Fuel economy and CO2 emissions of ethanol-gasoline blends in a turbocharged DI engine. *SAE Int J Eng* 2013;**6**:422–34.
[215] Janssen A, Balthasar F, Balzer C, Wang C, Wilbrand K, Warnecke W, et al. The role of high octane fuels in future mobility - a technical review *25th Aachen colloquium on outomobile and engine technology Aachen, Germany*; 2016.
[216] ASTM D4809-18. *Standard Test Method for Heat of Combustion of Liquid Hydrocarbon Fuels by Bomb Calorimeter (Precision Method)*. West Conshohocken, PA: ASTM International; 2018.
[217] Jung HH, Shelby MH, Newman CE, Stein RA. Effect of ethanol on part load thermal efficiency and CO2 emissions of SI engines. *SAE Tech Paper 2013-01-1634* 2013.
[218] Kolodziej CP, Pamminger M, Sevik J, Wallner T, Wagnon SW, Pitz WJ. Effects of fuel laminar flame speed compared to engine tumble ratio, ignition energy, and injection strategy on lean and EGR dilute spark ignition combustion. *SAE Int J Fuels Lubricants* 2017;**10**:82–94.
[219] Marshall SP, Taylor S, Stone CR, Davies TJ, Cracknell RF. Laminar burning velocity measurements of liquid fuels at elevated pressures and temperatures with combustion residuals. *Combust Flame* 2011;**158**:1920–32.
[220] Rallis CJ, Garforth AM. The determination of laminar burning velocity. *Prog Energ Combust* 1980;**6**:303–29.
[221] Andrews GE, Bradley D. Determination of burning velocities - critical review. *Combust Flame* 1972;**18**:133–53.
[222] Bradley D, Gaskell PH, Gu XJ. Burning velocities, markstein lengths, and flame quenching for spherical methane-air flames: a computational study. *Combust Flame* 1996;**104**:176–98.
[223] Law CK. Dynamics of stretched flames. *Symposium (Int) Combust* 1989;**22**:1381–402.
[224] Egolfopoulos FN, Hansen N, Ju Y, Kohse-Höinghaus K, Law CK, Qi F. Advances and challenges in laminar flame experiments and implications for combustion chemistry. *Prog Energ Combust* 2014;**43**:36–67.
[225] Williams FA. *Combustion Theory*. Menlo Park, CA: The Benjamin/Cummings Publishing Company, Inc.; 1985.
[226] Farrell JT, Weissman W, Johnston RJ, Nishimura J, Ueda T, Iwashita Y. Fuel effects on SIDI efficiency and emissions. *SAE Tech Paper 2003-01-3186* 2003.
[227] Hinton N, Stone R, Cracknell R. Laminar burning velocity measurements in constant volume vessels - Reconciliation of flame front imaging and pressure rise methods. *Fuel* 2018;**211**:446–57.
[228] Rahim F, Elia M, Ulinski M, Metghalchi M. Burning velocity measurements of methane-oxygen-argon mixtures and an application to extend methane-air burning velocity measurements. *Int J Engine Res* 2002;**3**:81–92.
[229] Rockstroh T, Burger V, Yates A, Smit D. Laminar flame speed characterization of synthetic gasoline components. *SAE Tech Paper 2014-01-2616* 2014.
[230] Gu XJ, Haq MZ, Lawes M, Woolley R. Laminar burning velocity and Markstein lengths of methane-air mixtures. *Combust Flame* 2000;**121**:41–58.
[231] Jerzembeck S, Sharma A, Peters N. Laminar burning velocities of nitrogen diluted standard gasoline-air mixture. *SAE Tech Paper 2008-01-1075* 2008.
[232] Johnston RJ, Farrell JT. Laminar burning velocities and Markstein lengths of aromatics at elevated temperature and pressure. *P Combust Inst* 2005;**30**:217–24.
[233] Kelley AP, Law CK. Nonlinear effects in the extraction of laminar flame speeds from expanding spherical flames. *Combust Flame* 2009;**156**:1844–51.
[234] Farrell JT, Johnston RJ, Androulakis IP. Molecular structure effects on laminar burning velocities at elevated temperature and pressure. *SAE Tech Paper 2004-01-2936* 2004.
[235] Metghalchi M, Keck JC. Burning velocities of mixtures of air with methanol, isooctane, and indolene at high-pressure and temperature. *Combust Flame* 1982;**48**:191–210.
[236] Sileghem L, Vancoillie J, Demuynck J, Galle J, Verhelst S. Alternative fuels for spark-ignition engines: mixing rules for the laminar burning velocity of gasoline-alcohol blends. *Energ Fuel* 2012;**26**:4721–7.
[237] Caton JA. Thermodynamic considerations regarding the use of EGR for conventional and high efficiency engines. In: Proceedings of the ASME ICEF technical paper WOS:000392464100023; 2016.
[238] Hesse R, Beeckmann J, Wantz K, Pitsch H. Laminar burning velocity of market type gasoline surrogates as a performance indicator in internal combustion engines. *SAE Tech Paper 2018-01-1667* 2018.
[239] Remmert SM, Campbell S, Cracknell R, Schuetze A, Warnecke W, lewis AGJ, et al. Fuel effects in a downsized, highly boosted direct injection spark ignition engine *23rd Aachen colloquium automobile and engine technology Aachen, Germany*; 2014.
[240] Broustail G, Halter F, Seers P, Moréac G, Mounaïm-Rousselle C. Experimental determination of laminar burning velocity for butanol/iso-octane and ethanol/iso-octane blends for different initial pressures. *Fuel* 2013;**106**:310–17.
[241] Sjöberg M, Reuss D. NOx-reduction by injection-timing retard in a stratified-charge DISI engine using gasoline and E85. *SAE Tech Paper 2012-01-1643* 2012.
[242] Li B, Liu N, Zhao RH, Zhang H, Egolfopoulos FN. Flame propagation of mixtures of air with high molecular weight neat hydrocarbons and practical jet and diesel fuels. *P Combust Inst* 2013;**34**:727–33.
[243] Ayala FA, Engines Heywood JBLean SI. The role of combustion variability in defining lean limits. *SAE Tech Paper 2007-24-0030* 2007.
[244] Chapman EM, Costanzo VS. A literature review of abnormal ignition by fuel and lubricant derivatives. *SAE Tech Paper 2015-01-1869* 2015.
[245] Michlberger A, Sutton M, Kocsis M, Anderson G, Van Horn A. On-road monitoring of low speed pre-ignition. *SAE Tech Paper 2018-01-1676* 2018.
[246] Jatana GS, Splitter DA, Kaul B, Szybist JP. Fuel property effects on low-speed pre-ignition. *Fuel* 2018;**230**:474–82.
[247] Wang Z, Liu H, Song T, Qi YL, He X, Shuai SJ, et al. Relationship between super-knock and pre-ignition. *Int J Engine Res* 2015;**16**:166–80.
[248] Wang Z, Qi YL, He X, Wang JX, Shuai SJ, Law CK. Analysis of pre-ignition to super-knock: Hotspot-induced deflagration to detonation. *Fuel* 2015;**144**:222–7.
[249] Zahdeh A, Rothenberger P, Nguyen W, Anbarasu M, Schmuck-Soldan S, Schaefer J, et al. Fundamental approach to investigate pre-ignition in boosted SI engines. *SAE Tech Paper 2011-01-0340* 2011.
[250] Zaccardi JM, Escudie D. Overview of the main mechanisms triggering low-speed pre-ignition in spark-ignition engines. *Int J Engine Res* 2015;**16**:152–65.
[251] Haenel P, Seyfried P, Kleeberg H, Tomazic D. Systematic approach to analyze and characterize pre-ignition events in turbocharged direct-injected gasoline engines. *SAE Tech Paper 2011-01-0343* 2011.
[252] Okada Y, Miyashita S, Izumi Y, Hayakawa Y. Study of low-speed pre-ignition in boosted spark ignition engine. *SAE Tech Paper 2014-01-1218* 2014.
[253] Wang Z, Qi Y, Liu H, Long Y, Wang J-X. Experimental study on pre-ignition and super-knock in gasoline engine combustion with carbon particle at elevated temperatures and pressures. *SAE Tech Paper 2015-01-0752* 2015.
[254] Gupta A, Seeley R, Shao H, Remias J, Roos J, Wang Z, et al. Impact of particle characteristics and engine conditions on deposit-induced pre-ignition and superknock in turbocharged gasoline engines. *SAE Tech Paper 2017-01-2345* 2017.
[255] Dahnz C, Han K-M, Spicher U, Magar M, Schiessl R, Maas U. Investigations on pre-ignition in highly supercharged SI engines. *SAE Tech Paper 2010-01-0355* 2010.

[256] Amann M, Mehta D, Alger T. Engine operating condition and gasoline fuel composition effects on low-speed pre-ignition in high-performance spark ignited gasoline engines. *SAE Tech Paper 2011-01-0342* 2011.
[257] Chapman E, Davis RS, Studzinski W, Geng P. Fuel octane and volatility effects on the stochastic pre-ignition behavior of a 2.0L gasoline turbocharged DI engine. *SAE Tech Paper 2014-01-1226* 2014.
[258] Mansfield AB, Chapman E, Briscoe K. Effect of market variations in gasoline composition on aspects of stochastic pre-ignition. *Fuel* 2016;**184**:390–400.
[259] Mansfield AB, Chapman E, Briscoe K. Impact of fuel octane rating and aromatic content on stochastic pre-ignition. *SAE Tech Paper 2016-01-0721* 2016.
[260] Dingle SF, Cairns A, Zhao H, Williams J, Williams O, Ali R. Lubricant induced pre-ignition in an optical SI engine. *SAE Tech Paper 2014-01-1222* 2014.
[261] Fletcher KA, Dingwell L, Yang K, Lam WY, Styer JP. Engine oil additive impacts on low speed pre-ignition. *SAE Tech Paper 2016-01-2277* 2016.
[262] Mayer M, Hofmann P, Geringer B, Williams J, Moss J, Kapus P. Influence of different oil properties on low-speed pre-ignition in turbocharged direct injection spark ignition engines. *SAE Tech Paper 2016-01-0718* 2016.
[263] Qi Y, Xu Y, Wang Z, Wang J. The effect of oil intrusion on super knock in gasoline engine. *SAE Tech Paper 2014-01-1224* 2014.
[264] Ritchie A, Boese D, Young AW. Controlling low-speed pre-ignition in modern automotive equipment part 3: identification of key additive component types and other lubricant composition effects on low-speed pre-ignition. *SAE Tech Paper 2016-01-0717* 2016.
[265] Welling O, Collings N, Williams J, Moss J. Impact of lubricant composition on low-speed pre-ignition. *SAE Tech Paper 2014-01-1213* 2014.
[266] Welling O, Moss J, Williams J, Collings N. Measuring the impact of engine oils and fuels on low-speed pre-ignition in downsized engines. *SAE Tech Paper 2014-01-1219* 2014.
[267] Whitby RD. Engine oils and low-speed pre-ignition. *Tribol Lubr Technol* 2015;**71**:88.
[268] Amann M, Alger T, Westmoreland B, Rothmaier A. The effects of piston crevices and injection strategy on low-speed pre-ignition in boosted SI engines. *SAE Tech Paper 2012-01-1148* 2012.
[269] Dahnz C, Spicher U. Irregular combustion in supercharged spark ignition engines - pre-ignition and other phenomena. *Int J Engine Res* 2010;**11**:485–98.
[270] Kalghatgi GT, Bradley D. Pre-ignition and 'super-knock' in turbo-charged spark-ignition engines. *Int J Engine Res* 2012;**13**:399–414.
[271] Kalghatgi GT, Bradley D, Andrae J, Harrison AJ. The nature of "superknock" and its origins in SI engines. Institution of mechanical engineers - internal combustion engines: performance. *Fuel Economy and Emissions* 2009:259–69.
[272] Peters N, Kerschgens B, Paczko G. Super-knock prediction using a refined theory of turbulence. *SAE Tech Paper 2013-01-1109* 2013.
[273] Mayer M, Hofmann P, Geringer B, Williams J, Moss J. Influence of different fuel properties and gasoline - ethanol blends on low-speed pre-ignition in turbocharged direct injection spark ignition engines. *SAE Tech Paper 2016-01-0719* 2016.
[274] Nomura T, Ueura H, Tanaka Y, da Y II, Yuan Z, Ando A. The effect of gasoline metallic additives on low speed pre-ignition. *SAE Tech Paper 2018-01-0936* 2018.
[275] Kassai M, Torii K, Shiraishi T, Noda T, Goh TK, Wilbrand K, et al. Research on the effect of lubricant oil and fuel properties on LSPI Occurrence in boosted S.I. engines. *SAE Tech Paper 2016-01-2292* 2016.
[276] Splitter D, Burrows B, Lewis S. Direct measurement and chemical speciation of top ring zone liquid during engine operation. *SAE Tech Paper 2015-01-0741* 2015.
[277] Splitter D, Kaul B, Szybist J, Speed L, Zigler B, Luecke J. Fuel-Lubricant Interactions on the Propensity for Stochastic Pre-Ignition. *SAE Tech Paper 2019-24-0103* 2019.
[278] Splitter D, Kaul B, Szybist J, Jatana G. Engine operating conditions and fuel properties on pre-spark heat release and SPI promotion in SI engines. *SAE Int J Eng* 2017;**10**:1036–50.
[279] Rudloff J, Zaccardi JM, Richard S, Anderlohr JM. Analysis of pre-ignition in highly charged SI engines: emphasis on the auto-ignition mode. *P Combust Inst* 2013;**34**:2959–67.
[280] Aikawa K, Sakurai T, Jetter JJ. Development of a predictive model for gasoline vehicle particulate matter emissions. *SAE Int J Fuels Lubricants* 2010;**3**:610–22.
[281] Swarts A, Chapman E, Costanzo VS. Detailed analyses and correlation of fuel effects on stochasti preignition. *SAE Tech Paper, 2020-01-0612* 2020.
[282] Pihl J, Thomas J, Sinha Majumdar S, Huff S, West B, Toops T. Development of a cold start fuel penalty metric for evaluating the impact of fuel composition changes on si engine emissions control. *SAE Tech Paper 2018-01-1264* 2018.
[283] Anderson J, Rask E, Lohse-Busch H, Miers S. A comparison of cold-start behavior and its impact on fuel economy for advanced technology vehicles. *SAE Int J Fuels Lubricants* 2014;**7**:427–35.
[284] Kessels JTBA, Foster DL, Bleuanus WAJ. Fuel penalty comparison for (Electrically) heated catalyst technology. *Oil Gas Sci Technol* 2010;**65**:47–54.
[285] Rodriguez JF, Cheng WK. Reduction of cold-start emissions through valve timing in a GDI engine. *SAE Int J Eng* 2016;**9**:1220–9.
[286] Rodriguez JF, Cheng WK. Cycle-by-cycle analysis of cold crank-start in a GDI engine. *SAE Int J Eng* 2016;**9**:1210–19.
[287] USDRIVE ACEC Tech Team Working Group on Low Temperature Aftertreatment. Aftertreatment protocols for catalyst characterization and performance evaluation: low temperature oxidation catalyst test protocol. 2017.
[288] Kang SB, Nam SB, Cho BK, Nam IS, Kim CH, Oh SH. Effect of speciated HCs on the performance of modern commercial TWCs. *Catal Today* 2014;**231**:3–14.
[289] Majumdar SS, Pihl J, Toops T. Reactivity of novel high-performance fuels on commercial three-way catalysts for control of emissions from spark-ignition engines. *Applied Energy* 2019;**255**:13640.
[290] Maricq MM, Szente JJ, Harwell AL, Loos MJ. How well can aerosol instruments measure particulate mass and solid particle number in engine exhaust? *Aerosol Sci Tech* 2016;**50**:605–14.
[291] Cole RL, Poola RB, Sekar R. Exhaust emissions of a vehicle with a gasoline direct-injection engine. *SAE Tech Paper 982605* 1998.
[292] He X, Ireland JC, Zigler BT, Ratcliff MA, Knoll KE, Alleman TL, et al. The impacts of mid-level biofuel content in gasoline on SIDI engine-out and tailpipe particulate matter emissions. *SAE Tech Paper 2010-01-2125* 2010.
[293] Khalek IA, Bougher T, Jetter JJ. Particle emissions from a 2009 gasoline direct injection engine using different commercially available fuels. *SAE Int J Fuels Lubricants* 2010;**3**:623–37.
[294] Maricq MM, Podsiadlik DH, Chase RE. Examination of the size-resolved and transient nature of motor vehicle particle emissions. *Environ Sci Technol* 1999;**33**:1618–26.
[295] Storey JM, Barone T, Norman K, Lewis S. Ethanol blend effects on direct injection spark-ignition gasoline vehicle particulate matter emissions. *SAE Int J Fuels Lubricants* 2010;**3**:650–9.
[296] Storey JME, Barone TL, Thomas JF, Huff SP. Exhaust particle characterization for lean and stoichiometric DI vehicles operating on ethanol-gasoline blends. *SAE Tech Paper 2012-01-0437* 2012.
[297] Zhang S, McMahon W. Particulate emissions for LEV II light-duty gasoline direct injection vehicles. *SAE Int J Fuels Lubricants* 2012;**5**:637–46.
[298] US EPA. Light-Duty Trucks: Tier 0, Tier 1, and Clean Fuel Vehicle (CFV) Exhaust Emission Standards. Report US EPA Report EPA-420-B-16-008, 2016.
[299] US EPA Part II: environmental protection agency: 40 CFR Parts 80, 85, and 86: control of air pollution from new motor vehicles: tier 2 motor vehicle emissions standards and gasoline sulfur control requirements; final rule. *Federal Register* 2010;**65**(28).
[300] US EPA. *Light-duty vehicles, light-duty trucks, and medium-duty passenger vehicles: tier 2 exhaust emission standards and implementation schedule. US EPA Report EPA-420-B-17-028*; 2017.
[301] US EPA. *Control of air pollution from motor vehicles: tier 3 motor vehicle emission and fuel standards final rule. US EPA Report EPA-420-R-14-005*; 2014.
[302] . California's advanced clean cars midterm review: appendix J: vehicle PM emission control technology assessment. California Environmental Protection Agency, California Air Resources Board; 2017. p. 1–34.
[303] Delphi Technologies. Delphi technologies worldwide emissions standards: passenger cars and ligh duty vehicles 2018-2019. Delphi Technologies. p. 1–128.
[304] Giechaskiel B, Arndt M, Schindler W, Bergmann A, Silvis W, Drossinos Y. Sampling of non-volatile vehicle exhaust particles: a simplified guide. *SAE Int J Eng* 2012;**5**:379–99.
[305] Giechaskiel B, Mamakos A, Andersson J, Dilara P, Martini G, Schindler W, et al. Measurement of automotive nonvolatile particle number emissions within the european legislative framework: a review. *Aerosol Sci Tech* 2012;**46**:719–49.
[306] Maricq MM, Szente J, Loos M, Vogt R. Motor vehicle PM emissions measurement at LEV III levels. *SAE Int J Eng* 2011;**4**:597–609.
[307] Joshi A. Review of vehicle engine efficiency and emissions. *SAE Tech Paper 2019-01-0314* 2019.
[308] Joshi A, Johnson TV. Gasoline particulate filters—a review, 4. Emission Control Science and Technology; 2018. p. 219–39.
[309] . California's advanced clean cars midterm review: appendix j: vehicle pm emission control technology assessment. California Environmental Protection Agency, California Air Resources Board; 2017. p. 1–34.
[310] Stach T, Schlerfer J, Vorbach M. New generation multi-hole fuel injector for direct-injection si engines - optimization of spray characteristics by means of adapted injector layout and multiple injection. *SAE Tech Paper 2007-01-1404* 2007.
[311] He X, Ratcliff MA, Zig BT. Effects of gasoline direct injection engine operating parameters on particle number emissions. *Energ Fuel* 2012;**26**:2014–27.
[312] Hoffmann G, Befrui B, Berndorfer A, Piock WF, Varble DL. Fuel system pressure increase for enhanced performance of GDi multi-hole injection systems. *SAE Int J Eng* 2014;**7**:519–27.
[313] Bromberg L, Cohn D. Optimized PFI+DI operation for minimizing DI gasoline engine particulates. *SAE Tech Paper 2018-01-1415* 2018.
[314] Chen W, Xia C, Mao K, Tao J, Fang J, Huang Z. The effects of injection strategies on particulate emissions from a dual-injection gasoline engine. *SAE Tech Paper 2019-01-0055* 2019.
[315] Ikoma T, Abe S, Sonoda Y, Suzuki H, Suzuki Y, Basaki M. Development of V-6 3.5-liter engine adopting new direct injection system. *SAE Tech Paper 2006-01-1259* 2006.
[316] Husted H, Spegar TD, Spakowski J. The effects of GDi fuel pressure on fuel economy. *SAE Tech Paper 2014-01-1438* 2014.
[317] Sobotowski RA, Butler AD, Guerra Z. A pilot study of fuel impacts on pm emissions from light-duty gasoline vehicles. *SAE Int J Fuels Lubricants* 2015;**8**:214–33.
[318] Coordinating Research Council Enhanced speciation of gasoline. *CRC Report AVFL-29* 2019.
[319] Barrientos EJ, Anderson JE, Maricq MM, Boehman AL. Particulate matter indices using fuel smoke point for vehicle emissions with gasoline, ethanol blends, and butanol blends. *Combust Flame* 2016;**167**:308–19.
[320] Ratcliff MA, Burton J, Sindler P, Christensen E, Fouts L, Chupka GM, et al. Knock resistance and fine particle emissions for several biomass-derived

oxygenates in a direct-injection spark-ignition engine. *SAE Int J Fuels Lubricants* 2016;**9**:59–70.
[321] Ratcliff MA, Windom B, Fioroni GM, John P St, Burke S, Burton J, et al. Impact of ethanol blending into gasoline on aromatic compound evaporation and particle emissions from a gasoline direct injection engine. *Appl Energy* 2019;**250**:1618–31.
[322] Smith BL, Bruno TJ. Improvements in the measurement of distillation curves. 3. Application to gasoline and gasoline plus methanol mixtures. *Ind Eng Chem Res* 2007;**46**:297–309.
[323] Burke S, Rhoads R, Ratcliff M, McCormick R, Windom B. Measured and predicted vapor liquid equilibrium of ethanol-gasoline fuels with insight on the influence of azeotrope interactions on aromatic species enrichment and particulate matter formation in spark ignition engines. *SAE Tech Paper 2018-01-0361* 2018.
[324] Burke SC, Ratcliff M, McCormick R, Rhoads R, Windom B. Distillation-based droplet modeling of non-ideal oxygenated gasoline blends: investigating the role of droplet evaporation on PM emissions. *SAE Int J Fuels Lubricants* 2017;**10**:69–81.
[325] Tibshirani R. Regression shrinkage and selection via the Lasso. *J Roy Stat Soc B Met* 1996;**58**:267–88.
[326] Das DD, John PCS, McEnally CS, Kim S, Pfefferle LD. Measuring and predicting sooting tendencies of oxygenates, alkanes, alkenes, cycloalkanes, and aromatics on a unified scale. *Combust Flame* 2018;**190**:349–64.
[327] Storey JM, Moses-DeBusk M, Huff S, Lewis S, Li F, Thomas J, et al. Characterization of GDI PM during start-stop operation with alcohol fuel blends *2016 heal effects institute workshop on the effects of fuel composition on PM Chicago, IL*; 2016.
[328] Pihl JA, Ratcliff MA, Kim S, St John P, Moses-Debusk M, Storey JM, et al. *Co-optima emissions, emissions control, and merit function development*, Washington, D.C.: US Departmment of Energy Vehicle Technologies; 2018. Office Annual Merit Review FT057.
[329] Chan TW, Meloche E, Kubsh J, Brezny R, Rosenblatt D, Rideout G. Impact of ambient temperature on gaseous and particle emissions from a direct injection gasoline vehicle and its implications on particle filtration. *SAE Int J Fuels Lubricants* 2013;**6**:350–71.
[330] Kern B, Spiess S, Richter JM. Comprehensive gasoline exhaust gas aftertreatment, an effective measure to minimize the contribution of modern direct injection engines to fine dust and soot emissions? *SAE Tech Paper 2014-01-1513* 2014.
[331] Mamakos A. *Joint research centre scientific and policy reports EUR 25297 EN*; 2011.
[332] Mamakos A, Steininger N, Martini G, Dilara P, Drossinos Y. Cost effectiveness of particulate filter installation on direct injection gasoline vehicles. *Atmos Environ* 2013;**77**:16–23.
[333] Yang J, Roth P, Durbin TD, Johnson KC, Cocker DR, Asa-Awuku A, et al. Gasoline particulate filters as an effective tool to reduce particulate and polycyclic aromatic hydrocarbon emissions from gasoline direct injection (GDI) vehicles: a case study with two GDI vehicles. *Environ Sci Technol* 2018;**52**:3275–84.
[334] Milkulic I, Koelman H, Majkowski S, Vosejpka P. A study about particulate filter application on a state-of-the-art homogeneous turbocharged 2L DI gasoline engine. *Aachener Kolloquium Fahrzeug und Motorentechnik* 2010.
[335] Lambert CK, Chanko T, Dobson D, Liu X, Pakko J. Gasoline particle filter development. *Emission Control Sci Technol* 2017;**3**:105–11.
[336] Lambert CK, Chanko T, Jagner M, Hangas J, Liu X, Pakko J, et al. Analysis of ash in low mileage, rapid aged, and high mileage gasoline exhaust particle filters. *SAE Int J Eng* 2017;**10**:1595–603.
[337] Liu X, Chanko T, Lambert C, Maricq M. Gasoline particulate filter efficiency and backpressure at very low mileage. *SAE Tech Paper 2018-01-1259* 2018.
[338] Hirshfeld DS, Kolb JA, Anderson JE, Studzinski W, Frusti J. Refining economics of U.S. gasoline: octane ratings and ethanol content. *Environ Sci Technol* 2014;**48**:11064–71.
[339] Anderson JE, Leone TG, Shelby MH, Wallington TJ, Bizub JJ, Foster M, et al. Octane numbers of ethanol-gasoline blends: measurements and novel estimation method from molar composition. *SAE Tech Paper 2012-01-1274* 2012.
[340] Ji CS, Dames E, Wang H, Egolfopoulos FN. Propagation and extinction of benzene and alkylated benzene flames. *Combust Flame* 2012;**159**:1070–81.
[341] Moses-Debusk M, Pihl JA, Storey JM, Lewis S, Sinha Majumdar S. Co-optima emissions and emissions control for SI/ACI multimode combustion. US Department of Energy Vehicle Technologies Office Annual Merit Review FT073. Washington, D.C. 2019.
[342] McCormick RL, Fioroni G, Fouts L, Christensen E, Yanowitz J, Polikarpov E, et al. Selection criteria and screening of potential biomass-derived streams as fuel blendstocks for advanced spark-ignition engines. *SAE Int J Fuels Lubricants* 2017;**10**:442–60.
[343] Anderson JE, Kramer U, Mueller SA, Wallington TJ. Octane numbers of ethanol- and methanol-gasoline blends estimated from molar concentrations. *Energ Fuel* 2010;**24**:6576–85.
[344] Foong TM. *On the autoignition of ethanol/gasoline blends in spark-ignition engines*. University of Melborne; 2013.
[345] Gary JH, Handwerk GE. *Petroleum refining: technology and economics*. 4 ed. New York, NY: Marcel Decker, Inc.; 2001.
[346] Gaspar DJ. *Top ten blendstocks derived from biomass for turbocharged spark ignition engines: bioblendstocks with potential for highest engine efficiency*. Pacific Northwest National Laboratory; 2019. PNNL-28713.
[347] Splitter D, Szybist J. Intermediate alcohol-gasoline blends, fuels for enabling increased engine efficiency and powertrain possibilities. *SAE Tech Paper 2014-01-1231* 2014.

James P. Szybist: Dr. Szybist leads the Fuel Property technical team within the Co-Optima initiative and is a principle investigator at Oak Ridge National Laboratory where he leads studies to better develop a better understanding of engine and fuel interactions. His current research interests include the autoignition processes that result in knock in spark ignited engines and autoignition in low temperature combustion engines and using kinetics to develop an improved conceptual understanding of the phenomenon. He is a Fellow of the Society of Automotive Engineers (SAE) and the 2015 recipient of the SAE Harry L. Horning Award. He received his Ph.D. from Penn State University in Fuel Science in in 2005 and then joined Oak Ridge National Laboratory as a post-doc, where he is currently a Distinguished Research Scientist.

Stephen Busch: Stephen Busch is a Principal Member of the Technical Staff at Sandia National Laboratories, where he is responsible for medium-duty diesel combustion research. His research interests include laser-based optical combustion diagnostics and high-speed imaging; 0D, 1D, and 3D fluid- and thermodynamic process analyses; science-driven approaches to diesel combustion system design, catalyst heating operation, and heat transfer measurements. He is a member of the Society of Automotive Engineers (SAE). He received his doctorate degree from the Karlsruhe Institute of Technology in 2013 and started his career as a postdoc at Sandia.

Robert L. McCormick: Dr. Robert L. McCormick is a Senior Research Fellow in the Fuels and Combustion Science group at the National Renewable Energy Laboratory. This group's research is focused on biofuels properties and fuel-engine interactions including biofuel quality and quality specifications, compatibility with modern engines, combustion, pollutant emissions effects, and leveraging fuel properties for design of more efficient engines. He has worked extensively on ethanol and biodiesel, as well as next generation and futuristic fuels. Bob has a PhD in chemical engineering. Before joining the National Renewable Energy Laboratory in 2001 he was a research professor at the Colorado School of Mines. He has coauthored over 120 peer reviewed technical articles and is a Fellow of SAE International.

Josh A. Pihl: Josh Pihl is the Group Leader for the Applied Catalysis and Emissions Research Group at Oak Ridge National Laboratory. His work focuses on developing emissions control solutions that enable high efficiency engines and alternative fuels to achieve emissions compliance. He relies on his background in chemical engineering and chemistry to identify the underlying chemical processes that control the performance of emissions control devices, and uses that information to develop improved catalyst formulations, aftertreatment system architectures, control strategies, and component models. He chairs the CLEERS (Crosscut Lean Exhaust Emissions Reduction Simulations) coordinating committee and serves as the Co-Optima Advanced Engine Development deputy team lead. He received a M.S. in Chemical Engineering from the University of Wisconsin, Madison in 2005 and a B.S. in Chemistry from the University of California, San Diego in 1999.

Derek A. Splitter: Derek Splitter holds a PhD in Mechanical Engineering from the University of Wisconsin Engine Research Center. He currently is a staff researcher at Oak Ridge National Laboratory, where he studies stoichiometric, dilute, and abnormal combustion processes including stochastic pre ignition. He is active in the engine combustion community and has authored over 60 publications in fuels and combustion processes ranging conventional spark and compression ignition processes to advanced combustion processes including HCCI, RCCI, PPC, SA-HCCI, and RCCI. Some of his work has been distinguished with the SAE Horning Memorial, and Myers Awards, and he is an active member in SAE and the Combustion Institute.

Matthew A. Ratcliff: Matt is a senior Chemist with NREL's Transportation and Hydrogen Systems Center where his research focuses on the intersection of fuel chemistry, internal combustion engine performance, and exhaust emissions. On-going investigations involve the use of next generation biofuels in direct injection spark ignition and advanced compression ignition engines, as part of the US Department of Energy's initiative Co-Optimization of Fuels and Engines. Previously Matt worked in NREL's National Bioenergy Center (NBC) integrating an indirect biomass gasifier with spark-ignition and microturbine engines for electric power generation. While at NBC he also collaborated with industry for several years developing biomass gasification systems with syngas tar reforming catalysts for power generation and liquid fuels synthesis. Matt received a B.S. in Chemistry from Colorado State University and a M.S. in Analytical Chemistry from Colorado School of Mines.

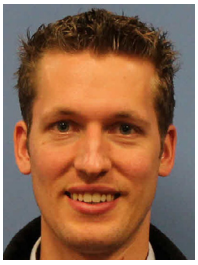

Christopher P. Kolodziej: Christopher P. Kolodziej has been a research engineer at Argonne National Laboratory, in the Center for Transportation Research, for three years. He previously worked at Delphi as a Senior Engineer and a postdoctoral appointee at Argonne National Laboratory. He conducts research in the areas of fuel composition effects on autoignition reactivity, fuel reactivity rating methods, and gasoline compression ignition (GCI) engine combustion. Christopher holds bachelor and master degrees in Mechanical Engineering from the University of Wisconsin-Madison and a doctoral degree from the CMT-Motores Termicos, an engine research department within the Universidad Politecnica de Valencia in Valencia, Spain.

John M.E. Storey: Dr. Storey retired in 2020 as a distinguished research staff member from the Oak Ridge National Laboratory where he led the emissions characterization efforts at the Fuels, Engines, and Emissions Research Center. Storey joined Oak Ridge in 1992. His research was focused on engine particulate emissions, including real-world mobile source emissions. His research also emphasized air toxics and particulate characterization. His other areas of interest included health effects of exhaust nanoparticles, decomposition products in urea-Selective Catalytic Reduction (SCR) systems, and real-time exhaust composition measurement. Storey's research has led to more than 75 publications and three patents. He has served on the Transportation and Air Quality Committee of the Transportation Research Board, and has co-chaired the Department of Energy committees on emissions from advanced petroleum-based fuels. Storey is a Fellow of the Society of Automotive Engineers (SAE) and a 30 year member of the American Chemical Society. During his career, he received three R&D 100 Awards, the Partnership for a New Generation of Vehicles Award for Technical Accomplishment, and six Significant Event Awards from Oak Ridge National Laboratory. Storey earned his bachelor's in chemistry at Harvard University, his master's in environmental engineering from Duke University and his doctorate in environmental chemistry from the Oregon Graduate Institute of Oregon Health Sciences University.

Melanie Moses-Debusk: Dr. Melanie Moses-DeBusk is a Staff R&D Scientist at Oak Ridge National Laboratory (ORNL) and leads projects at the National Transportation Research Center in emissions characterization, catalyst development and aftertreatment control. Moses-DeBusk joined ORNL 2004 as a Post-Doctoral Associate before transition to staff. Her current research focuses are in engine particulate and gaseous hydrocarbon emissions and natural gas aftertreatment development. Other areas she has worked in at ORNL have ranged from single atom catalysis to inorganic membrane separation. She has authored over 34 publications, 3 book chapters and holds 4 patents. Moses-DeBusk earned her bachelor's in chemistry from Bellarmine University (formerly Bellarmine College) and her PhD in chemistry from the University of Maryland, College Park.

David Vuilleumier: Dr. David Vuilleumier studies the interactions between internal combustion engines and the fuels they consume, with the goal of elucidating the relationships between fuel composition and engine performance, in order to improve our utilization of energy in the transportation system. Dr. Vuilleumier has investigated fuel – engine interactions in a variety of different combustion systems, including stoichiometric spark-ignition engines, lean-burn spark-ignition engines, stratified-charge engines, homogeneous charge compression ignition engines, and gasoline compression ignition engines, using a variety of techniques, including metal-engine performance testing, engine and benchtop optical-diagnostics, 1-D engine modeling, and detailed kinetic simulations. Dr. Vuilleumier received his Ph.D. in Mechanical Engineering from the University of California at Berkeley where he investigated the low-temperature autoignition behavior of gasoline-ethanol blends under Homogeneous Charge Compression Ignition and Gasoline Compression Ignition type conditions.

Magnus Sjöberg: Dr. Magnus Sjöberg is a Principal Member of Technical Staff in the Engine Combustion Department at Sandia National Laboratories. He is also the AED Team Lead in DOE's Co-Optima initiative. Magnus is Principal Investigator in Sandia's Alternative Fuels Direct-Injection Spark-Ignition (DISI) Engine Lab, where he leads research on fuel effects on advanced SI engine combustion. This research spans from performance testing and exhaust-emissions measurements to detailed optical measurements of in-cylinder processes. One focus area is fuel-spray mixture formation and emissions-formation processes in stratified-charge SI combustion. Another focus area include end-gas autoignition phenomena in both conventional stoichiometric combustion as well as in lean spark-assisted mixed-mode combustion. Prior research at Sandia involved fundamental research on fuel effects for Homogeneous Charge Compression Ignition (HCCI) engine combustion. Magnus holds a PhD in Mechanical Engineering from the Royal Institute of Technology in Stockholm, Sweden, where his studies focused on diesel-engine combustion and emissions-formation processes.

C. Scott Sluder: Scott Sluder is a Senior Research Engineer at Oak Ridge National Laboratory's Fuels, Engines, and Emissions Research Center. He received a B.S. in 1994 and an M.S. degree in 1995 in Mechanical engineering from the University of Tennessee. He joined the staff of Oak Ridge National Laboratory in 1998. Scott is actively involved in SAE International, having organized and chaired numerous technical sessions and symposia and authored more than 30 SAE technical paper. Scott received SAE's Forest R. McFarland Award in 2008 and has also twice received SAE's Excellence in Oral Presentation Award. Scott is currently serving as the Chairman of SAE's Land & Sea Operating Group and as an Associate editor of the SAE International Journal of Fuels and Lubricants.

Toby Rockstroh: Toby Rockstroh is a staff research engineer in the Energy Systems Division at Argonne National Laboratory (ANL). His experience in the field of internal combustion engines ranges from work in the South African automotive industry (Volkswagen), synthetic fuels research in academia (Sasol) and engine combustion research at a US national laboratory. At ANL he is the principle investigator for light duty engine research, focusing on studying fuel effects on the combustion behavior in spark as well as compression ignition gasoline engines. He holds a PhD in mechanical engineering from the Sasol Advanced Fuels Laboratory at the University of Cape Town.

Paul Miles: Paul Miles manages the Engine Combustion Research department at Sandia National Laboratories and has actively researched or guided research in engine combustion processes since 1984. Dr. Miles joined Sandia in 1992, and transitioned from his technical work as a Distinguished Member of the Technical Staff into a management role in 2014, where he works closely with the U.S. Department of Energy and other government-industry partnership organizations to define research roadmaps for advanced engine combustion. Dr. Miles is a Fellow of the Society of Automotive Engineers (SAE), and has been recognized with several awards for technical and programmatic accomplishments by the SAE, ASME, and USDRIVE. He is a past co-chair of the SAE Powertrain, Fuels and Lubricants activities and serves as the Operating Agent for the International Energy Agency Combustion Technology Collaboration Programme. Dr. Miles also serves as an associate editor of the SAE Journal of Engines, is a member of the editorial board of the International Journal of Engine Research, and serves on the advisory or organizing committees of several international conferences. He received his PhD in Mechanical Engineering from Cornell University, following a BSME from the Georgia Institute of Technology.